

An Investigation of the Radioecology of the Carbonatite deposits in the Homa
Mountain region in South Nyanza, Kenya

by

David Otwoma

Registration Number: I80/80187/2010

A thesis submitted in fulfillment of the requirements for the degree of Doctor of
Philosophy, University of Nairobi

A Thesis submitted in December 2012

DECLARATION

This thesis is my original work and has not been presented for a degree in any other University

David Otwoma



31st Dec 2012

I80/80187/2010

Signature

Date

Department of Physics

University of Nairobi

P.O. Box 30197

Nairobi, Kenya

This thesis has been submitted for examination with the approval of my supervisors:

1. **Prof. J. P. Patel**



4/12/2012

Signature

Date

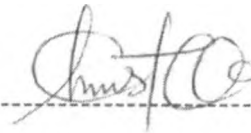
Department of Physics

University of Nairobi

P.O. Box 30197

Nairobi, Kenya

2. **Dr. A. O. Mustapha**



4-12-12

Signature

Date

Department of Physics

Federal University of Agriculture

P.M.B. 2240

Abeokuta, Nigeria

ABSTRACT

The level of radiation due to the naturally occurring radioactive materials was investigated and the radiological hazard was calculated for Homa Mountain located at the intersection of longitude 33° 26' E and 34° 34' E latitude 0° 30' N and 0° 20' N in southwestern Kenya. The absorbed dose rate in air at 1 meter above the ground was measured using calibrated hand held survey meters that could be coupled to sodium iodide (NaI) radiation detector. The measured mean dose rate of 474.1 nSv h⁻¹ translated to annual dose due to external radioactivity of 4.15 mSv y⁻¹. The radioactivity concentrations of ⁴⁰K, ²²⁶Ra and ²³²Th in rock and soil samples were measured using gamma ray spectroscopy from two different institutions for comparison purposes of accuracy and precision. The cumulative mean activity concentrations obtained were 915.6, 195.3 and 409.5 Bq kg⁻¹ of ⁴⁰K, ²²⁶Ra and ²³²Th, respectively. The calculated mean absorbed dose rate was 383.33 nGy h⁻¹; the radium equivalent activity mean was 838.6 Bq kg⁻¹; the representative level index mean value was 5.93; the gamma activity index mean value was 2.96; the external hazard index mean was 2.26 and the internal hazard index mean was 2.77. It was observed that the pattern of high values of the radiological indices follows that of the corresponding activity concentrations. These indices are important parameters for the radiological protection of the population since soils are used for making earthen huts and pottery while bricks and rocks for building human habitations. The resultant total effective dose (TED) equivalent was 5.03 mSv y⁻¹. Using RESRAD software program, the impact of these naturally occurring radioactive materials on the environment was evaluated for different age sets of the population and the results showed that infants and teenagers receive more effective doses than other segments of the populations. The RESRAD code enabled modeling of ⁴⁰K, ²³²Th and ²³⁸U environmental pathways. This led to exposure pathways of external radiation, inhalation and ingestion resulting in total effective dose equivalent to exposed individuals estimated as 4.93 mSv y⁻¹. The excellent correlation of similar TED derived from the different

measurements and modeling methodologies increased the certainty of the conclusions arrived at for the work done. The Homa Mountain study has established data on radiation dose to the population and qualifies the region as a high background radiation area due to dominance of carbonatite rocks. Investigations of the health hazards of radiation and the impacts of high levels of background radiation on the local inhabitants can be done in future epidemiological studies. The exploration of the possible economic benefits that can be derived from the minerals associated with carbonatite deposits, Rare Earth Elements and Thorium is open for consideration.

TABLE OF CONTENTS

Title	i
Declaration	ii
Abstract.....	iii
Table of Contents	v
Acknowledgements.....	vii
List of Figures	ix
List of Tables.....	xi
List of Abbreviations	xii
Chapter 1: INTRODUCTION.....	1
1.1 Radioecology of Natural Occurring Radiation Materials.....	1
1.2 Geography and Geology of Homa Mountain Area.....	4
1.3 Gamma Dose Rates of NORM.....	10
Chapter 2: LITERATURE REVIEW.....	14
2.1 Review of Activity Concentration of Natural Radioactivity.....	14
2.2 Review of Significant Radiation Hazard	19
2.3 Studies done in Kenya on Radiological Exposure.....	24
2.4 Statement of the Research Problem.....	28
2.5 Objective of the Research.....	29
2.6 Rationale of the Research.....	30
Chapter 3: THEORETICAL BACKGROUND.....	32
3.1 Theory of Radioecological Assessment of Naturally Occurring Radioactive Materials.....	32
3.2 Dosimetric Radiation Quantities and Units.....	33
3.3 Theory of Different Radiation Indices	38
3.4 Background Information of RESRAD.....	42
Chapter 4: MATERIALS AND METHODS.....	59

4.1	Summary.....	59
4.2	Equipment and Calibration Procedures.....	59
4.3	Method of Sampling after surveying.....	66
4.4	Sample Preparation	66
4.5	Measurement of Activity Concentration.....	67
4.6	Computer Hardware and RESRAD Software.....	77
Chapter 5: RESULTS AND DISCUSSIONS		80
5.1	Summary.....	80
5.2	Background Radiation Dose Measurements using Hand Held Survey Meters.....	80
5.3	Concentration of Uranium, Thorium and Potassium in Samples..	86
5.4	Exposure Pathways and Dose Estimation using RESRAD.....	99
Chapter 6: CONCLUSIONS AND RECOMMENDATIONS		112
6.1	Dose Rates using hand held Survey Meters Conclusions	112
6.2	Radiation Hazard/Indices Conclusions	112
6.3	RESidual RADIation (RESRAD) Adaptation Conclusions	113
6.4	Recommendations	114
REFERENCES		118
Appendix A: Geology and Geography of Homa Mountain		137
Appendix B: List of Surveyed Areas		147
Appendix C: Reference Materials isotopic Data for ^{40}K , ^{232}Th and ^{238}U		165

ACKNOWLEDGEMENTS

I wish to express my profound gratitude to Prof. J. P. Patel who opened up in-situ measurements of radioactivity in Kenya. He occupies a special place and deserves accolades for always encouraging, guiding, and offering very useful suggestions throughout the course of the research. Appreciation to Dr. A. O. Mustapha for pioneering in-situ followed by laboratory background radiation measurements in Kenya before he left University of Nairobi (UoN) in 2007 and hence encouraging many of us into this field of research. I thank Dr. H. A. Kalambuka of UoN for his incisive insight and being available at the completion of this study; Mr. Joel Kioko for approving and Mr. Stanislaus Masinza for being present when performing calibration of equipment at the Secondary Standards Dosimetry Laboratory (SSDL) at Kenya Bureau of Standards (KeBS); Ms. Ruth Nguti of National Council of Science and Technology (NCST) for conscientiously typing most of the thesis. Ms. Irene Gichira, Stellah Wambui and Ms. Marcellah Ojiambo for assisting in sample preparations at the Materials Testing and Research Laboratories (MTRL) of the Ministry of Roads (MoR), Mr. David Kabiga of NCST for ever encouraging me to persist with the study; Mr. Simon Bartlol for facilitating gamma radiation measurements at the Institute of Nuclear Science and Technology (INST), UoN; Michael Mangala for his positive appraisal that enabled polishing of this thesis, Samuel Mngongo of MoR for assisting with internet connectivity. During my field trips and all the friendly people I had the privilege of meeting on those occasions, I am grateful to them too.

Recognition to the authorities and staff of the NCST, KeBS, MoR, INST, Radiation Protection Board (RPB) and Ministries of Energy (MoE) and Livestock Development for providing logistic resources, facilitating and hosting me when doing most of the research work. I am also grateful to my sponsors Ministry of Higher Education Science and Technology for paying for two years tuition fee, and my host institutions, initially NCST for providing me with logistics and

required facilitation that enabled the bulk of the work to be done and recently the Nuclear Electricity Project. Special gratitude too goes to Mr. Patrick Nyoike, the Permanent Secretary in the MoE, for encouraging me to complete the work and facilitating sponsorship for the final year cost. Gratitude to the International Atomic Energy Agency who enabled meeting peers internationally and having equipped INST, MTRL, RPB and KeBS with the instruments I used for this research.

Finally, this study alienated me from people very close to me, and I am very grateful for their patience and perseverance. My family especially my cherished wife Amina and my wonderful children Luiza, Eva and Nasio Omutsani were a source of encouragement and their invaluable support makes me very grateful for their understanding and calmness.

LIST OF FIGURES

1.1	Map of Kenya in relation to its position in Africa	5
1.2	Position of Homa Mountain (in red star) next to Lake Victoria.....	7
1.3	Sketch map of the Homa Mountain area.....	8
1.4	Exposure Dose percentage from Natural and Artificial Radiation Sources.....	11
3.1	Schematics of a 4π Geometry.....	38
3.2	Exposure Pathways Considered in RESRAD.....	43
3.3	Schematic Representation of RESRAD Pathways.....	46
3.4	Exposure Geometry Considered for Area Factor Calculation.....	52
3.5	Cross Section of Exposure Geometry Showing Element of Integration for Area Factor Calculation.....	53
4.1	Radiogem with α , β and Υ Probes.....	59
4.2	Calibration Factor and Response normalized for RPB Radiagem.....	62
4.3	Linearity of the Response versus the True H^* (10).....	63
4.4	Responses for different X-ray keVs.....	65
4.5	Calibration Factors against X-ray Energies.....	65
4.6	Peak Efficiency Calibration Curve for the HpGe of RPB.....	73
4.7	Peak Efficiency Curve for the HpGe detector of INST.....	74
5.1	Box Plot of the Absorbed Dose Rates values.....	82
5.2	Distribution fit superimposed on Histogram for Absorbed Dose Rates values.....	84
5.3	Normal Q-Q Plot of Dose Rate values.....	85
5.4	Detrended Normal Q-Q Plot of Dose Rate values.....	86
5.5	Annual Dose when ^{40}K , ^{224}Ra and ^{232}Th all pathways summed for mean activity concentration.....	104
5.6	Annual dose when ^{40}K , ^{224}Ra and ^{232}Th all pathway summed for 1,000 Year extrapolation for sample with highest Th.....	106
5.7	Annual Dose when ^{40}K , ^{224}Ra and ^{232}Th all Pathways Summed for 1,000	

Year extrapolation for Sample with highest U.....	107
5.8 Annual dose when ^{40}K , ^{224}Ra and ^{232}Th all Pathways Summed for 1,000 Year extrapolation for Sample with highest K.....	108
A.1 Nyasanya peak – the forest cover have been cleared by charcoal burners.....	137
A.2 A lineament cutting across the northern side of Homa Mountain in a NE- SW direction.....	138
A.3 Rawe beds composed of brown clay, ash and gravel beds overlain by alluvials.....	139
A.4 Veins, a common feature in the hot water discharge zones.....	140
A.5 Veins, a common feature in the hot water discharge zones.....	141
A.6 An inclusion of welded pyroclastics in Rawe beds exposed on the banks of Nyagot Pala stream.....	142
A.7 Clear water discharging from a formation contact zone.....	143
A. 8 Habitations encroaching Got Chiewo viewed from Ndiru Mbili.....	144
C. 1 Decay schemes of ^{40}K and ^{87}Rb	169
C. 2 Decay schemes of ^{235}U	170
C. 3 Decay schemes of ^{238}U	171
C. 4 Decay schemes of ^{232}Th	172

LIST OF TABLES

1.1	Exposure Dose Rates as mSv from Natural and Artificial Sources in the World.....	11
4.1	Comparison of the Responses of the Radiogem used (RPB), at SSDL (IAEA) and Ion Chambers (PTW).....	62
4.2	Calibration Factor and Responses for different x-ray keVs.....	64
4.3	Gamma ray Energies used for Calibration of Spectrometer and for Measurement of Activity of the Radionuclides	68
4.4	Measured Activity Concentrations (Bq kg ⁻¹) of ²³² Th, ²²⁶ Ra and ⁴⁰ K in the IAEA Reference Samples Compared to Others.....	70
5.1	Descriptive Statistical Analysis of the Absorbed Dose Rates.....	81
5.2	Test of Normality for Data from Homa Mountain.....	82
5.3	Activity Concentration (Bq Kg ⁻¹) of ²³² Th, ²²⁶ Ra and ⁴⁰ K in the Rock and Soil samples.....	87
5.4	Comparison of mean activity concentration values (Bq Kg ⁻¹) of Rock and Soil samples from different Countries.....	91
5.5	Calculated Radiological Indices for Homa Mountain area.....	93
5.6	Total Effective Dose contributions for individual radionuclides and pathways for water independent pathways (inhalation excludes Rn)....	100
B.1	List of sites at and around Homa Mountain that the hand held survey meters were used showing the dose rates.....	147
C.1	IAEA -RGU-1.....	165
C.2	IAEA -RGTh-1.....	167
C.3	IAEA -RGK-1.....	168

LIST OF ABBREVIATIONS

Abbreviations

ALARA	as low as reasonably achievable
ANL	Argonne National Laboratory (in United States of America)
BEIR	Committee on the Biological Effects of Ionizing Radiation
BIOMASS	Biosphere Model Validation Study
CEDE	Committed Effective Dose Equivalent
DCF	Dose Conversion Factor(s)
DOE	U.S Department of Energy
DSR	dose/source ratio
EDF	Environmental Dose Factor(s)
EPA	U.S Environmental Protection Agency
ETF	Environmental Transport Factor(s)
HPGe	Hyper Pure Germanium detector
IAEA	International Atomic Energy Agency
ICRP	International Commission on Radiological Protection
INST	Institute of Nuclear Science and Technology
KeBS	Kenya Bureau of Standards
LLD	Lower Limit of Detection
MoE	Ministry of Energy (in Kenya)
MoR	Ministry of Roads (in Kenya)
MTRL	Materials Testing and Research Laboratories (in Kenya)
NCST	National Council for Science and Technology (in Kenya)
ND	Non Detectable
NORM	Naturally Occurring Radioactive Material
NRC	U.S. Nuclear Regulatory Commission
RESRAD	Residual Radioactivity (model)
RPB	Radiation Protection Board (in Kenya)
SF	Source Factor
SPSS	Statistical Package for the Social Sciences
TEDE	Total Effective Dose Equivalent
TP	Time since Placement

Chapter 1

INTRODUCTION

1.1. Radioecology of Naturally Occurring Radiation Materials

Radioecology is defined as the scientific discipline that gathers all the environmentally related knowledge required to assess the impacts of radioactive substances on the environment. Radioecology includes the study of transfer pathways through which radionuclides traverse, and thereby expose or contaminate the environment, and consequently human populations. Ionizing radiation and radioactive matter are natural and permanent features of the environment. Naturally occurring radioactive material (NORM) includes most radioactive substances found in surroundings (UNSCEAR 2000). NORM are sources of low level radiation, in comparison to artificial high level radiation, although some areas have anomalously high values. Radioactive elements such as uranium (U), thorium (Th), potassium (K) and their decay products such as radium (Ra) and radon (Rn) are examples of NORM. The distribution of naturally-occurring U, Rn, and other radionuclides, depends on the distribution of rocks from which they originate and the processes that concentrate them (Aliyeva 2004; Bolivar et al. 1996; Chowdhury et al. 2005; Elegba and Funtua 2004; Gbadago et al. 2011). Knowing the distribution of source-rock materials containing elevated levels of NORM and understanding the physical and geochemical processes that concentrate radionuclides is useful in radioecological studies.

Radioactivity in soil results from the rock from which they are derived. Therefore, the NORM mainly depends on geological and geophysical conditions. Radionuclides are present in rocks in varying amounts, and they are easily mobilized into the environment. Additional processes which result to NORM removal from the soil and migration results in their distribution leading to

human exposure (Hashim et al.2004; Ivanov et al. 2009; Mustapha et al. 1997; Otansev et al. 2012). The concentration of natural radionuclides in the rock varies considerably depending on the rock formation and lithologic character. The natural rocks such as granite, limestone, dolomite, marble, rhyolites, shale and so on, are widely used as building materials (El-Mageed et al. 2010; Ademoli et al. 2008; Al-Saleh et al. 2007; Malozewski et al. 2004; Viruthagiri and Ponnarasi 2011). It follows that the annual dose due to NORM in the Earth's crust principally from ^{232}Th and ^{238}U series and ^{40}K may be severe when these natural materials are used, for building human habitations or activities such as farming is done. It is therefore important to measure the concentration of radionuclides in rocks that are used and those that have the potential of being used as building materials. Additionally knowledge of concentrations in rocks and soils enable, for human habitations, settlements and where farming activities are, knowledge of environmental transfer of radionuclides. Finally assessing the radiological risks to the human health and studying trends in ailments due to radiation hazards needs can be done. This should be the case where monazite and carbonatite igneous rocks are found in abundance.

Carbonatite rock intrusions found in various parts of the world have been associated with high concentrations of ^{40}K , ^{232}Th and ^{238}U radio-nuclides. These radionuclides are a natural source of radiation exposure. Data on population and health effects when living in high background radiation areas is not conclusive despite various studies done in several parts of the world. Such studies have not been addressed adequately in Kenya. Carbonatites are carbonate-rich rocks which are formed through magmatic processes in the upper mantle. Field studies have established several carbonatite and alkaline rock provinces associated with fold belts and rifted continental margins (Bell 1989). Extrusive carbonatites are widespread illustrating low viscosity carbonatite melts can form most of the typical volcanic products normally associated with silicate melts. Natural radioactive mineral deposits can be

found in geological environments. The occurrences of out crops of such rocks enhances the background radiation of the area. Therefore, it is important to determine trace elements in carbonatites. Erosion and other vagaries of nature result in soil formation from the rocks. The soil, if foodstuffs are grown on it can also result in internal intakes of NORM by consumers of the food products.

Artificial radionuclides can also be present such as Cesium (^{134}Cs and ^{137}C), resulting from fallout from weapons testing and nuclear power plants accidents such as those of Chernobyl and Fukushima. The growing worldwide interest in natural radiation exposure has lead to extensive surveys in many countries. In radiological protection, the emphasis is usually on limiting exposure to artificial radiation (Kenya Government 1982). There is a well established approach to the protection of staff in hospitals from X-rays and the public in general from the radioactive consumer goods. Although current radiation protection standards for the public are generally judged to be acceptably robust, there remain considerable scientific uncertainties with regard to dose and health risk assessments.

Some of these uncertainties originate from the exposure assessment, which is largely dependent on knowledge of the occurrence and behavior of natural and artificial radionuclides in the environment. This thesis seeks to emphasize that for Homa Mountain area the dose to human beings is persistent specifically due to presence of carbonatites. Radioecology also examines the effects of radionuclides on ecosystems (i.e. ecotoxicology of radionuclides). Such studies are important to optimize radiation protection (Akerblom 1995; Degrange and Lepicard 2004; EC 1994; Henrich et asl. 2004; ICRP 1984). They are also important to society because any over- or under-estimation of contaminant exposure or radiological effects could lead to unnecessary and costly restrictions, or alternatively, to a lower level of protection for the public or the environment.

The radiological implication of radionuclides from U, Th and their daughters is due to the gamma (γ -) ray exposure of the body and irradiation of lung tissue from inhalation of radon and its daughters (ICRP 1991; Latourneau et al. 1984; Nair et al. 2009). These dose rates vary depending upon the concentration of the natural radionuclides, ^{238}U , ^{232}Th , their daughter products, principally Radon (^{222}Rn) and ^{40}K , present in soil, rocks and aqua system, which in turn depend upon the local geology of each region in the world (Myrick et al., 1983). ^{222}Rn is a natural radioactive gas. When the gas and its decay products are inhaled into the respiratory system, they will attach to the lung tissue and increase the risk of lung cancer.

1.2. Geography and Geology of Homa Mountain Area

The total population of Kenya is 38,340,000 (July 2010 estimate) living in a total area of 582,650 km². The annual population growth rate is 3.53% with a life expectancy at birth of 51.3 years. The GDP per capita is US \$980. Kenya lies along the equator in East Africa (see Fig 1). Most of the country consists of high plateau areas and mountain ranges that rise up to 3,000 m and more. The plateau area is dissected by the Eastern Rift Valley, which is 40-50 km wide and up to 1,000 m lower than the flanking plateaux. The narrow coastal strip along the Indian Ocean is backed by a zone of thornbush-land. Some areas in central Kenya, at the flanks of the Rift Valley, and in western Kenya, close to Lake Victoria, are very densely populated. The backbones of Kenya's economy are agriculture and tourism. Large parts of the population make their living from subsistence agriculture. The predominant food crops are maize, rice, wheat, bananas and cassava. The main export crops are coffee, tea, pyrethrum, sisal, tobacco and horticultural products mainly flowers

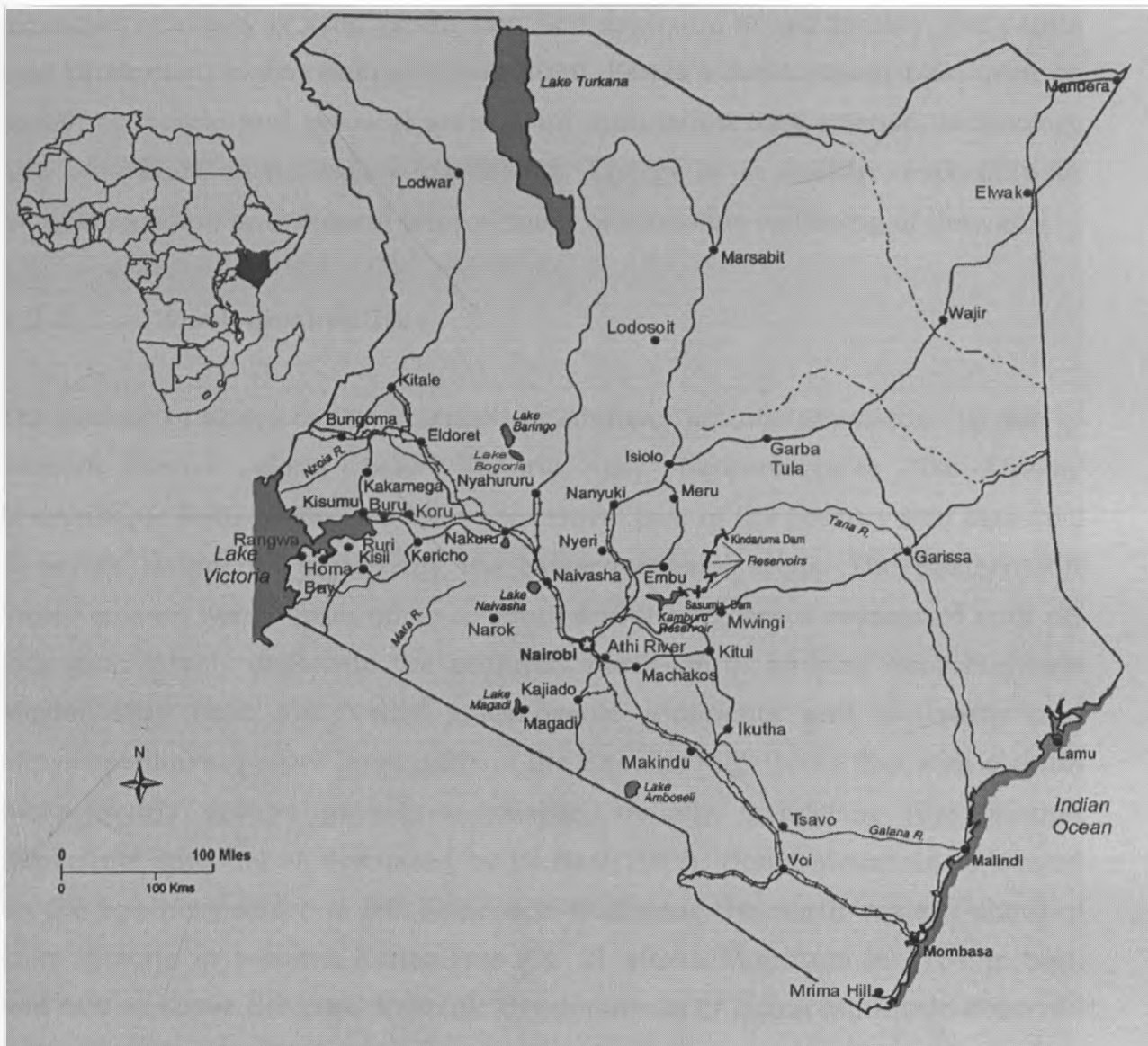


Fig. 1.1 Map of Kenya in relation to its position in Africa (Mustapha 1999)

The mineral industry is small, with the main minerals of economic significance being soda ash (from Lake Magadi), limestone for the cement industry, and other industrial minerals. Small gold deposits are exploited by small-scale miners in the western part of the country. The International Labour Organization estimates the number of persons involved in small-scale mining in Kenya to be 30,000 to 40,000. Increased population density has resulted in

increased intensity of crop production and depletion of soil fertility. Per capita food production is decreasing. Vision 2030, Kenya's development blue print on social, economic and political arenas, on foundation lists science, technology and innovation as necessary ingredients. Energy is an enabler, especially for industrialization and general improvement of economic wellbeing of Kenyans.

1.2.1 Geological outline

The geology of Kenya is characterized by Archean granite/greenstone terrain in western Kenya along Lake Victoria, the Neoproterozoic 'Pan-African' Mozambique Belt, which underlies the central part of the country and Mesozoic to recent sediments underlying the eastern coastal areas. The Eastern Rift Valley crosses Kenya from north to south and the volcanics associated with rift formation largely obliterate the generally north-south striking Neoproterozoic Mozambique Belt. Rift Valley volcanogenic sediments and lacustrine and alluvial sediments cover large parts of the Eastern Rift. Homa Bay area contain rocks nearly always potassium-feldspar, usually orthoclase (Carbonatite-Nephelinite igneous) as discussed by Le Bas (1977). Homa Mountain is located on the southern shore of the Kavirondo Gulf near the north-eastern shore of Lake Victoria in western Kenya (see Fig. 2). Homa Mountain is 1754 m high and 600 m above the lake. Volcanic developments of Homa Mountain occurred in four stages of carbonatite intrusion and have been reported from 8 Ma (10⁶ years) to 2 Ma periods

Because of their low viscosity, carbonatite melts tend to move fast with minimal effects of crustal contamination during ascent to the surface of the earth. The chemical composition of carbonatite can be used as chemical tracers for studying the nature of the upper mantle. Beyond such purely scientific reasons for the enormously expanded interest in carbonatites, the investigation of these rocks has been accelerated because of the discovery of Rare Earth

Elements (REE) concentration in them. Carbonatites are commercially exploitable sources of Niobium, light REEs and Thorium.



Fig. 1.2. Position of Homa Mountain (in red star) next to Lake Victoria

Such rocks containing 75% or more K-feldspar are called orthoclasite, or trachyte if fine-grained. Phonolites are defined by the alkali-feldspar content constituting between 40% and 90% of the total felsics. The phonolites of Homa Bay are characterized by the presence of euhedral phenocrysts of nepheline, some of tubular alkali-feldspar and zoned prismatic aegirine-augite. The map (Fig A.3) was divided into eight areas (Personal Communication with Wanjie and Chebet, 2007) namely Homa Mountain peak, Awaya, Chiewo, Ndiru, Nyasanja, Ndiru Mbili, Rongo Hills, Bala gulley and Rawe beds.

In the Homa and Kendu Bay areas of South Nyanza extrusive carbonatites occur in several centres, including Rangwa cladera, the Ruri carbonanite

complexes and the satellite vents of Homa Mountain. All extrusive carbonatite volcanic of the Homa Bay area are spatially and temporally related to alkavite dykes corresponding to the C2, C3, and C4 carbonatite stages of Les Bas (1977), Nyamai (1989), Mulaha (1989) and (Bell 1989).

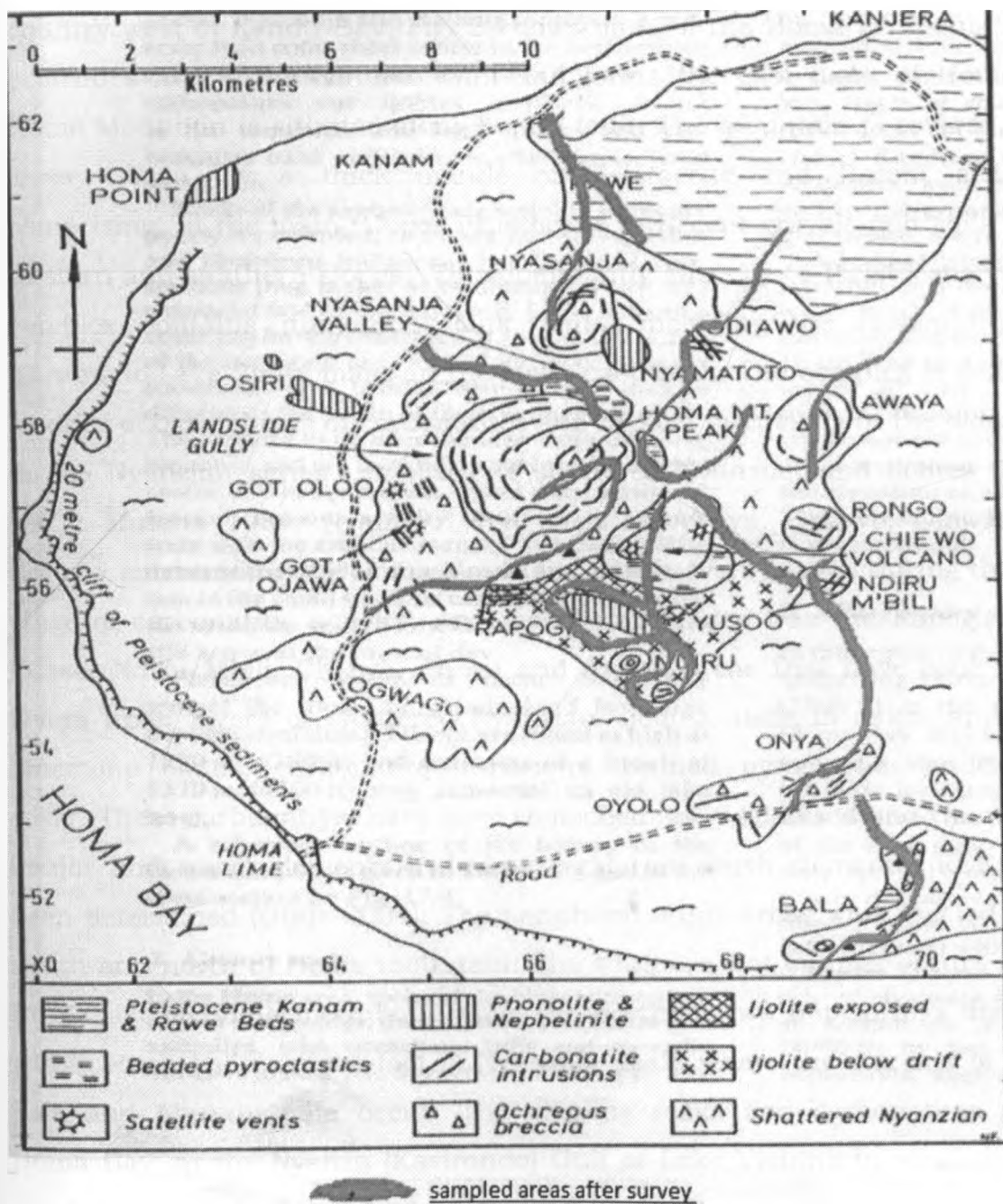


Fig. 3 Sketch map of the Homa Mountain area (Le Bas 1977)

Homa Mountain is a large carbonatitic complex that forms a broad peninsula on the eastern shore of Lake Victoria. It is located in West Karachuonyo division, Rachuonyo district in Homa Bay County and is bound by latitude $0^{\circ} 30' N$ and $0^{\circ} 20' N$ and longitude $33^{\circ} 26' E$ and $34^{\circ} 34' E$. Homa Mountain, the site of an active volcano in Tertiary and Pleistocene times, dominates the country west of Kendu Bay. Fig. 3 shows most of the Homa peninsula, which protrudes into the Kavirondo Gulf and forms the east flank of Homa Bay. Homa Mountain is situated along Kendu fault. The mountain is covered, on its lower slopes, by a thick mantle of Pleistocene and Recent sediments comprising, in the main, Upper Pleistocene to Recent gravels and soils on the western and southern slopes. This dominantly Miocene-to-Pleistocene volcanic complex contains numerous flank vents, including the carbonatitic and ultramafic Lake Simbi maar on the lower east flank. The complex is defined as a series of cone sheets of carbonatites and breccia intrusions in the oldest rock in the Nyanzian series composed of shattered Nyanzian and ijolites (Le Bas 1977; Mulaha 1989; Nyamai 1989) such as Awaya, Chiewo, Ojawa, Oloo, Rongo, surrounding the Homa Mountain, which were formed during the latest stage of carbonatitic activity. An area of importance was the Rapogi, Ndiru-Yusso, Ndiru Mbili, Chiewo, Rongo and Awaya areas that have cone shaped layers upon layers of shattered Nyanzian, ijolites, tuffs in dykes and vents, limestone bands, carbonatite intrusions, bedded pyroclastics and alluvial cover. These carbonatites have been radiochemically analysed and twenty eight (major and trace) elements including eight rare earth elements (REEs) have been determined (Ohde 2004). The peripheral study areas were located on the south and north of Homa mountain. The southern hot springs occurs around Bala, east of Homa mountain, while the northern two hot springs are found within Rawe beds, on the foot of Nyasanja peak, where the streams of Nyagot pala and Abundu pala occur. The alkaline rocks and carbonatites around Homa Bay on the Nyanza (Kavirondo) Gulf of Lake Victoria in western Kenya are fully and comprehensively described by Le Bas (1977). Appendix A gives details general area studied composed of a number of separate peaks which

include Nyasanja, Odiawo, Rongo, Chiewo, Ndiru. Ojawa, Oloo, Nyamatoto and Awaya, the largest being Homa which rises to a height of over 1584 m.

1.3. Gamma Dose Rates of Natural Occurring Radioactive Materials

Naturally occurring radioactive material (NORM) are wide spread in the earth's environment and they exist in enhanced forms in geological formations in soil, rocks, plants, water and air in certain areas. There have been many surveys to determine the background levels of radionuclides in rocks and soils, which can in turn be related to the absorbed dose rates in air. The latter can be measured directly, and these results provide an even more extensive evaluation of the background exposure in different countries (Ibrahiem et al. 1993; Aly-Abdo et al. 1999; Singh et al. 2003). The specific levels that give rise to external exposure outdoors are related to the types of rock from which the soil originate. Higher radiation levels are associated with igneous rocks, such as granite and lower levels with sedimentary rocks (Hashim et al. 2004).

Rocks are used for various purposes, mainly building and construction of houses and roads (Al-Saleh and Al-Berzan 2007). Soils that are in the surrounding areas are also used for building but additional food crops and cattle graze on grass that grow from the soil. These terrestrial primordial radionuclides, ^{40}K , rubidium (^{87}Rb) and the radionuclides in the decay chains of ^{232}Th and ^{238}U found in soils, rocks, building materials, water, air and foodstuffs cause exposure to human beings and the environment nearby. The members of the radioactive decay chain of ^{232}Th (14%), ^{235}U and ^{238}U (55.8%), along with ^{40}K (13.8%) are responsible for the main contributions to the dose and Table 1 shows the exposure dose rates from both natural and artificial sources (UNSCEAR 2000). UNSCEAR reports the greatest contribution to human exposure comes from natural background radiation due to NORM. The worldwide average annual effective dose from all sources as detailed in Table 1

is 2.4 mSv. For inhabitants living in areas with radioactive mineral deposits, they are exposed at higher levels due to NORM. The terrestrial source alone would be above 1 mSv y⁻¹ which is a limit applied for building materials in some countries (OECD 1979; EC 1999; Al-Saleh and Al-Berzan 2007).

Table 1. Exposure dose rates as mSv from natural and artificial sources in the World (UNSCEAR 2000)

Radiation		UNSCEAR	
Type	Source	World Average (mSv)	Typical Range (mSv)
Natural	Air	1.26	0.2-10.0
	Internal	0.29	0.2-1.0
	Terrestrial	0.48	0.3-1.0
	Cosmic	0.39	0.3-1.0
	Total	2.40	1.0-13.0
Man Made	Medical	0.60	0.03-2.0
	Fallout	0.007	0-1+
	others	0.0052	0-20

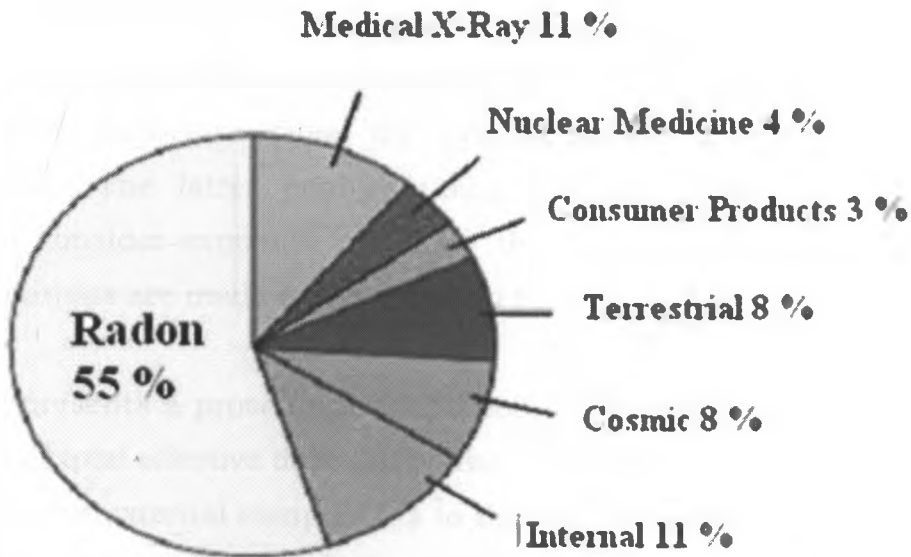


Fig. 4 Exposure dose percentage from natural and artificial radiation sources

By collecting the rock and soil samples and using gamma ray spectrometry to analyze the activity concentration of NORM in them it was possible to estimate by calculations both the indoor and outdoor external exposure to the public. Field surveys done giving dose rate were compared to estimated dose values calculated using the activity concentrations, occupancy factors and conversion factors. U and Th have been found in naturally occurring minerals such as monazite, rutile, zircons, ilmenite etc. are some heavy radioactive minerals which are found abundantly in Kenya (Mangala 1987; Bell 1989). Carbonatite melts are considered to be stable mantle fluids responsible for transporting volatiles and trace elements (B, Sn, Li, Rb, Sr and rare earth elements) in the upper mantle. Because of their low viscosity, carbonatite melts tend to move fast with minimal effects of crustal contamination during ascent to the surface of the earth. The chemical composition of carbonatite can be used as chemical tracers for studying the nature of the upper mantle. Beyond such purely scientific reasons for the enormously expanded interest in carbonatites, the investigation of these rocks has been accelerated because of the discovery of Rare Earth Elements (REE), which are of economic value. Where REE are found elevated levels of U and Th are found and these are sources of exposure to radiation. Accurate radiation dose assessment for areas affected or not affected by mining is important from the concentrations of U and Th in the environment. The latter enables using Residual Radioactivity (RESRAD) program to consider exposure scenarios that are discussed and appropriate recommendations are made for actions and further studies.

This study presents a procedural adaptation of RESRAD code for novel use in calculation of total effective dose (TED) due to NORM. TED is the summation of the internal and external components to the effective dose, whereas committed effective dose (CED) includes only contribution from external components. Additionally, a method is presented which uses the procedural adaptation of RESRAD to compute factors that can be used to directly estimate the annual TED appropriate to chronic exposures to NORM based on activity

concentrations in rocks and soils. These factors are defined as environmental dose factors (EDFs). The EDFs for uranium and thorium in rocks and soils have been calculated and are represented for different exposure scenarios and age groups ranging from infant to adult. Both the procedural adaptation of RESRAD and EDFs could be used to support in baseline dose assessments for Uranium mining or to calculate or estimate the biological implications of NORM.

The radioecology of Homa Mountain documents possible enhanced activity concentrations of radioactivity and the dose exposure due to NORM. Field measurements with hand held gamma dose rate meters combined with in situ gamma ray spectrometry for collected samples measured in the laboratory were done. IAEA reference standards were used to validate the gamma ray spectroscopy equipment while inter comparisons of different hand held equipment ensured quality control. By use of dose conversion factors the activity concentrations of NORM yielded a second independent way of deducing dose received by populations. Lastly the results compiled were compared and additionally the RESRAD code used to create possible scenario that are discussed and appropriate recommendations are made for actions and further studies.

LITERATURE REVIEW

2.1 Review of Activity Concentration of Natural Radioactivity

Natural Occurring Radioactive Materials (NORM) in rocks and soils results in exposure to radiation of human beings and biota. High levels of NORM are due to presence of definite radioactive minerals and are usually embedded in the rock system of the area. The study of the distribution of primordial radionuclides allows the understanding of the radiological deduction of the exposure to human beings and better consideration of the environment and in addition the economic implications.

The growing worldwide interest in natural radiation exposure has lead to widespread surveys in many countries (Ibrahim 1999; Singh et al. 2003; Harb et al. 2008). External gamma dose estimation owing to the terrestrial sources is essential not only because it contributes considerably (0.46 mSv y^{-1}) to the collective dose but also for the reason that the variations of the individual doses related to this pathway is not well known. These doses vary depending upon the concentrations of the natural radio nuclides, ^{238}U , ^{232}Th , their daughter products and ^{40}K , present in the soils and rocks, which in turn depend upon the local geology of each region in the world (Al-Sulaiti et al. 2008; Ivanov et al. 2009; Beauvais et al. 2009; Gonzalez et al. 2009; Nair et al. 2009; Yii et al. 2009).

Heaviest radioactive element uranium is toxic and it is found in traces in more or less all types of rocks, soils, sands and waters. Due to its property to get dissolved in aqueous solution in hexavalent (U6+) form

and to precipitate as a separate mineral in tetravalent (U⁴⁺) form, U forms deposits in the earth's crust where the geological conditions turn out to be favorable (Mustapha 1999). It is extremely important to evaluate the terrestrial gamma dose rate for outdoor occupation so as to estimate the natural radioactivity level in soils. The natural radioactivity of soil samples is usually determined from the ²²⁶Ra, ²³²Th and ⁴⁰K within. Since 98.5% of the radiological effects of the Uranium series are produced by radium and its daughter products, the contribution from the ²³⁸U and the other ²²⁶Ra precursors are usually overlooked. Nationwide surveys have been carried out to determine the radium equivalent activity of soil samples in many countries (Ibrahim 1999; Singh et al. 2003; El-Mageed et al. 2010; Alharbi et al. 2011; Gbadago et al. 2011).

In Brazil stand out the studies at Guarapari, coastal region of Espirito Santo and in the Ilha Grande, Rio de Janeiro State (Bolívar et al. 1996; Malance et al. 1996; Briquet et al. 2004; Alencar and Freitasn 2004; Martínez-Aguirre et al. 1996; Veiga et al. 2006). Most carbonatites regions of the Amazon area in South America were located by aerial surveys. They occur as outstanding topographic expressions associated with radiometric anomalies. In spite of difficult logistic problems, some of these complexes were explored in considerable detail, primarily for U. However, because of the intense oxidation in these areas and the vastly mobile nature of U, it is improbable that any appreciable concentrations would be found in this type of environment. Two types of areas in Brazil are well known for their elevated background radiation: namely the region of volcanic intrusions in the State of Minas Gerais and the region of monazite sands along the Atlantic coast. Radiological studies have been made in monazite sand locations, mainly in India, because along its coastline there are quite a few monazite sand bearing placer deposits that are a source of natural high background radiation areas (UNSCEAR

2000); in Kerala and Tamilnadu in Kalpakkam and in recent work in the coast of Orissa (Singha et al. 2005; Sugahara 2009; Shanthi et al. 2009 and Shanthi et al. 2010).

Activity concentrations of ^{238}U , ^{226}Ra , ^{232}Th and ^{40}K in soil samples collected from different locations of Punjab and Himachal Pradesh were studied to see the inclination in variation of these values from Punjab to Himachal Pradesh. The activity concentrations of ^{226}Ra , ^{232}Th and ^{40}K in collected soil samples were estimated by gamma ray spectrometry and the fission track registration technique was used for the investigation of uranium concentration in these samples (Singha et al. 2005). They established the air-absorbed dose rates in air at a height of about 1m above the ground level due to terrestrial gamma radiation and the corresponding outdoor annual effective dose calculated utilizing a conversion coefficient of 0.7 Sv Gy^{-1} for an absorbed dose in air to effective dose in human body. The gamma dose rate calculated from the concentration of radionuclides of ^{226}Ra , ^{232}Th and ^{40}K ranged between 8.40 and 29.88, 21.68 and 77.67, and 3.33 and 7.51 nGy h^{-1} , respectively. According to UNSCEAR (2000) report, the dose rate in air outdoors from terrestrial gamma rays in normal circumstances is about 57 nGy h^{-1} and the world average ranges from 20 to 1100 nGy h^{-1} .

The half-life (3.8 days) of radon (^{222}Rn) is long enough so that much of the radon formed either in building materials or in the ground within approximately a meter of building understructures can reach the indoor environment (Nair et al. 2009). It decays into a series of short-lived daughter products, out of which ^{218}Po and ^{214}Po emit high energy α -particles. ^{222}Rn and its progeny, when inhaled during breathing enter the human lungs and may lead to serious diseases like lung cancer. Thus radon is a health hazard (UNSCEAR 2000; Lazar et al. 2003). In recent years substantial attention has been paid to ^{222}Rn , particularly to the

problems of exposure to ^{222}Rn and its progeny in dwellings because of its apparent health implications. Many indoor national surveys have been carried out in countries with cold climate, where inhabitants spend a great deal of time indoors especially in winter, such as Austria (Friedmann 2002), Azerbaijan (Aliyeva 2004), Poland (Faanhof and Kempster 2004; Pietrzak-Flis et al. 2004; Malozewski et al. 2004), Russia (Iakovleva and Karataev 2001), France (Degrange and Lepicard 2004), United Kingdom (Oatway et al. 2004), United States of America (Myrick et al. 1983; NCRP 1987) to determine the level of Radon and its progeny in the dwellings. Even in the warm countries such as Mexico (Espinosa and Gammage 2003), Latin America (Canoba et al. 2001), Bangladesh (Viruthagiri and Ponnarasi 2011), Malaysia (Mohsen et al. 2007 and Yii et al. 2009), Nigeria (Elegba and Funtua 2004; Joshua et al. 2009) and Zambia (Hayumbu et al. 2004), considerable attention is being paid to indoor ^{222}Rn problems.

In India, many research workers (Singha et al. 2005; Sugahara 2009; Shanthi et al. 2009 and Shanthi et al. 2010) are engaged in the measurement of indoor ^{222}Rn levels in dwellings for health risk assessments and its control. Though a lot of work has been reported for indoor ^{222}Rn studies in Himachal Pradesh, the data available for Punjab is very meager. Thus considering the health hazards of ^{222}Rn , the indoor ^{222}Rn survey has been carried out in the dwellings belonging to 22 villages of Bathinda district, Punjab. The yearly exposure to the occupants, the annual effective dose received by the population and the lifetime fatality risk estimations have been assessed in the light of guidelines given by the International Commission on Radiological Protection (ICRP 1984, 1995 and 2007). Since U and Ra present in the soil, rocks and building materials are the main sources of indoor ^{222}Rn , the estimation of U and Ra content along with the ^{222}Rn exhalation rate in the soil has also been carried out.

Due to a recent upward trend in the price of U and subsequent increased interest in U mining, accurate modeling of baseline dose from environmental sources of radioactivity is of growing importance. Survey results have been useful to mappers and explorers and have led to additional surveys in subsequent years when new knowledge is acquired (McCall 1958; Patel et al. 1987; Doyle et al. 1990). Quantitative methodology developed 30 years ago for measuring the surface distribution of γ -emitting isotopes, allows data to be expressed in terms of element concentrations and dose rate (Akerblom 1995). Homa Mountains contain mineral deposits formed through weathering and erosion of either igneous or metamorphic rocks. Among the rock constituent minerals are some natural radionuclides that contribute to ionizing radiation exposure on Earth. Carbonatites are igneous rocks, inclusive of the structures and textures characteristic of basaltic or granitic rocks. As with more widespread igneous rocks, understanding the origins and petrology of carbonatites depends on accepting the nature of carbonatite magmas and the processes which can ensue in carbonatite magma bodies. Two classes of critical data are needed to treat carbonatites as igneous rocks; thermochemical (associated to melting, solution, and crystallization) and thermophysical (linked to low styles and speeds, and to motion of crystals). Carbonatite rocks continue to be a resource of niobium (Nb), phosphate, and rare earth elements (REEs). Other commodities associated with carbonatites comprise barite, Cu, fluorite, Sr, V, Th, and U. Th and U are enriched in carbonatites and alkaline igneous rocks relative to crustal abundances. In carbonatites Th is usually more abundant than U (Mustapha et al. 1999).

Case histories from the Canadian Cordillera in British Columbia and Yukon Territory document the powerful exploration vectoring provided by γ -ray spectrometry, during detection of intense potassium enrichment in

the core and periphery of many of these deposits (Shives 1997). For ^{222}Rn gas in the home, Health Canada considers 800 Bq/m^3 to be the limit above which remedial action is optional. Studies in Canada (Letourneau et al. 1984; Cocksedge et al. 1993; Jackson 1992; Doyle et al. 1990), the United States (Otton et al. 1995), Sweden (Akerblom 1995) and United Kingdom (Oatway et al. 2004) have shown that the ground concentration of U determined using an airborne gamma-ray spectrometer gives a qualitative, first-order approximation of regional variation in indoor ^{222}Rn levels and can be used to identify and outline high risk areas.

Results over the famous Sullivan Mine and the surrounding Sullivan-North Star Corridor, suggest that the radiometric data do offer exploration guidance when used in combination with the magnetic and electro-magnetic data. The mineralization lies within delicate Th/K ratio laws, related to potassium adjustment in the form of muscovite. Many are based on using U and Th variations to map mineralizing intrusive phases or variation that may be late or post-magmatic, such as the Sn, W deposits common in Carboniferous peraluminous granites in Nova Scotia (Doyle et al. 1990; Cocksedge et al. 1993). In other particular intrusions, U may provide a pathfinder for molybdenum or other gold-enriched zones. Unusual intrusions such as carbonatites often contain elevated U and/or Th in association with various rare or strategic metals, including Be, Nb, Ta, Ce, La, Y, Zr, Mo, P and others.

2.2 Review of Significant Radiation Hazard

While knowledge about NORM and Technically Enhanced NORM areas has increased substantially over the previous few years estimation of doses in many studies still needs to be improved (Salman and Amany 2008). Estimates of absorbed dose to particular organs for individuals are necessary and can be made from measurements of exposure, air

kerma, or personal dose equivalent. Ansoborlo et al. 2002 have limited its role to assembling the vital scientific information and, in recent years, to estimating the risk coefficients, that is, the increased probability of occurrence of genetic effects or cancer per unit of radiation dose per unit of population. UNSCEAR (2000) does not recommend limits of acceptable dose.

Tomazini da Conceica et al., 2009 have done studies on distribution of ^{226}Ra , ^{232}Th and ^{40}K in soils and sugar cane crops at Corumbatai river basin, Sao Paulo State in Brazil utilizing soil-to-sugar transfer factors to explore potential risk to human health. Phosphate ore used as raw material for fertilizer production is commonly rich in U. Distribution of Ra, Th and K due to phosphate fertilizers and amendments applications comprise an additional source of radiation exposure and may become readily available to plants and be transferred to the human food chain. Geraldo et al. 2010 noted that the most important Brazilian fertilizer industries located near Cubatao River Basin discharged pollutant materials resulting in U accumulation in waters, sediments and soils of the estuarine region of Santos and Sao Vincente. They observed that the presence of U in large scale in these environment compartments can induce an accumulation in living beings and consequently represented a potential radiological hazard to the population of these areas.

The half life (3.82 days) of ^{222}Rn decays allows sufficient time to diffuse from rock and soil to the atmosphere where it decays to ^{210}Po and ^{210}Pb . These radionuclides are no longer in a gaseous form, therefore, come back to the earth's surface by both dry and wet deposition and its existence in all foodstuffs is predictable. ^{210}Po and ^{210}Pb , decay products of the U series, dissolve in water and are primarily transferred into plants and afterward conveyed from plants to human. Ekdal et al., 2006 detected activity concentration of ^{210}Po and ^{210}Pb in soil and vegetable

from Kucuk Menderes basin, one of the most important agricultural regions of Turkey. They concluded that plants may be given radionuclides both by deposition of radioactive fallout and by sorption from the soil. Therefore, a detailed study of ^{210}Po and ^{210}Pb in rock and soil in the environmental samples of a region constitute an important aspect which assumes a special significance in the surroundings. Their results revealed that extensive applications of phosphate fertilizers to soils may slightly increase the activity concentration of ^{210}Po and ^{210}Pb .

The determination of ^{226}Ra , in environmental samples is very significant principally due to its radiotoxicity, it has a long half-life ($T_{1/2} = 1600$ yr) and has been associated to human bones for a long time. It amplifies the risk of cancer. Anthropomorphic enhancements of the NORM, such as discharges from phosphoric factories, increases ^{226}Ra and ^{222}Rn activity concentrations in sediments (Martínez-Aguirre 1996). Although activity concentrations of ^{226}Ra in environmental and geological samples have been usually determined by α - (Crespo 2000) or γ - (Bolívar et al. 1996) spectrometry, these methods have some drawbacks. In the case of γ -spectrometry the results obtained must be properly corrected due to self-absorption effects, and long counting times are needed to obtain adequate limits of detection. On the other hand, radiochemical procedures used for α - spectrometry are tedious and time consuming.

A weak positive correlation of indoor ^{222}Rn with U and ^{222}Rn exhalation rate was observed by Singha (2005). U, however, showed a good correlation with ^{222}Rn exhalation rate in rock and soil. An attempt was also made to study the correlation between the content of U and ^{226}Ra in soil and the indoor ^{222}Rn activity in dwellings. Singha et al. 2005 reported that the annual effective dose in the study area varied from 1.63 to 3.45 mSv y^{-1} with a mean value of 2.62 mSv y^{-1} . Thus the average value of annual effective dose due to ^{222}Rn and its progeny is greater

than the annual external gamma radiation dose (0.3 to 1.0 mSv). From the distribution pattern of annual effective dose it was evident that in about 70% of the dwellings the annual effective dose was less than the lower limit of the recommended level (ICRP 1984) i.e. 0.3–10 mSv y⁻¹. The average value of the lifetime fatality risk of 2.03×10^{-4} (0.02%) is relatively a small fraction (about 4%) of the lifetime risk of lung cancer due to cigarette smoking and chewing of tobacco.

Most of the studies of NORM focus on investigating places of high levels and evaluating exposure of population to radiation from the consumption of water, and correlation between the levels of these radionuclides in water and other parameters, such as geological structure, radioactivity content of underlying bedrock and disequilibria in the uranium series (Ivanov et al. 2009). Several advantages are provided by the new scintillations counters: no self-absorption effects, high efficiency, simultaneous determination of α - and β - emissions and low background.

It has frequently been suggested that the risks of low-level radiation might be determined by studies of people who live in areas of the world in which the radioactive background is elevated above the normal range of values. Such places exist in Sudan (Osman et al. 2008), Nigeria (Oladele 2009; Jibiri et al. 2009), Egypt (Aly Abdo et al. 1999; Harb et al. 2008), Brazil (Malance et al. 1996; Alencar and Freitasn 2005), India (Nair et al. 2009), and Russia (Ivanov et al. 2009). The most meaningful study thus far completed has been in China, where no effects were found in a study of about 80,000 people who have lived for generations in an area in which the soil is enriched in Th, and the average gamma radiation dose is about 3.3 mSv y⁻¹. In fact, cancer mortality adjusted for age was found to be lower among residents of the high-background area than in the control population (NCRP 1993; NRPB 2002). No differences

were found in the prevalence's of genetic disease or congenital defects. The cancer incidence study in Karunagappaly, India, which is a coastal belt of Kerala known for high background radiation (HBR) from Th containing monazite sand concluded no HBR related excess of cancer risk from exposure to terrestrial gamma radiation. This was after following close to 70,000 residents for 10.5 years.

Whicker and McNaughton (2009) conducted a ^{222}Rn survey to compute and document indoor ^{222}Rn levels across a broad spectrum of office type workspaces and neighboring homes. The measured concentrations were compared against those measured across United States and across the world. The results were also compared against a wide variety of radiation protection thresholds such as (1) the action level of 148 Bq m^{-3} (the U.S. EPA action level for public housing), (2) $1,200 \text{ Bq m}^{-3}$ OSHA threshold for office spaces, (3) effective dose threshold of 1 mSv threshold for defining a radiological worker, (50 mSv occupational effective dose limit), and (4) 0.1 mSv and 1 mSv limits for public exposure from the air pathway and all pathways, respectively. They concluded that those who spent more hours at the workplaces received less dose than at their residences.

Beauvias et. Al., 2009 developed a procedural adoption of RESRAD in order to use the code to estimate dose due to chronic exposure to and intake of NORM. The models of radionuclide distribution into plants, livestock, and other sectors of the environment were highly useful in considering the full range of dose pathways for chronic exposures. The dose calculations and estimations made with the procedural adaptation of RESRAD represented the use of hypothetical values of certain hydrological, geological, and site specific parameters considered by RESRAD code. An assumption of secular equilibrium of decay products within a series (U or Th) was made for the calculations they presented. For future site assessments, using the procedural adaptation they

presented, they recommended that it's proper to abandon some assumptions when more information is known about the activity concentrations of the various radionuclides present. The exposure scenarios are used as base generalizations to allow for the hypothetical scenarios for better representation of different segments of the population. Several assumptions regarding the dietary habits of occupants to a site under consideration were factored into the input parameters listed for each of the specified exposure scenarios. It is suggested that when additional information is known about the lifestyle habits of occupants of a site under consideration, the exposure scenarios should be discarded in exchange for the more accurate data available. A resident farmer scenario can be used in the calculation of the estimated TED due to United States national average concentration of enhanced NORM, in particular K, U and Th.

2.3 Studies done in Kenya on Radiological Exposure

McCall (1958) described small and insignificant phosphate occurrences at the Homa Bay carbonatite complex and at the Ruri carbonatite complexes south of the Kavirondo Gulf in western Kenya. He analyzed radioactive iron stone without finding obvious radioactive mineral. He identified monazite and pyrochlore, and it's now known that the former contains principally Th and its radioactive daughters along with several rare earth metals. The Ol Doinyo Lengai volcano, in the Great Rift Valley, Africa, is the world's only active carbonatite volcano. Other older carbonatite volcanoes are located in the same region, including Homa Mountain.

Economically viable concentrations of radionuclides mostly occur in beach placer deposits. Generally coastal regions of various countries are designated as very high background radiation areas (HBRAs) due to

enrichment of radioactive placer deposits. Mrima hills in south coast of Kenya, swaths across the Rift Valley traversing Kenya and Nyanzian belt in Western Kenya have been exploited for commercial deposits of various minerals notably rare earth elements (REE). REE are widely applied in material science research and high technology industries.

Mangala (1987) performed elemental analysis of sediment samples from Mrima hills and found high concentrations of thorium and rare earth metals. Mulaha's (1989) work involved detailed geological mapping, sampling, petrographical work and geochemical analysis of Ndiru Hills an offshoot from Homa Mountain. It showed carbonatites of Ndiru Hills as magmatic in origin, Nyamai (1989) performed petrographic mineralogical and geochemical studies south of the alkaline silicate rocks of Rangwa complex. He added more knowledge of the rock type stretching from Homa Mountain to Ruri Hills and to the Rangwe complex of South Nyanza. Patel (1991) in follow up studies established that the area is composed of weathered carbonatite rock. Some of these areas have been evacuated so that mineral prospecting firms e.g. Tiomin, can mine, while others have been taken by electricity generating power companies for geothermal energy production (Personal Communication with Riario 2007) and others are under study to determine the risks and effects of long term, low level natural radiation exposure (Otwoma 1999) and geochemical study of REE (Ohde 2004).

Th bearing minerals are found in igneous complexes, mainly associated with the granites, syenites and pegmatite of all ages, however, the main source base is confined to beach and inland placer deposits. Beach placer deposits occur at several places along both the north and south coasts of Kenya. There are areas with appreciable concentrations of inland placers containing monazites: Ruri hills, Homa Mountain, on the south coast of Lake Victoria where Japanese exploration companies were

looking for REE and niobium (Ohde 2004). They found only small amounts of these elements and very low-grade phosphates in the primary and weathered rocks. Jombo and Mrima hills on the south coast of Kenya are such areas. These are associated with mainly carbonatite complexes, conglomerates, sandstones, granites, syenites and pegmatites as reported by Mangala (1987), Patel (1991) and Mustapha (1999). Homa Mountain geothermal prospects was not an earlier area ranked for geothermal potential, but with the need to develop electricity for small scale use, Homa Mountain has now been targeted for investigation for electricity generation for direct utilization (Personal Communication with Riario 2007).

Otwoma (1998) extensively tested drinking water, and Mustpaha (1999 to 2002) performed measurements in building materials from soils and rock, establishing presence of elevated levels of radioactivity across seven provinces in Kenya. Against a background of increasing concern over the health risks associated with exposure to natural sources of radiation, Mustapha et al., 1997 measured in Kenya, the activity concentrations of the major radionuclides in some natural building materials and from different types of rock and soil samples analyzing them with a gamma ray spectrometer. The external gamma ray absorbed doses in indoor air, and the corresponding effective dose equivalents in a typical dwelling were presented. Exposures to various components of the natural background radiation in Kenya were estimated using measured activity concentrations of natural radionuclides and dose conversion factors. Ranges of; 50 to 1500 Bq kg⁻¹ for ⁴⁰K; 5 to 200 Bq kg⁻¹ for ²²⁶Ra; and 5 to 300 Bq kg⁻¹ for ²³²Th were encountered. Contributions to the total effective dose included: 0.1 to 2.0 mSv y⁻¹ from terrestrial gamma radiation; 0.2 to 0.7 mSv y⁻¹ and a *per capita* of 0.4 mSv.y⁻¹ from cosmic radiation; and 0.4 to 6.0 mSv y⁻¹ from inhalation of ²²²Rn. ²²²Rn concentrations ranged from 5 to 1200 Bq.m⁻³ in indoor air and from 1 to

410 Bq L⁻¹ in drinking water. Considering the population distribution in relation to living habits of the people and to the relief and the geology in Kenya, it was concluded that the average annual effective dose in Kenya was higher than the global average. Ingestion of volcanic ash by some people, particularly pregnant women, was also identified as a supplementary (unusual) internal exposure pathway.

Mustapha et al., 2002 did a screening survey to determine activity concentrations of ²²²Rn in drinking water and indoor air in various locations in Kenya. The concentration of ²²²Rn in water was measured using a liquid scintillation counter (LSC). Three different passive integrating devices were used in the measurements of ²²²Rn in air. In the short-term measurements, ²²²Rn was absorbed in activated charcoal and analysis was carried out using either LSC or gamma ray spectrometry. The long-term measurements were carried out using solid-state nuclear track detectors (SSNTD). The mean and maximum values of ²²²Rn concentrations in water were 37 and 410 Bq L⁻¹ and 100 and 1160 Bq m⁻³, respectively, in air. The highest values were obtained from groundwater sources and in the basements of buildings. When these values are compared with the internationally recommended reference levels, there were implications of existence of ²²²Rn problems in some of the water sources and the dwellings tested in the survey.

Hashim et al., 2004 measured samples of sediments from selected areas of Kenya coast. He obtained effective dose rates varying widely from 0.01 to 0.2 mSv y⁻¹ which were all below ICRP (1991) limit. The main sources of the abnormal levels of radiation were attributed to the presence of Th rich monazites and pyrochlore in the carbonatite rocks. NORM were estimated to result to an average annual effective dose of 3.9 mSv y⁻¹. At the Buru hill carbonatite, east of Kisumu, Japanese exploration companies were looking for REE and Niobium. Ohde (2004) used

instrumental neutron activation analysis to determine twenty eight elements including rare earth elements from samples of carbonatite rocks from Homa Mountain. They found only small amounts of these elements and very low-grade phosphates in the primary and weathered rocks. Follow-up work by Finnish and Kenyan geologists indicated low and sporadic concentrations of apatite in parts of these carbonatite complexes. In addition, grade and volume are too low to be of any economic interest, even from a small-scale mining point of view.

Le Bas (1977) explained the volcanic development of Homa Mountain in four stages of carbonatite intrusion from 8 Ma (10^6 years) to 2 Ma (250,000 years). Carbonatites are comparatively rare and small in volume compared to marine limestones, and they are important for monitoring the chemical evolution of the upper mantle. They are stable mantle fluids responsible for transporting volatiles and trace elements (B, Sn, Li, Rb, Sc and rare earth elements) in the upper mantle. Carbonatites are commercially exploitable sources of niobium, light REEs and Th. The carbonatite cone-sheet complex of Homa Mountain farther east is associated with earlier ijolite and fenites; after a period of erosion, igneous activity was resumed with the eruption of vents of phonolitic nephelinite, melilitite and carbonatite.

2.4 Statement of Research Problem

Although current radiation protection standards for the public are generally judged to be acceptably robust, there lingers a considerable scientific uncertainty with regard to dose and health risk assessments. Some of these uncertainties originate from the exposure assessment, which is largely dependent on knowledge of the behavior of natural and artificial radionuclides in the environment. The acquisition of new scientific knowledge through research in radioecology is therefore a

crucial element in improving the public's protection. The need for a system to protect the environment from ionizing radiation has, over the past decade, been recognized internationally.

While radiation levels from man-made radiation sources and associated risks have been thoroughly studied and regulated through a single Government agency (Kenya Government 1982), less attention has been paid to the measurement and regulatory control of NORM both in homes and the environment. Existing exposure situations include naturally occurring exposures as well as exposures from past events and accidents, and practices conducted outside the recommendations of ICRP (2007). Human settlements continue to increase with rise in population and areas previously not occupied are now accommodating people. Local land use includes building of houses and using the land for among other farming. According to international recommendations, the Basic Safety Series 115 (IAEA 1996), the use of building materials for human habitation containing enhanced concentrations of NORM should be controlled and restricted under application of radiation safety standards.

2.5 Objective of Research

Carbonatite rock intrusions found in various parts of the world have been associated with high concentrations of ^{40}K , ^{232}Th and ^{238}U radionuclides. These radionuclides are a natural source of radiation exposure. Data on population and health effects when living in high background radiation areas is not conclusive despite various studies done in several parts of the world. Such studies have not been addressed adequately in Kenya. The main purpose of the investigation was to study the radioecology, environmental and dosimetric impacts of the carbonatite deposits in the Homa Mountain region in South Nyanza so as to produce a record on NORM and probable exposure of the human

population. The objective of this study was focused on determining the activity concentrations of ^{238}U , ^{226}Ra , ^{232}Th and ^{40}K in rock and soil samples collected from different locations of Homa mountain and estimate dose due to NORM inhabitants are exposed to using Dose Conversion Factors, calculations and the RESRAD code.

The specific objectives were to:

1. record the surface distribution of gamma radiation dose rate in Homa Mountain area;
2. measure the concentrations of ^{238}U , ^{226}Ra , ^{232}Th and ^{40}K radionuclides in rock and soil samples;
3. determine external exposure of people to terrestrial gamma rays from the primordial radionuclides in the ground;
4. model the dose rate from activity concentrations in using assumed lifestyle declarations for various exposure scenarios; and,
5. examine and identify any new natural radiation exposure pathways as well as any critical populations or groups.

2.6 Rationale of Research

The magnitude of the effective dose rates that result from NORM both in homes and the environment, presents an interesting opportunity to contrast effective dose rates from NORM exposure with regulatory limits, both public and occupational. The measurement of activity or activity

concentration levels in NORM materials can often be very difficult due to the fact that many radionuclides are part of long radioactive decay chains. The data collected and used to assess exposure from NORM will be beneficial to, among others:

- The regulatory authorities, in the current set up being the Radiation Protection Board and National Environmental Management Authority, can identify non man made exposure scenarios due to NORM or technically enhanced NORM that may require controls. The application of dose constraints or reference levels as part of the optimization process is required and the results of this research will allow visualization of various exposure scenario.
- The data of concentrations of NORM will act as baseline data for drawing a radiological map of the Homa Mt. area. Any future technically enhanced NORM from industrial activities and/or contamination of the environment will enable assessment of increased radiation exposure and confirmation of significant health hazard accompanying the practice(s).
- Accurate background radiation dose assessment for areas yet unaffected by mining is necessary because of potential environmental impacts when mining commences and/or nuclear power plants are built.
- When modeling exposure pathways there are lots of assumptions made which cover a wide variety of situations. Information about high background radiation areas will provide a record that may be applied as guidelines than can be used for epidemiological studies on the effects of radiation exposure to human population.

Chapter 3

THEORETICAL BACKGROUND

3.1. Theory of Radioecology Assessment of Naturally Occurring Radioactive Materials

The naturally occurring radioisotopes, which produce the radiation fields, are associated predominantly with the elements of Uranium (U), Thorium (Th) and Potassium (K). In the case of U and Th, particular parent radioisotopes (^{238}U , ^{235}U and ^{232}Th) undergo radioactive decay and generate daughter radioisotopes. Their 'daughters' are the radioisotopes which emit γ rays producing the measurable radiation fields. The radioactive decays of the parent radioisotopes U and Th are multistage processes in which the unstable 'daughters' that are produced, in turn, become 'parents'. The decay process of each parent radioisotope eventually terminates with the production of a stable isotope of lead (Pb). Annex C shows the decay chains of ^{40}K , ^{87}Rb , ^{235}U , ^{238}U and ^{232}Th .

Direct measurement of the radiation emitted or calculation can provide levels of exposure a particular individual receives from natural occurring radioactive materials (NORM). Radioecological assessment models are necessary tools for estimating the radiation exposure of humans and non-human biota. While such an approach may be appropriate and sufficient for demonstrating compliance with dose limits, for other applications, radiation exposure may need to be estimated as realistically as possible and with a high degree of reliability. Gamma-Ray Spectrometry (GRS) provides a direct measurement of the surface of the earth, with no significant depth of penetration. This at-surface characteristic allows us to reliably relate the measured radioelement contrasts to mapped bedrock and surface geology, and alteration associated with mineral deposits. All rocks, and materials derived from

them especially soil are radioactive, containing detectable amounts of a variety of radioactive elements. Methods for derivation of gamma dose rate in air from an in situ gamma ray spectra, both spectrum stripping and peak area are in use.

Model calculation may provide estimations of the level of exposure experienced by a population or by an average individual in the population. Dosimetric models are used to link measurable radiation quantities, such as flux density or fluence, with dosimetric quantities like kerma (kinetic energy released in matter) or absorbed dose.

3.2 DOSIMETRIC RADIATION QUANTITIES AND UNITS

3.2.1 Absorbed dose and Absorbed Dose Rate

The ICRP (1984, 1995 and 2007), ISO (1993 and 2000) and IAEA (2004) set of definitions for the quantities and units to be used for radiation dose measurements are used. Absorbed dose, D , is a statement of the amount of energy absorbed per unit mass of an irradiated material, formal definition is:

$$D = \frac{d\varepsilon}{dm} \quad 3.1$$

where $d\varepsilon$ is the mean energy imparted by ionizing radiation to matter of mass dm . Absorbed dose is a point function and is continuous and differentiable and one may refer to its gradient and its rate. The unit of absorbed dose is $J. kg^{-1}$ and the special name is gray (Gy). "Radiation dose" is defined here as the effective dose equivalent (EDE) from external radiation and the committed effective dose equivalent (CEDE) from internal radiation (ICRP 1984). "Total dose" is the sum of the external radiation EDE and the internal radiations CEDE and are referred to as

the total effective dose equivalent (TEDE). The absorbed dose rate, D_R , is defined by:-

$$D_R = \frac{dD}{dt} \quad 3.2$$

Where dD is the absorbed dose and dt is time. The unit for absorbed dose rate is $J. kg^{-1}. s^{-1}$.

3.2.2 Gamma Dose Rate determination by the 'spectrum stripping' method

A count registered by the Sodium Iodide [NaI(Tl)] and/or Germanium (HpGe) detector can be caused by the full or partial absorption of an incident photon or by the passage of a cosmic ray producing a charged particle. In order to convert to gamma dose rate the spectrum must be stripped from the partial absorption and cosmic ray events leaving only the events corresponding to the full absorption of a gamma ray. Hence the contribution of every radionuclide to the total dose rate is not possible. However, knowledge of the detector's geometry is required while the source geometry is not needed. Using manufactures data as input we tried to reproduce by simulation the measured spectra obtained with ^{137}Cs , ^{60}Co , ^{133}Ba and ^{131}I point sources.

The ^{131}I point source, with an activity of 1.85 MBq has been used for the experimental determination of the detector efficiency. The source was placed several meters from the detector and a spectrum was taken. A shield sufficient to stop essentially all primary gamma rays from the source was then interposed so as to geometrically shadow the detector from the source, and a spectrum was taken and subtracted from the original. In this manner, scattered radiation from the rooms walls floor

and ceiling as well as any background radiation is canceled out leaving a spectrum that represents the direct parallel flux from the source. This flux is simply given by the relation by Clouvas (2010) as:

$$\varphi = \frac{S \cdot e^{-\mu r}}{4\pi \cdot r^2} \quad 3.3$$

where

φ = unscattered flux incident to the detector ($\gamma \text{ cm}^{-2}\text{s}^{-1}$)

S = intensity of the source ($\gamma \text{ s}^{-1}$)

r = distance between source and the detector (cm)

μ = attenuation coefficient in air for the specific energy

Point-kernel method is macroscopic approach used for gamma radiation exposure rate calculations. Within this approach gamma radiation propagation is assumed beam-like. Effects of radiation interaction in matter are described using macroscopic linear attenuation factors. Consistent scattered radiation accounting could not achieved within macroscopic approach. The events corresponding to fractional absorption in the detector are determined by Monte Carlo simulations for different incident photon energies and angles. The spectrum is first stripped of the partial absorption and cosmic-ray events leaving only the events corresponding to the full absorption of a gamma ray. Applying to the resulting spectrum the full absorption efficiency curve of the detector determined by calibrated point sources and Monte Carlo simulations using Eq.3.2, the photon flux energy distribution as deduced by Clouvas et al., 2010 was obtained.

$$\varphi = -S \cdot \frac{\int_0^1 \frac{e^{\left(\frac{\mu}{\rho}\delta\right)\frac{h}{\omega}} [e^{-\left(\frac{\mu}{\rho}\delta\right)\frac{z}{\omega}} - 1]}{\frac{\mu}{\rho}} d\omega}{2\rho} \quad 3.2$$

Where

S: intensity of the source in photons/cm³ s

Z: depth till the source is distributed

ω : $\cos \theta$

δ : air density

ρ : soil density

$\frac{\mu}{\rho}$: mass attenuation coefficient in soil

h: detectors distance from soil

According to the main idea of point-kernel method radiation source volume is cut up into elementary cells (point kernels). Each point kernel gives contribution to the dose rate at the detecting point for radiation energy E. Knowing the computed shapes of partial absorption continuum deduced by the Monte Carlo simulation for different incident photon energies and angles, it is therefore feasible to convert the measured in-situ spectra to total incident flux spectra by applying the full absorption efficiency curve of the detector, which is determined by calibrated point sources and Monte Carlo simulations. Good simulated spectra must not only predict the experimental full absorption peak count rate (efficiency of the detector) but also the partial absorption of photons in the detector, in other words the shape of the continuum. Having calculated the flux energy distribution, the absorbed dose rate in air due to gamma radiation is straightforwardly as done by Clouvas et al., 2010 from Eq 3.4.

$$D_R = \sum_{E=0}^{E=E_{max}} \phi(E) \cdot E \cdot \frac{\mu_a}{\rho}(E) \quad 3.4$$

3.2.3 Gamma Dose Rate Determination by “Peak Area Method”

This method for deriving simple calibration factors (for the outdoor measurements) which convert the measured full absorption peak count rate to activity in the soil and dose rate in air is explained by Takoudis (2010). The only parameters that are needed are the efficiency and the crystal dimensions of the NaI(Tl) and/or HpGe detector used. This can be adopted and modified the technique for measurements in an indoor environment and particularly in case of masonry structure. The contribution of each radionuclide to the total dose rate is possible to deduce. The detector's geometry knowledge is not needed while the source geometry is required. The procedure starts with the measurement of an indoor or outdoor gamma spectrum. What is directly deduced by the in situ gamma spectrometry measurement is the number N of counts in each photopeak per unit of time (in counts per minute). The main problem point-kernel method encounters is account for scattered radiation which is usually implemented through semi-empirical approximation. Additional "build-up" factor must be introduced as a multiplier to the attenuated dose. Determination of the appropriate build-up factor can be rather complex as it depends upon the energy, the thickness and type of material. Uncertainties in determining build-up factor essentially limit the accuracy of point-kernel method.

For 4π geometry the buildup factor does not depend strongly on parameters such as: (a) dimensions of the rooms, (b) the thickness of walls, (c) the density of the building materials, and (d) the gamma source geometry. If only approximate results are desired it is possible to use those factors derived for half-space geometry also for the indoor environment. In the case of a masonry structure this approach is adequate, due to the fact that the ratio of primary to scattered flux is

approximately the same for the two environments. Total gamma dose rates can be directly deduced from in situ gamma spectra using a “spectral stripping method” which does not require any assumptions concerning the source geometry as shown in Fig 3.1.

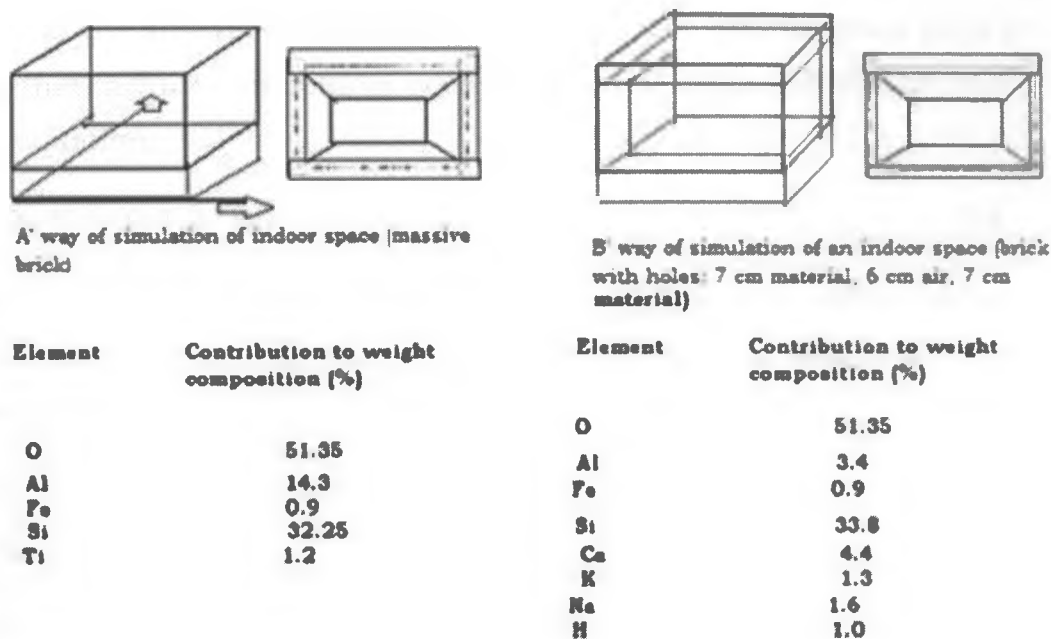


Fig. 3.1 Schematics of a 4π Geometry (Clouvas et al. 2010)

3.3. THEORY OF DIFFERENT RADIATION INDICES

3.3.1. Absorbed dose rate

The absorbed dose rate in outdoor air, D_R (nGy h^{-1}), at about 1 m (average gonad height) above the surface of the ground were calculated by Chowdhury et al. (2005), Al-Saleh and Al-Berzan (2007), Harb et al. (2008), Viruthagiri and Ponnarasi (2011), Alharbi et al. (2011) and Gbadago et al. (2011) using:

$$D_R = 0.043C_K + 0.427C_{Ra} + 0.666C_{Th} \quad 3.5$$

Where C_K , C_{Ra} and C_{Th} are the activity concentrations ($Bq\ kg^{-1}$) of ^{40}K , ^{226}Ra and ^{232}Th , respectively in the samples.

3.3.2. Annual outdoor effective dose equivalent

The annual outdoor effective dose equivalent was calculated for each sample using the conversion factor of $0.7 \times 10^{-6}\ mSv\ nGy^{-1}$ that translates the absorbed dose rate ($nGy\ h^{-1}$) in air to effective dose ($mSv\ y^{-1}$) and that includes an outdoor occupancy factor of 0.2 (UNSCEAR 2000) using equation:

$$H_R = D_R N_h \times 0.7\ Sv\ Gy^{-1} \times 0.2 \quad 3.6$$

where D_R is the absorbed dose rates in air ($nG\ h^{-1}$) and N_H ($=8766\ h$) is the number of hours in 1 year ($= 365.25$ days taking the leap year into account).

3.3.3. Radium equivalent activity

In calculating the absorbed dose rates in air, a homogeneous distribution of natural radionuclide in the rock and soils being investigated was implicit. In reality, however, the distribution is not uniform. Therefore, a common radiological index that can be used to assess the real activity level of ^{40}K , ^{226}Ra and ^{232}Th in the soil sample is required. This common radiological index, called the radium equivalent activity Ra_{eq} , provides a very useful guideline in regulating the safety standard in radiation protection for human population. The index was calculated by Chowdhury et al. (2005), Al-Saleh and Al-Berzan (2007), Harb et al. (2008), Viruthagiri and Ponnarasi (2011), Alharbi et al. (2011) and Gbadago et al. (2011) according to:

$$Ra_{eq} = C_{Ra} + 1.429C_{Th} + 0.077C_K \quad 3.7$$

where C_{Ra} , C_{Th} and C_K are the activity concentrations ($Bq\ kg^{-1}$) of ^{40}K , ^{226}Ra and ^{232}Th , respectively, in the samples. The formula is based on the assumption that $37\ Bq\ kg^{-1}$ of ^{226}Ra , $25.9\ Bq\ kg^{-1}$ of ^{232}Th and $481\ Bq\ kg^{-1}$ of ^{40}K produce the same gamma ray dose rate. A value of $370\ Bq\ kg^{-1}$ corresponds to $1\ mSv\ y^{-1}$.

3.3.4. Representative level index

The representative level index I_{γ} of a construction material is used to estimate the level of the gamma radiation hazard associated with natural gamma emitter in the material. It was calculated by Chowdhury et al. (2005), Al-Saleh and Al-Berzan (2007), Harb et al. (2008), Viruthagiri and Ponnarasi (2011) and Alharbi et al. (2011) using Eq:

$$I_{\gamma} = \frac{C_{Ra}}{150} + \frac{C_{Th}}{100} + \frac{C_K}{1500} \leq 1 \quad 3.8$$

where C_{Ra} , C_{Th} and C_K are activity concentrations ($Bq\ kg^{-1}$) of ^{226}Ra , ^{232}Th and ^{40}K , respectively, in the samples.

3.3.5. Gamma activity index

The gamma activity index I as proposed is one of the health indices dealing with assessment of the excess external and indoor gamma radiation from building materials. In the present work, the relation given by EC (1999) is used as Eq:

$$I = \frac{C_{Ra}}{300} + \frac{C_{Th}}{200} + \frac{C_K}{3000} \leq 1 \quad 3.9$$

where C_{Ra} , C_{Th} and C_K are activity concentrations ($Bq\ kg^{-1}$) of ^{226}Ra , ^{232}Th and ^{40}K , respectively, in the samples.

A value of 0.5 or less for I corresponds to an effective dose equivalent rate of $\geq 0.3 \text{ mSv y}^{-1}$, while a value of 1 or less for I corresponds to a dose rate of 1.0 mSv y^{-1} .

3.3.6. External hazard index

Safety requirements are issued by different countries to limit the radiation exposure caused by the use of building materials containing elevated concentrations of natural radionuclides. This has given rise to different models based on different criteria. The model used by Chowdhury et al. (2005), Harb et al. (2008) and Alharbi et al. (2011) is based on a criterion called external hazard index (H_{ex}) as shown below:

$$H_{\text{ex}} = \frac{C_{\text{Ra}}}{370} + \frac{C_{\text{Th}}}{259} + \frac{C_{\text{K}}}{4810} \quad 3.10$$

where C_{Ra} , C_{Th} and C_{K} are activity concentrations (Bq kg^{-1}) of ^{226}Ra , ^{232}Th and ^{40}K , respectively, in the samples.

H_{ex} is a criterion of the model proposed to limit the radiation exposure attributable to NORM in building materials to 1.5 mSv y^{-1} .

3.3.7. Internal hazard index

To reduce the acceptable maximum activity concentration of ^{226}Ra to half the normal limit, has been recently used by Chowdhury et al. (2005), Harb et al. (2008) and Alharbi et al. (2011) as another criterion called internal hazard index (H_{in}). This criterion is defined as:

$$H_{\text{in}} = \frac{C_{\text{Ra}}}{185} + \frac{C_{\text{Th}}}{259} + \frac{C_{\text{K}}}{4810} \quad 3.11$$

where C_{Ra} , C_{Th} and C_{K} are activity concentrations (Bq kg^{-1}) of ^{226}Ra , ^{232}Th and ^{40}K , respectively, in the samples. For unrestricted use of building raw materials in construction, H_{in} should be less than 1.0.

3.4. BACKGROUND INFORMATION ON RESRAD

RESRAD (Yu et al. 2001) computer code was used for biosphere modeling and dose computation. RESidual RADioactive materials aka RESRAD was developed by the Environmental Assessment Division at Argonne National Laboratory as a tool to aid in the development of cleanup criteria for residual radioactive materials, but it is also used to conduct site-specific dose assessment for observed and measured radionuclide concentrations. RESRAD is a free, publicly available code with extensive benchmarking of its dose computation and environmental models, and has become an industry standard for residual radioactivity modeling. Accurate baseline radiation dose assessment for areas yet unaffected by mining is necessary because of potential environmental impacts when mining commences and/or nuclear power plants are built. In this research a novel use of RESRAD for calculation of dose from non-enhanced NORM is presented. In order to use RESRAD to calculate the total effective dose (TED) due to NORM, a procedural adaptation was developed to negate the time progressive distribution of radioactive materials

Detailed discussions of the exposure pathways are considered in the RESRAD code. For calculation of effective dose due to background NORM at a given site, it is essential to accurately model the distribution of radioactive materials throughout the site. NORM radionuclides in a decay series ought to be, or nearly in, secular equilibrium with the head of the series. This was the assumption for most hypothetical situations calculated and considered for this research. RESRAD allows the user to input radionuclide concentrations in rock, soil and water reflecting this assumption and consequently carries the concentrations reflective of secular equilibrium, through its environmental distribution models.

RESRAD dose estimations are accounted by contributing pathway and by radionuclide, allowing straightforward manipulation and analysis. These exposure pathways are illustrated in Figure 3.2.

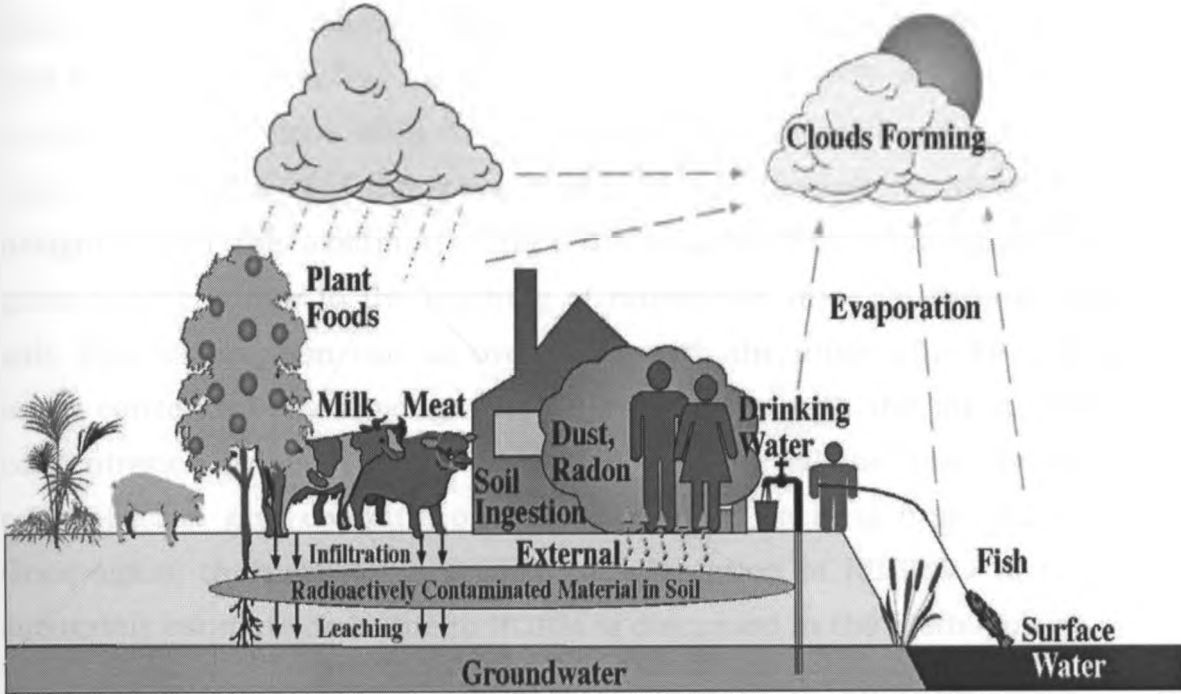


Fig 3.2 Exposure Pathways Considered in RESRAD (Yu et al. 2001)

Other major improvements to the RESRAD code include its ability to run uncertainty analyses, additional options for graphical and text output, a better dose conversion factor editor, updated databases, a better groundwater transport model for long decay chains, an external ground radiation pathway model, an inhalation area factor model, time-integration of dose and risk, and a better graphical user interface.

In order to directly enter a radionuclide water concentration in RESRAD, the user must specify a 'Time Since Material Placement' (TP). Since RESRAD is primarily used to model the movement of radioactive materials following a spill, leak, or artificial placement, the use of a TP stands to reason. However, with respect to NORM and the general assumption of time constant concentration, a TP cannot be determined and has no true meaning. Additionally, ^{40}K , ^{238}U and ^{232}Th are primordial in origin and the time since their placement into the environment is not relevant and outside of the scope of possibility for modeling. RESRAD is designed with the assumption that the radionuclide concentration in groundwater is due to the leaching of radioactive material through the soil. This assumption can be overridden with the input of a TP and a water concentration, although the TP must agree with the input water concentration or else the code is designed to prevail the user specified concentration and compute one based on the leaching from the soil. Once again, the need for a procedural adaptation of RESRAD to more accurately estimate dose due to NORM is discussed in the methodology.

The pathway analysis for deriving soil concentration guidelines from a dose limit has four parts as shown in Fig 3.3 representing briefly (1) source analysis, (2) environmental transport analysis, (3) dose/exposure analysis, and (4) scenario analysis.

Source analysis addresses the problem of deriving the source terms that determine the rate at which residual radioactivity is released into the environment. This rate is determined by the geometry of the contaminated zone, the concentrations of the radionuclides present, the in growth and decay rates of the radionuclides and the removal rate by erosion and leaching. The radiation dose calculated by RESRAD for a given site is organized in the output by the pathway in which it is

received. The results presented in this thesis reflect this by separating the annual TED into its respective contributions for each radionuclide and pathway. Pathways are further separated into water independent pathways, for which the dose depends upon the soil radionuclide concentrations, and water dependent pathways, for which the dose depends upon the radionuclide concentration in groundwater.

The water independent pathways are as follows: 'Ground,' the dose due to external exposure ; 'Inhalation,' the dose due to non radon inhalation of particulates; 'Radon,' the dose due to the inhalation of terrestrial radon; 'Plant,' the dose due to ingestion of vegetables grown in radioactive soil; 'Meat,' the dose due to ingestion of meat contaminated with radioactive materials; 'Milk,' the dose due to ingestion of milk contaminated with radioactive materials; and 'Soil,' the dose due to inadvertent ingestion of soil containing radionuclides.

The water dependent pathways are as follows: 'Water,' the dose due to ingestion of water containing radionuclides; 'Fish,' the dose due to ingestion of aquatic animals containing radionuclides; 'Radon,' the dose due to inhalation of radon released from water sources; 'plant,' the dose due to ingestion of vegetables grown with water containing the radionuclides; 'Meat,' the dose due to the ingestion of meat from animals that drank water contaminated with radionuclides; and 'milk,' the dose due to the ingestion of milk from animals that drank water contaminated with radionuclides.

RESRAD modeled the movement of NORM into food sources through soil and water, into homes through radon exhalation, and into each of the multiple pathways considered by RESRAD. Since the times required for uniform distribution of radioactive materials into food sources and the

clearance rates of air within a home are short relative to the time that the site has been with NORM those models hold. Related to the assumption of secular equilibrium, it is assumed that the concentrations of background NORM are constant for a specific site.

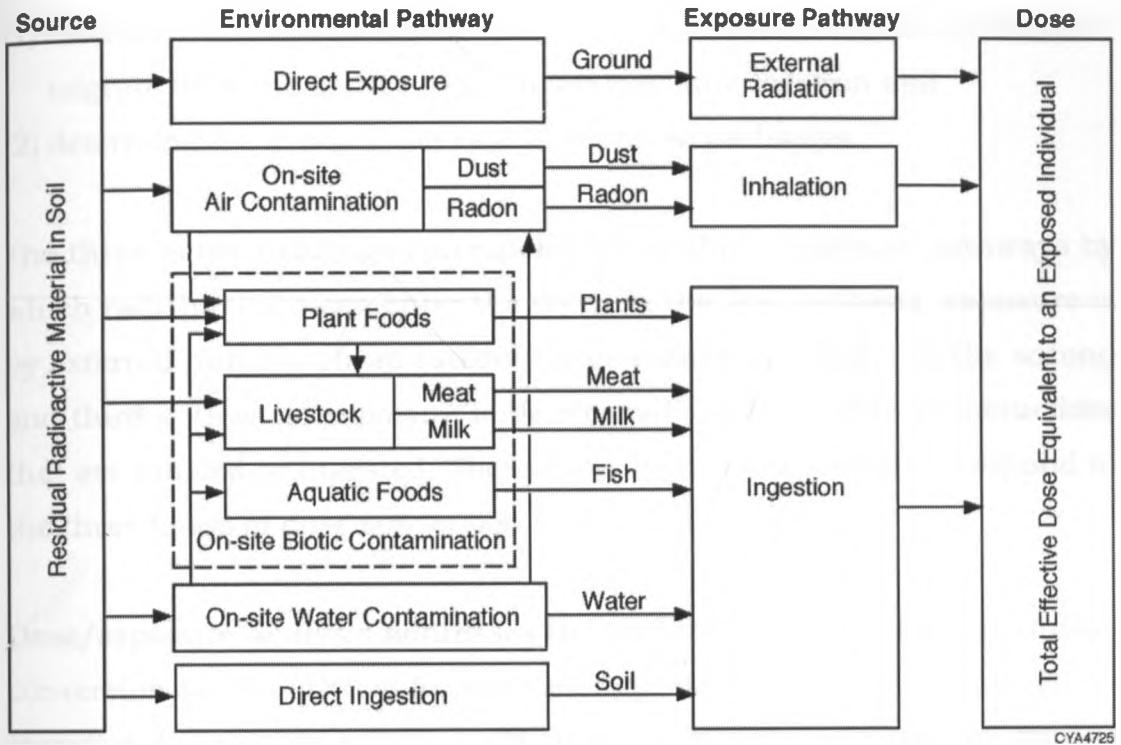


Fig 3.3 Schematic Representation of RESRAD Pathways (Yu et al. 2001)

The TED calculated by RESRAD reflects a time integration of dose over a one year period in which RESRAD models the movement and decay of radionuclides present. Thus, under the default procedure, the TED calculated by RESRAD reflects a variable concentration in violation of the assumption for ancient NORM. In order to more accurately calculate the dose due to constant a constant concentration of radioactive material,

which is the case of NORM, a procedural adaptation of RESRAD is required.

Environmental transport analysis addresses the problems of

- (1) Identifying environmental pathways by which radionuclides can migrate from the source to a human exposure location and
- (2) determining the migration rate along these pathways.

The three major headings correspond to the three exposure pathways by which radionuclides can enter the body. In the first pathway, exposure is by external radiation from radionuclides outside the body. In the second and third pathways, exposure is by internal radiation from radionuclides that are inhaled or ingested. These three types of exposure correspond to the three kinds of dose conversion factors

Dose/exposure analysis addresses the problem of the derivation of dose conversion factors (DCFs) for the radiation dose that will be incurred by exposure to ionizing radiation. The parameters that control the rate of radionuclide release into the environment and the severity and duration of human exposure at a given location are determined by patterns of human activity referred to as exposure scenarios.

In general, the radiation dose resulting from these secondary sources is minimal compared with the dose resulting from direct exposure to the primary source. The contribution to the effective dose equivalent (EDE) from the external ground radiation pathway for the i th principal radionuclide at time t following the radiological survey is given by the dose/source ratio $DSR_{i1}(t)$. This dose/source ratio may be expressed as the sum of the products of the dose conversion factor (DCF_{ij}), the

environmental transport factor (ETF_{j1}), branching factor (BRF_{ij}), and the source factor (SF_{ij}) from each decay product (j) of the principal radionuclide (i).

The dose conversion factor DCF_{i1} for the external ground radiation pathway is the annual EDE received from exposure to radiation from the i th principal radionuclide present at the unit concentration in a uniformly contaminated zone of infinite depth and lateral extent. The dose is calculated at a distance of 1 m above the ground surface.

The environmental transport factor ETF_{i1} for the external ground radiation pathway is the ratio of the EDE for the actual source to the EDE for the standard source, multiplied by an occupancy and shielding factor.

To further extend this model for actual geometries (i.e., finite irregular areas), an area-and-shape factor was derived by using the point-kernel method. The ETF at time, t , for the external ground radiation pathway is expressed as the product

$$ETF_{i1}(t) = FO_1 \times FS_{i1}(t) \times FA_{i1}(t) \times FCD_{i1}(t) \quad 3.12$$

where

FO_1 = occupancy and shielding factor (dimensionless),

$FS_{i1}(t)$ = shape factor (dimensionless),

$FA_{i1}(t)$ = nuclide-specific area factor (dimensionless), and

$FCD_{i1}(t)$ = depth-and-cover factor (dimensionless).

The occupancy and shielding factor accounts for the fraction of a year that an individual is located on site and the reduction in the external

exposure rate afforded by on-site buildings or other structures while the individual is indoors. It is expressed as

$$FO_1 = f_{otd} + (f_{ind} \times F_{sh}), \quad 3.13$$

Where

f_{otd} = fraction of a year spent outdoors, on site (0.25, dimensionless);

f_{ind} = fraction of a year spent indoors, on site (0.50 dimensionless); and

F_{sh} = indoor shielding factor for external gamma (0.7, dimensionless).

The depth factor (FD_{i1}) is based on the regression analysis of the Eckerman and Ryman (1993) dose conversion factors (DCF_i^{FGR}) as a function of depth to the following function:

$$FD_{i1} = \frac{DCF_i^{FGR} [T_s = T(t)]}{DCF_i^{FGR} (T_s = \infty)} = 1 - A_i e^{-100KA_{ipb}^{cz} T(t)} - B_i e^{-100KB_{ipb}^{cz} T(t)} \quad 3.14$$

Where

$DCF_i^{FGR} [T_s = T(t)]$ = Eckerman and Ryman (1993) DCFs with different source contamination depths,

$T(t)$ = thickness of contaminated zone at time t (m),

ρ_b^{cz} = bulk density of soil material in the contaminated zone (g/cm^3),

A_i, B_i = fit parameters (dimensionless), and

KA_i, KB_i = fit parameters (cm^2/g).

The four unknown parameters (A_i, B_i, KA_i , and KB_i) were determined for all radionuclides in the RESRAD database.

Erosion rates for both the cover and the contaminated zone may be estimated by means of the Universal Soil Loss Equation, an empirical model that has been developed for predicting the rate of soil loss by sheet and rill erosion (Yu et al. 2001). If sufficient site-specific data are available, a sites specific erosion rate can be calculated. Estimates based on the range of erosion rates for typical sites in humid areas east of the Mississippi River (based on model site calculations for locations in New York, New Jersey, Ohio, and Missouri) were used. For a site with a 2% slope, these model calculations predict a range of 8×10^{-7} to 3×10^{-6} m/yr for natural succession vegetation, 1×10^{-5} to 6×10^{-5} m/yr for permanent pasture, and 9×10^{-5} to 6×10^{-4} m/yr for row-crop agriculture. The rate increases by a factor of about 3 for a 5% slope, 7 for a 10% slope, and 15 for a 15% slope. If these generic values are used for a resident farmer scenario in which the dose contribution from food ingestion pathways is expected to be significant, an erosion rate of 0.06 cm/yr should be assumed for a site with a 2% slope. This would lead to erosion of 0.6 m of soil in 1,000 years. The time dependence of the contaminated zone thickness is given by

$$\begin{aligned}
 T(t) &= T(0), \quad 0 \leq t \leq t_c \\
 &= T(0) - V^{(cz)}(t - t_c), \quad t_c < t,
 \end{aligned}
 \tag{3.15}$$

Where

$T(t)$ = thickness of the contaminated zone at time t (m)

$T(0)$ = initial thickness of the contaminated zone (2 m),

$t_c = C_d(0)/V^{(cv)}$ = time for the cover to be removed by erosion (yr),
and

$V^{(cv)}$ = erosion rate of cover material (0.001 m/yr).

The following depth and cover factor (FCD_{i1}) was derived on the basis of depth factor function, by considering both dose contribution and attenuation from different depths:

$$FCD_{i1} = \frac{DCF_i^{FGR} [T_c = C_d(t), T_s = T(t)]}{DCF_i^{FGR} (T_c = T_s = \infty)} \quad 3.16$$

$$= A_i e^{-100KA_{ipb}^{cv} C_d^{(t)}} \left(1 - e^{-100KA_{ipb}^{cz} T(t)}\right) + b_i e^{-100KB_{ipb}^{cv} C_d^{(t)}} \left(1 - e^{-100KB_{ipb}^{cz} T(t)}\right)$$

Where

$C_c(t)$ = cover depth at time t (m),

ρ_b^{cv} = bulk density of cover material (g/cm^3),

$T(t)$ = thickness of contaminated zone at time t (m), and

ρ_b^{cz} = bulk density of contaminated zone at time t (g/cm^3).

The time dependence of the cover depth is given by

$$C_d(t) = C_d(0) - V^{(cv)} t, \quad 0 \leq t < t_c,$$

Where

$C_d(t)$ = cover depth at time t (m).

$C_d(0)$ = initial cover depth (0 m),

The energy-dependent area factor, $FA_y(E_y)$, can be derived by considering the point-kernel dose integral, $D(R, t_a, C_d(t), T(t))$, over the source thickness ($T(t)$), radius R , distance from the receptor midpoint to the plane of the source and air interface (T_a), and thickness of the shielding material ($C_d(t)$) for the geometry depicted in Fig 3.4.

The area factor is the ratio of the dose integrals for the geometry being considered and the infinite slab geometry:

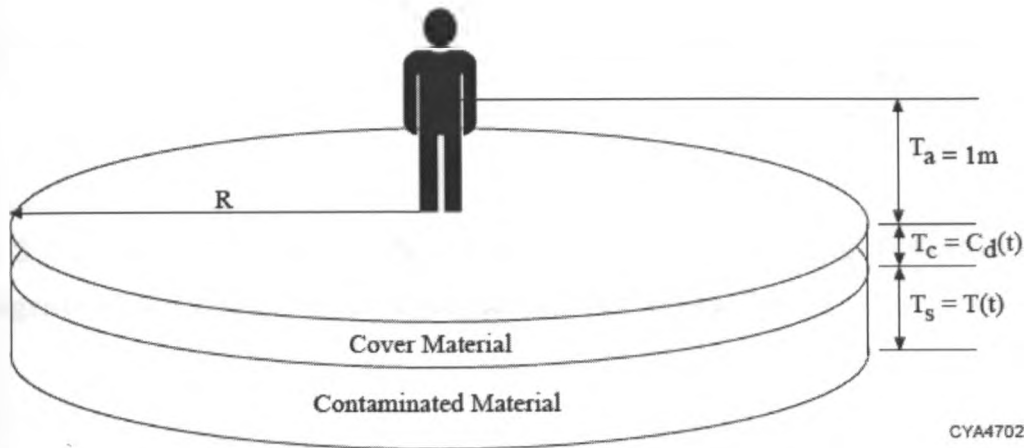


Fig 3.4 Exposure Geometry Considered for Area Factor Calculation (Yu et al. 2001)

$$FA'_Y = \frac{D [R=r, T_a = 1m, T_c = C_d(t), T_s = T(t)]}{D [R = \infty, T_a = 1m, T_c = C_d(t), T_s = T(t)]}, \quad 3.17$$

Where the function D is the dose rate evaluated by using the point-kernel method as shown on Figure 3.5:

$$D[R, T_{Ra}, C_d(t),] = K \int_{V_s} e^{-z} \frac{B(z)}{4\pi l^2} dV, \quad 3.18$$

where

$$z = \frac{\mu_a T_a + \mu_c C_d(t) + \mu_s y}{T_a + C_d(t) + y} l;$$

$$l^2 = r^2 + (T_a + C_d(t) + y)^2;$$

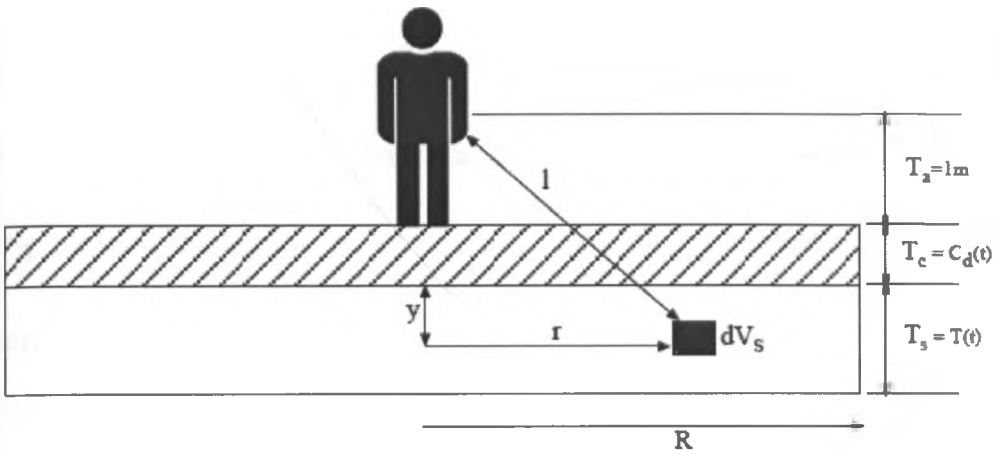


Fig 3.5 Cross Section of Exposure Geometry Showing Element of Integration for Area Factor Calculation (Yu et al. 2001)

$$dV_s = 2\pi r y dr dy;$$

μ_a = attenuation coefficient for air (energy-dependent);

μ_c = attenuation coefficient of the source material (energy-dependent);

μ_s = attenuation coefficient of the source material (energy-dependent);

$B(z)$ = buildup factor for length measured in mean free paths, z (energy-dependent); and

K = energy-dependent conversion factor.

The volume integral can be written more explicitly as

$$\int_0^{T_s} dy \int_0^R \frac{e^{-z} B(z)}{4\pi l^2} 2\pi dr. \quad 3.19$$

Note that in the inner integral,

$$\frac{dz}{z} = \frac{d1}{1} = \frac{r dr}{1^2}$$

The volume integral can then be written as

$$\frac{1}{2} \int_0^{T_s} dy \int_{Z_0}^{Z_f} \frac{e^{-z} B(z)}{z} dz \quad 3.20$$

Where

$$Z_0 = \mu_a T_a + \mu_c C_d(t) + \mu_s t \text{ and}$$

$$Z_f = Z_0 \sqrt{1 + \frac{R^2}{(T_a + C_d(t) + y)^2}} .$$

The photon energies and yields of different radionuclides were obtained by condensing International Commission on Radiological Protection Publication 38 (ICRP 1983) photon spectra. The radionuclide-specific area factor, FA_{i1} , is obtained by combining the energy-dependent area factors weighted by their photon fraction, FPT_γ , and dose contribution at the reference point:

$$FA_{i1} = \frac{\sum_\gamma FA_\gamma (E_\gamma) FPT_\gamma D_{slab} (E_\gamma)}{\sum_\gamma FPT_\gamma D_{slab} (E_\gamma)} \quad 3.21$$

where

$D_{slab} (E_\gamma)$ = dose from the FGR-12 (Eckerman and Ryman 1993) infinite slab geometry.

An ETF for dust inhalation is the ratio $ETF_{i2}(t) = E_{i2}(t)/S_i(t)$ of the annual intake $E_{i2}(t)$ of the j th principal radionuclide by dust inhalation to the concentration $S_i(t)$ of that radionuclide in the soil for the t th year following the radiological survey. It can be expressed as the product

$$ETF_{i2}(t) = ASR_2 \times FA_2 \times FCD_2(t) \times FO_2 \times Fl_2, \quad 3.22$$

Where

$ETF_{i2}(t)$ = environmental transport factor at time t for dust inhalation for the i th principal radionuclide (g/yr).

ASR_2 = air/soil concentration ratio = average mass loading of airborne contaminated soil particles (1×10^{-4} g/m³),

FA_2 = area factor (dimensionless),

$FCD_2(t)$ = cover and depth factor (dimensionless),

FO_2 = occupancy factor (0.25), and

Fl_2 = annual intake of air (8,400 m³ yr⁻¹).

The methodology used in RESRAD is designed to reflect site-specific soil characteristics and meteorological conditions. The site-specific parameters considered include the size of the source area, average particle diameter, and average wind speed. Other site-specific parameters (particle density, atmospheric stability, raindrop diameter, and annual precipitation rate) were assumed to be constant. The model uses the Gaussian plume model combined with removal processes, such as dry and wet deposition of particulates. The annual air intake of 8,400 m³/yr used in the RESRAD code is the value recommended by the International Commission on Radiological Protection (ICRP 1991). The fraction of time outdoors (on site) is defined as the average fraction of time during which an individual stays outdoors on the site. A typical value, used for the default scenario in RESRAD, lies is 0.25. The fraction of time spent indoors is defined as the average fraction of time during which an individual stays inside the house. A typical value, used for the default scenario in RESRAD, is 0.5. The default shielding factor of 0.7

implies that the indoor levels of external radiation are 30% lower than the outdoor levels. The area factor was fitted by least squares regression to the formula

$$FA_2 = \frac{a}{1+b(\sqrt{A})^c}, \quad 3.23$$

where

A = area of contaminated zone (10,000 m²) and

a,b,c = least squares regression coefficients.

For the default particle size of 1 µm used in the RESRAD code (Yu et al. 2001), the regression coefficients for Equation 3.23 are given for wind speeds not listed (i.e., those between 1 and 10 m/s), the area factor is calculated by interpolation.

Computation of Environmental Dose Factors (EDFs)

The relationship between the Total Effective Dose (TED) calculated using the procedural adaptation of RESRAD for a given set of input parameters was done. The respective concentrations of radionuclides in rock, soil and groundwater on which the TED calculated was based on evaluation obtained from the concentrations of ⁴⁰K, ²³²Th and ²²⁶Ra (²³⁸U). The latter were compared with dose rate values measured using hand held survey.

Here, EDFs are defined as factors that relate TED due to a chronic exposure to NORM to the elemental activity concentration of a given element in rock, soil or water for a certain age group and exposure scenario. Only EDF values for K, U and Th were calculated for this study because it was assumed that all progeny radionuclides remain in secular equilibrium with their precursors. Natural abundance of mass of U in

rock and soil is assumed as 99.2745% ^{238}U , 0.0055% ^{234}U and 0.7200% ^{235}U ; while ^{232}Th is assumed to be 100% of natural Th. RESRAD exposure scenarios are also used to classify the various EDFs, where ingestion of well water is still assumed for suburban residents. Furthermore, the annual TED to a given age group for a given exposure scenario is estimated as the sum of the activity concentrations of all of the radionuclides in both rock/soil and water, multiplied by their proper respective EDFs. This is expressed mathematically as:

$$\text{TED}_{\text{Age, Exposure Scenario}} = \sum_z \cdot \sum_m \text{EDF} \cdot C \quad 3.24$$

where z is the element under consideration, m is the environmental medium, and C is the activity concentration of element z in media m . For this work, z was K, U and Th and m was soil/rock and water.

To calculate an EDF, it is first necessary to calculate the CED per unit activity concentration in a given environmental medium, for each pathway, and for each of the decay progeny for all of the naturally abundant radioisotopes of the element using the procedural adaptation of RESRAD. An EDF for a given element, exposure scenario, age of applicability, and environmental medium is calculated as the sum over all of the natural isotopes of the given element of the product of that element's fractional abundance by mass multiplied by its maximum specific activity. This is multiplied again by the sum of the CED per unit activity concentration over all dose pathways for the given environmental medium for all decay progeny of that isotope, and everything is divided by the sum of the products of the fractional abundances by mass and the maximum specific activity of each of the natural isotopes of the element. This is expressed mathematically as:

$$EDF_{z,m} = \frac{\sum_k \left(F_k (SA)_{\cdot k} \sum_i \sum_j P F_{ij} \right)}{\sum_i (F_k (SA)_{\cdot k})} \quad 3.25$$

Where k is a naturally occurring radionuclide of element z , i is a decay product of radionuclide k and j is the dose pathway. F is fractional abundance by mass of radionuclide k with respect to element z , SA is the maximum specific activity of radionuclide k , and P is the CED per unit activity concentration of radionuclide i in pathway j calculated using the procedural adaptation of RESRAD. For this work, k will be ^{40}K , ^{232}Th and ^{238}U . Consequently, the radionuclides, i , will correspond to those in U and Th series. The pathways, j , are the dose pathways considered by RESRAD for given exposure scenario.

MATERIALS AND METHODS

4.1. Summary

The surveyed area was mapped using hand held radiation detectors. The sampling sites were selected from different major geological terrain, as detailed in Appendix A, in order to assess the influence of geology on the distribution of radioactivity and consequently on the distribution of radiation exposure in Homa Mountain area. Measurement of activity concentration of naturally occurring radioactive materials (NORM) in samples were performed using conventional experimental procedures. These include measurement of ^{40}K , ^{226}Ra and ^{232}Th in pulverized soil and rock samples. RESRAD code is used to deduce possible doses inhabitants and individuals in the population receive from exposure to NORM.

4.2 EQUIPMENT AND CALIBRATION PROCEDURES

4.2.1. Description of Radiagem

The Radiagem personal dose rate and survey meter (see Fig 4.1) was capable of measuring ambient dose equivalent rate up to 100 mSv h^{-1} .



Fig. 4.1 Radiagem with the α , β and γ probes

The Radiagem™ 2000 was easy to handle and had a LCD display showing average digital reading with visual and audible alarms. Radiagem's external smart α , β and γ probes extend the capabilities of the instrument to a range of general surveying applications. The probe is a fully integrated subsystem, taking and transmitting the measurement to the instrument, which is used for display. In this "smart" design, key components of hardware circuitry (high voltage, amplifier, discriminator, etc.) are located directly inside of the probe housing rather than in the host survey instrument. Also, the intelligence associated with controlling those components is located in the probe i.e. control and storage of key parameters, settings, calibrations, probe ID, alarm settings, etc. The probes can be plugged in "hot" without powering down the instrument as it immediately recognizes the probe and automatically switches measurement mode to the mode required for that specific probe.

4.2.2. Quality Assurance and Calibration of Hand held survey meters

Measurement uncertainties and characteristic limits were factored in the data of Homa Mountain area. Due to the fact that measurement uncertainties and characteristic limits are increasingly referred to in legislation and legal regulations, internationally standardized procedures were applied to quantify measurement uncertainties and characteristic limits. To satisfy these needs with respect to measurement uncertainties, ISO (1993 and 2000) published the ISO Guide to the Expression of Uncertainty in Measurement (GUM) which allows a standardized quantification of measurement uncertainties. The ISO methodology, which is widely accepted and has been adopted also by national and international bodies (Van 2004; EURACHEM/CITAC 2000; IAEA 1999 and 2004), was used for quality assurance and calibration of the hand held dose rate survey meters.

Radiagem was used at all locations where samples were collected in and around Homa Mountain and its readings were compared to similar equipment

kept at the SSDL at KeBS. The traceability is intimately linked to uncertainty because it provides the means of placing all related measurements on a consistent measurement scale, while uncertainty characterizes the 'strength' of the links in the chain and the agreement to be expected between laboratories making similar measurements. The uncertainty calculation of gamma dose measurements using hand held survey meter is presented in Figs 4.2, 4.3, 4.4 and 4.5. The influence of each parameter and the identification of the major contributor, in the relative difference between the methods of uncertainty calculation is as explained by Gonzalez et al. (2008).

From Equations 3.1 and 3.2 one can relate the absorbed dose to air factor, N, defined as:

$$N = D_{SSDL} / D_{RPB} \quad 4.1$$

Where D_{SSDL} is the dose rate reading from the Radiagem of the SSDL and D_{RPB} is the dose rate reading of the Radiagem used in the study. The Radiagem performance used in the field (RPB) was compared to a similar one (IAEA) kept at the Secondary Standard Dosimetry Laboratory (SSDL) and ion chambers traceable to the National Standards Laboratory of Germany (PTW). Table 4.1 shows the different dose rates exposure scenarios using ^{137}Cs calibration source, the correction factors (c.f.) deduced by dividing the reading of the Radiagem of IAEA with that of RPB. The response is the reciprocal of c.f.

From Table 4.1 the mean c.f. value of 1.027 implies very good metrological traceability which is a property of a measurement result whereby the result can be related to a reference (PTW) through a documented unbroken chain of calibrations (SSDL). Each (RPB, SSDL and PTW) contributed to the measurement uncertainty.

Table. 4.1. Comparison of the Responses of the Radiagem used (RPB), at SSDL (IAEA) and ion chambers (PTW)

SSDL	PTW	RPB				
TRUE		Indication	N=c.f.	Response	% differ	
H*(10)		H*(10)		1/N		Mean
μSv/h		μSv/h				N =c.f.
5.2	5.01	6.60	0.79	1.27	31.74%	
8.3	8.02	7.71	1.08	0.93	-3.87%	
20.7	20.04	21.12	0.98	1.02	5.39%	1.027
51.9	50.20	49.93	1.04	0.96	-0.54%	
82.9	80.26	81.39	1.02	0.98	1.41%	
206.6	199.9	198.4	1.04	0.96	-0.75%	
518.9	502.1	516.5	1.00	0.99	2.87%	

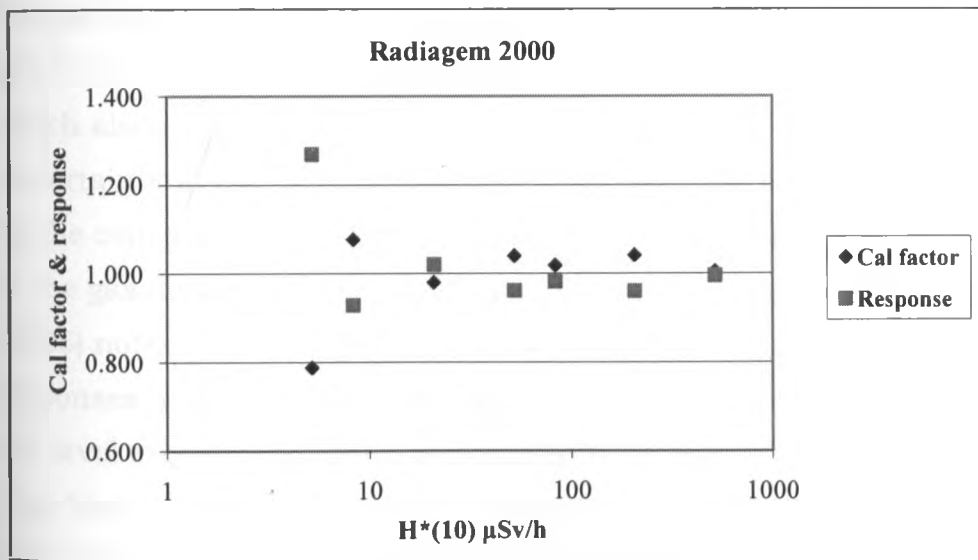


Fig. 4.2 Calibration Factor (c.f) and Response normalized for RPB Radiagem

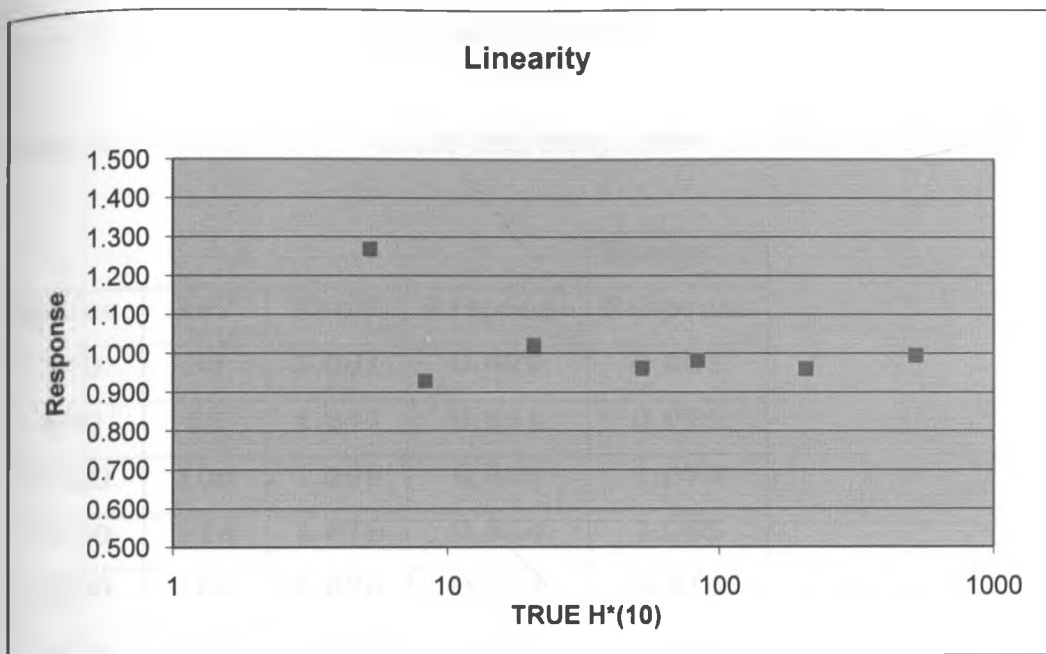


Fig. 4.3 Linearity of the Response versus the True H*(10)

An issue that calls for clarification is the appreciable percentage difference (31.74%) between the calibration factor and response at low doses ($5.2 \mu\text{Sv h}^{-1}$) which also comes out clearly on linearity shown on Figs 4.2 and 4.3. The uncertainty in the determination of absorbed dose to the dosimetry is affected by the composition and geometry of the ionization chamber. The radiation field in the gas filled cavity will have more uncertainties at low doses because ICRP (2005) notes that emerging results with regard to radiation-related adaptive responses, genomic instability, and bystander effects suggest that the risk of low-level exposure to ionizing radiation is uncertain, and a simple extrapolation from high-dose effects may not be wholly justified in all instances. The focus is on evidence regarding linearity of the dose-response relationship for all cancers considered as a group, but not necessarily individually, at low doses [the so-called linear, non-threshold (LNT) hypothesis]. The (ICRP 2005) report concludes that while existence of a low-dose threshold does not seem to be

unlikely for radiation-related cancers of certain tissues, the evidence does not favor the existence of a universal threshold.

Table 4.2 Calibration Factor and Responses for different X-ray keVs

Source	keV	N=c.f.	Response	Energy
				Response
N40	33	2.001	0.499	0.855
N80	65	1.847	0.541	0.926
N120	100	1.598	0.625	1.070
N150	118	1.576	0.634	1.085
N200	164	1.870	0.534	0.914
S-Cs	662	1.710	0.584	1.000

The LNT hypothesis remains a prudent basis for radiation protection at low doses and low dose rates. Tables 4.2 and Figs 4.4 and 4.5 show the correctness of the ICRP interpretation for x-ray energies (N40 to N200) too which are compared to cesium (Cs) source for the 662 energy. In part because of the insurmountable intrinsic and methodological difficulties in determining if the health effects that are demonstrated at high radiation doses are also present at low doses, current radiation protection standards and practices are based on the premise that any radiation dose, no matter how small, may result in detrimental health effects, such as cancer and hereditary genetic damage. Further, it is assumed that these effects are produced in direct proportion to the dose received, that is, doubling the radiation dose results in a doubling of the effect. These two assumptions lead to a dose-response relationship, often referred to as the linear, no-threshold model, for estimating health effects at radiation dose levels of interest. There is, however, substantial scientific evidence that this model is an oversimplification.

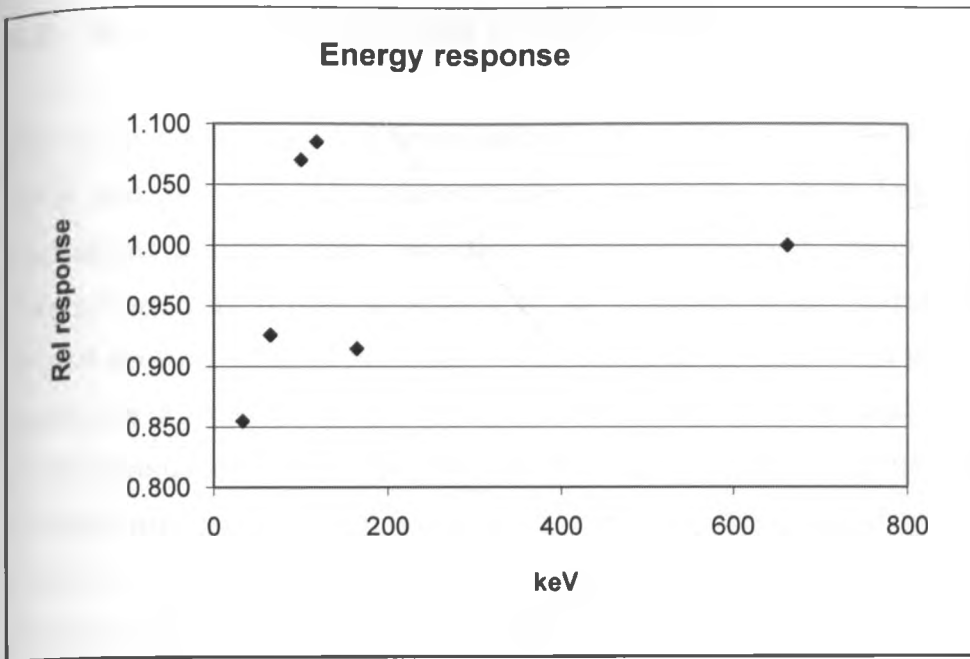


Fig 4.4 Responses for different X-ray keVs

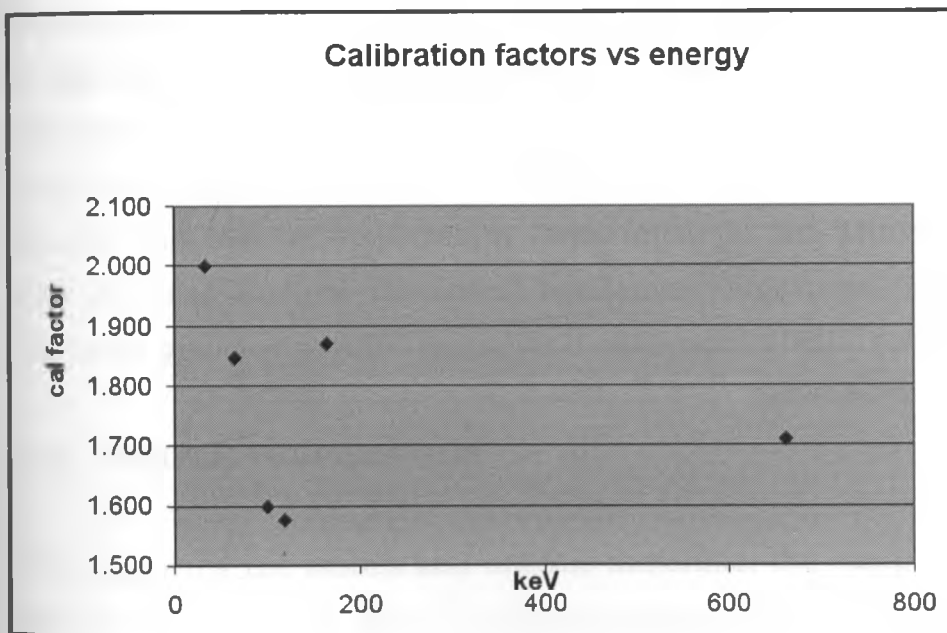


Fig 4.5 Calibration Factors against X-ray Energies

4.3. METHOD OF SAMPLING AFTER SURVEYING

The study area extended from latitude $0^{\circ} 30'N$ and $0^{\circ} 20'N$ and longitude $33^{\circ} 26' E$ and $34^{\circ} 34'E$. Altitude extended above 600 m from Lake Victoria surface. Radiagem, a hand held radiation measuring survey meter coupled with NaI detector gamma probe, was used at all locations where samples were collected in and around Homa Mountain. The study area, shown in green in Figure A.3, Appendix A was traversed on foot, and ambient dose equivalent rates in air were measured at suitable sites including around dwellings, farmlands, water sources and yet to be settled areas currently used for growing crops, grazing cattle or recreation. The coordinates of the readings were determined by global positioning system. At chosen sites rock were chipped from outcrops and soil samples were scooped after removing stones and organic materials before being transferred to the laboratory. A total 250 point measurements were done and 44 samples were taken, as detailed in Appendix B. The sampling sites were selected from different geological terrain after field measurements. Assessment of the influence of geology on the distribution of NORM and consequently on the radiation exposure in Homa Mountain area was done. Identification of the rock samples was done at the Geological Department of the University of Nairobi and the Geo-exploration Department in the Ministry of Energy. The rock samples include rhyolites, sandstone, limestone, ijolite, carbonatites, Nyanzian pyroclasts, tuffs, quartz and associated alkalic rocks.

4.4. SAMPLE PREPARATION

After removing the stones and organic materials, the samples were dried in an oven at about $100^{\circ}C$ for 1–2 hour to remove the moisture content and then crushed to pass through a $150\ \mu m$ mesh sieve to homogenize it. The samples were weighed using an analytical balance, calibrated with a calibrated weight set traceable to the Kenya Bureau of Standards kilogram, which is directly traceable to the BIPM (Bureau International des Poids et Mesures, Sevres,

France) kilogram. A typical sample of $200 \pm 0.05\%$ g was weighed and finally, a split of the prepared sample was packed in a standard plastic container (7.5 cm × 6.5 cm diameter) before properly tightening the threaded lid to the containers. These containers were hermetically sealed with aluminum foil to prevent the escape of gaseous ^{222}Rn and ^{220}Rn from the samples and left for at least 4 weeks (>7 half-lives of ^{222}Rn and ^{224}Ra) before counting by gamma spectrometry in order to ensure that the daughter products of ^{226}Ra up to ^{210}Pb and of ^{228}Th up to ^{208}Pb achieve equilibrium with their respective parent radionuclides. The standard sources for ^{226}Ra and ^{232}Th (in secular equilibrium with ^{228}Th) were prepared using known activity contents and mixing with the matrix material of phthalic acid powder. Analar grade potassium chloride (KCl) of a known amount in the same geometry was used as the standard source for ^{40}K .

4.5. MEASUREMENTS OF ACTIVITY CONCENTRATION

The high-resolution hyper purity germanium (HPGe) gamma ray spectrometry system belonging to the National Radiation Protection Laboratory and Institute of Nuclear Science and Technology were used. They have a 25% relative efficiency, and were used to determine the activity concentration of radionuclides due to ^{232}Th , ^{238}U (^{226}Ra) and ^{40}K in the samples. They consisted of a p-type intrinsic germanium coaxial detector mounted vertically and coupled to a 3 keV digital high-voltage source. The detector were housed inside a massive 10 cm thick old lead shield with an inner layer of copper to reduce background radiation. The containers were tapped and placed directly on top of the detector end cap and measured for 1 to 15 hours each. The standards were measured for shorter periods i.e. less than an hour for those whose activity concentration was appreciable. By collecting the spectrum of each reference material for 3,600 seconds, the efficiency calibration of the system was done. The γ ray energies considered for calibration are given in Table 4.3.

Table 4.3 Gamma Ray Energies that may be used for Calibration of Spectrometer and for Measurement of Activity of the Radionuclides. Source (Reilly et al., 1991). Those in bold were used.

Parent Nuclide	Daughter Nuclide	Y-ray energy (keV)	Abundance (%) and half life i.e. $T_{1/2}$
^{232}Th	^{228}Ac	209.39	(3.81) 6.15 h
^{232}Th	^{212}Pb	238.63	(43.60) 10.64 h
^{232}Th	^{228}Ac	338.42	(1.25) 6.15 h
^{232}Th	^{228}Ac	463.10	(4.44) 6.15 h
^{232}Th	^{208}Tl	583.19	(84.50) 3.05 m
^{232}Th	^{212}Bi	727.33	(6.25) 1.01 h
^{232}Th	^{208}Tl	860.56	(12.42) 3.05 m
^{232}Th	^{228}Ac	911.16	(26.60) 6.15 h
^{232}Th	^{228}Ac	964.64	(5.11) 6.15 h
^{232}Th	^{228}Ac	968.97	(16.23) 6.15 h
^{232}Th	^{208}Tl	2614.60	(99.2) 3.05 m
^{137}Cs		661.66	(85) 30.17 y
^{60}Co		1173.20	(100) 5.172 y
^{60}Co		1332.00	(100) 5.172 y
^{238}U	^{214}Pb	241.98	(7.5) 26.8 m
^{238}U	^{214}Pb	295.21	(18.5) 26.8 m
^{238}U	^{214}Pb	351.92	(38.5) 26.8 m
^{238}U	^{214}Bi	609.32	(44.8) 19.9 m
^{238}U	^{214}Bi	768.30	(4.88) 19.9 m
^{238}U	^{214}Bi	1120.28	(14.8) 19.9 m
^{238}U	^{214}Bi	1238.11	(5.86) 19.9 m
^{238}U	^{214}Bi	1764.60	(15.96) 19.9 m
^{40}K		1460.8	(99.16) 1.277E+8 y

Gamma spectroscopy was used to determine the activities of ^{40}K , ^{226}Ra and ^{232}Th , with a p-type intrinsic hyper pure germanium (HpGe) coaxial detector mounted vertically and coupled to a 3 kV digital high voltage source. The HpGe detector was calibrated for energy, relative efficiency using calibration sources containing ^{133}Ba , ^{22}Na , ^{137}Cs , ^{54}Mn and ^{60}Co . A performance test using IAEA(1987) standard reference material Soil-375, RGU, RGTh and RGK was used for checking the efficiency, $\varepsilon(E,n)$ of the calibration of the system as done by Mustapha (1999), Hasham (2004) and Achola (2012) using the relation:

$$\varepsilon(E,n) = \frac{C(E,n)}{t.f(E,n).A} \quad 4.1$$

Where:

$C(E,n)$: net photo-peak count of gamma-ray transition with energy E of radionuclide n,

t: counting time, s,

$f(E,n)$: branching ratio, number of photon with energy E per hundred disintegration of radionuclide n,

A: activity concentration in Bq of radionuclide n.

However, the precise determination of the activity concentration of each radionuclide requires the determination of full energy efficiency calibration for a given geometry. Standard or reference samples should have the closest specifications, regarding geometry and matrices (apparently density and composition), to the analyzed samples. The accurate determination of the photopeak efficiency curve for a given sample matrix represent the main challenge in gamma-ray spectrometry. Practically, the samples geometry (shape and sample-detector geometry) can be easily reproduced. However, the major source of possible error in efficiency calibration remains due to the difficulties to reproduce the same matrix and chemical composition of the standard

samples as that of the other bulk samples that could have vast diversities in both densities and compositions. Table 4.4 shows the average values found in this work for SRM.

Table 4.4 Measured Activity Concentrations of ^{232}Th , ^{226}Ra and ^{40}K in the IAEA Reference Samples Compared to Others

Reference	Sample Code	^{40}K (Bq kg ⁻¹)	^{226}Ra (Bq kg ⁻¹)	^{232}Th (Bq kg ⁻¹)
This work	IAEA-375	424.0± 2.3	ND	21.5±15.1
This work	SR-16	412.3±8.1	449.4±9.7	18.9±10.2
This work	IAEA/RGU	ND	4940.4±0.3	ND
This work	IAEA/RGTh	ND	ND	3248.0±0.4
This work	IAEA/RGK	14245.3±0.7	ND	ND
This work	IAEA/RGMix	8097.8±0.3	837.0±1.2	830.1±0.7
Kebwaro et al. 2011 and Mustapha et al 2004	IAEA/RGU	< 0.6	4900±30	< 4
As above	IAEA/RGTh	6±3	77±5	3280±70
As above	IAEA/RGK	13400±90	<0.012	<0.04
As above	IAEA/RGMix	9100±140	810±11	810±23
IAEA 1987	IAEA/RGU	< 20	4940 (4910 - 4970)	< 4
IAEA 1987	IAEA/RGTh	6.3 (3.1 - 9.5)	78 (72 -840)	3250 (3160 - 3340)
IAEA 1987	IAEA/RGK	14000 (13600 - 14400)	ND	ND

Also for the purpose of this study, a secondary calibration material was prepared in our laboratory by mixing the three reference samples, and the product is referred to as RGMIX as explained by Mustapha (1999). The primary reference materials were counted from 600 to 1,800 s and the RGMIX for longer times since for the latter the γ lines of 238 keV (^{212}Pb for Th), 352 keV (^{214}Pb for Ra), 609 keV (^{214}Bi for Ra), 911 keV (^{228}Ac for Th) and 1460 keV (^{40}K) keV were clearly resolved without much interference. The results obtained in the SRM agree with the certificate data, within experimental uncertainties and the maximum relative difference between the values (method accuracy) was 14%. Results comparable to those of Mustapha et al (2004) and Kebwaro et al (2011) were obtained as displayed in Table 4.4. The overall uncertainties reported in these table and those in Chapter 5 Table 5.3 were determined taking into consideration the standard deviation of the average values obtained in the HpGe counting sample and SRM.

An important correction applied in gamma-ray spectrometry of bulk samples is the correction for photon attenuation within the source material itself that is known as self-attenuation or absorption correction. For a given geometric setup, the correction factor $[(C_s(E))]$ is expressed as the ratio of efficiency of standard $[\epsilon(E, \text{Standard})]$ to that of the sample $[\epsilon(E, \text{sample})]$ i.e.:

$$C_s(E) = \frac{\epsilon(E, \text{ standard })}{\epsilon(E, \text{ sample })} \quad 4.2$$

4.5.1. Efficiency Calibration of HpGe Detector

The high resolution γ -ray spectrometry method is an indirect method, using the detection system as a comparator of the sample to a SRM, and therefore it was calibrated with SRM traceable to the SI units and of the same geometry as that of the sample. The HpGe detector system employed in this work was calibrated for peak efficiency using a single nuclide point sources as well as IAEA (1987)

certified soil SRMs, RGU-1 (^{226}Ra), RGTh-1(^{232}Th) and RGK-1(^{40}K), with densities similar to the pulverised samples measured. The certified SRM was prepared and analyzed in the same experimental condition used in the rock and soil samples analysis. Therefore, a detection efficiency curve, known as efficiency calibration, over the energy region of interest must be established precisely in advance. The detection efficiency curve depends not only on a detection system but also on both the sample shape and matrix (Reilly et al. 1991). Using the detector's characteristics given by the manufacturer as input it was impossible to reproduce the efficiency and shape of the continuum of experimental spectra obtained with point sources. A transition zone of increasing charge collection efficiency had to be introduced in the simulated geometry, in the Ge crystal entrance window after the Ge dead layer, in order to obtain a good agreement between the simulated and experimental spectra. Knowing the computed shapes of partial absorption continuum deduced by the Monte Carlo simulation for different incident photon energies and angles it was therefore possible to convert the measured in-situ spectra to total incident flux spectra by applying the full absorption efficiency curve of the detector which was determined by calibrated point sources and Monte Carlo simulations. Having calculated the flux energy distribution the absorbed dose rate in air due to the gamma radiation was easily deduced. Experimentally, the detection efficiency curve was obtained using SRMs that contain a set of radionuclides with known activities and cover the gamma-ray energy range of interest (usually from 35 to 2000 keV).

Fig 4.5 shows the type of calibration curve resulting from use of different energies emitted by ^{60}Co , ^{137}Cs , ^{238}U , ^{232}Th and ^{40}K .

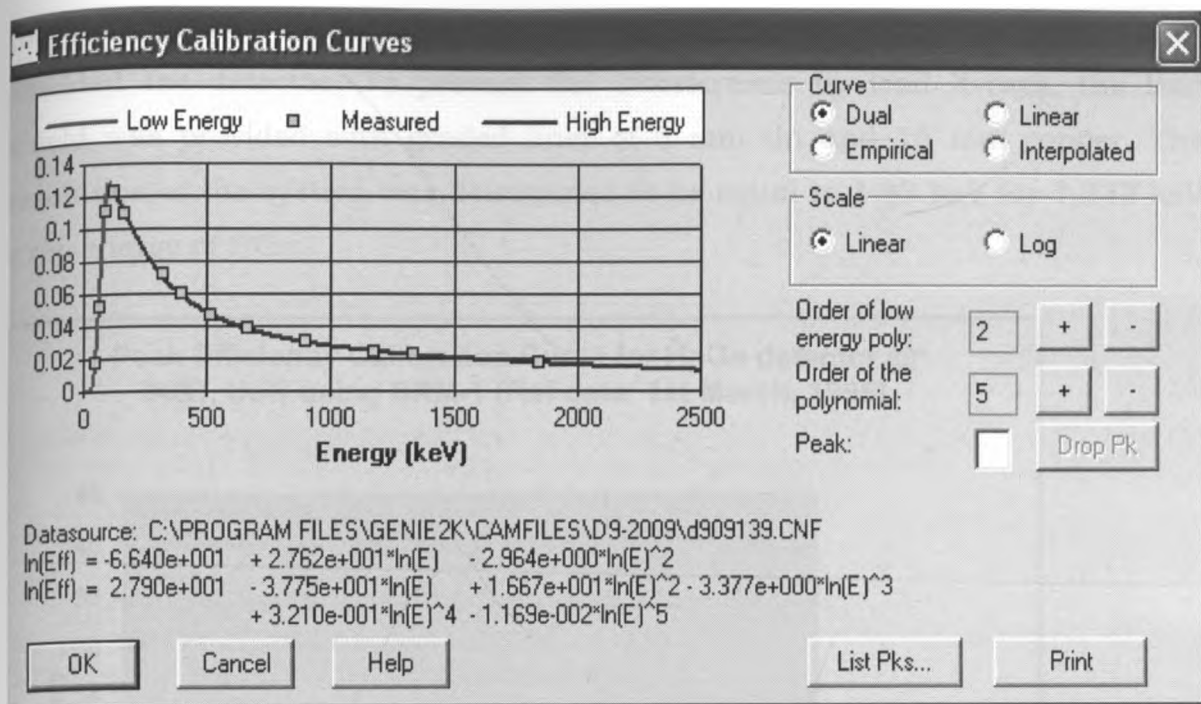


Fig. 4.6 Peak Efficiency Calibration Curve for HpGe of RPB

The efficiency curve for calibration shown in Fig 4.6 was determined after the analysis of the obtained gamma spectra was performed with the use of software's Maestro II (MCA, EG&G ORTEC) and MCC (by IRD/CNEN).

4.5.2 Calibration of HpGe Detector by Comparison

To identify the responsible radionuclides using the radiation laboratory measurements of soil and rock samples from the area the determination of the relative concentration of natural radioactive elements of ^{40}K and the series of ^{232}Th and ^{238}U contributing to the high radiation level was done. Soil and rock samples collected from Homa Mountain and surrounding areas were crushed before being sieved and 200 gm placed in plastic containers. After one month they were analyzed by γ -ray spectroscopy using HpGe detector. The detector consisted of a vertical dipstick mounted on liquid nitrogen dewar. To reduce

the γ ray background, a lead cylinder with fixed bottom and moveable cover, shielded the detector. To prevent the interference by lead X-rays, the lead shield was provided with graded liner of 5 mm tin and 16 mm copper. The resolution of the system was determined to be equal to 1.83 keV for 1,332 keV γ ray energy of ^{60}Co .

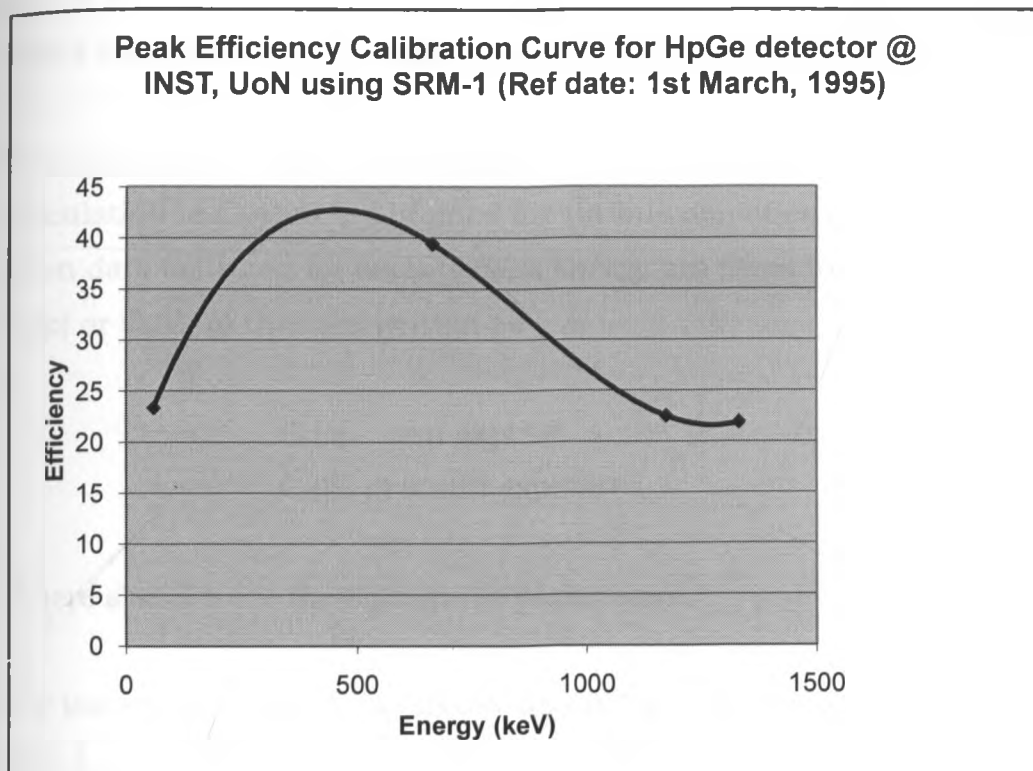


Fig 4.7 Peak Efficiency Calibration Curve for the HpGe of INST

For meaningful results, the γ ray spectroscopy system was calibrated, before performing qualitative and quantitative isotopic identification. The quality assurance of the measurements was carried out by the efficiency and energy calibration, by IAEA provided reference materials soil 6, soil 375, RGK, RGU and RGTh which were used for efficiency and energy calibration of the spectrometer. Fig 4.7 shows the peak efficiency calibration curve for the HpGe detector at INST, UoN using SRM whose reference date is 1st March 1995.

In practical applications, standard and sample materials might be entirely different. However, knowing the concentration of the standards one can deduce the concentrations of the samples. Environmental samples may greatly differ in their chemical composition, even of the same matrices (such as soil and sediment samples), and their density ranging from extremely low densities up to 2.0 g/cm³. Self-absorption correction can be determined experimentally or using the Monte Carlo computation techniques or using analytical methods.

The procedure for self-absorption factor determination includes firstly calculation of C_s that is obtained for various densities ρ and photon energies E . Then data collected for each photon energy are fitted to an appropriate function $C_s(\rho)$ or $C_s(E, \rho)$ that are written as

$$\begin{aligned} C_s(\rho) &= a \exp(-b \rho) && \text{or} && 4.3 \\ C_s(E, \rho) &= a(E) \exp[-b(E) \rho] \end{aligned}$$

Where a and b are the adjustable parameters.

For low energy gamma-ray (below about 100 keV) these formulae are applicable only for materials of similar composition on account of the relation between the mass attenuation coefficient and the atomic number. Gamma-ray photons are known to be attenuated through the material according to the following relation;

$$\begin{aligned} I &= I_o \cdot e^{(\mu \cdot x)} && \text{and} && 4.4 \\ I &= I_o \cdot e^{(\mu_m \cdot x \cdot \rho)} \end{aligned}$$

Where:

- I_o : the photons, with energy E , intensity without attenuation
- I : the photons, with energy E , intensity after attenuation

- μ : the linear attenuation coefficient, cm^{-1} ,
- μ_m : the mass attenuation coefficient, $\mu_m = \mu / \rho$, cm^{-2}/g .
- x : the sample thickness (or effective thickness)

Figures 4.5, and 4.6 shows the calibration curve using the standard reference materials (SRM) described in Appendix C.

When determining the detection threshold of a counting system, the measurement is expressed in terms of background count rates, n . The Minimum Detectable Activity (MDA) of a counting system is defined by the National Bureau of Standards as three standard deviations of the background count rate where the sample is counted for the same period of time, hereafter abbreviated MDA (B.S.). Thus, this value is associated with a 99.9% level of confidence that counts greater than MDA (B.S.) represent valid, detectable radioactivity (ISO 2000).

$$MDA (B.S.) = 3 \gamma \frac{\sqrt{n}}{\sqrt{T^2}} \quad 4.5$$

where

n = background count rate (cpm)

T = background counting period (min)

γ = correction factor(s) (e.g., $1/\epsilon$) to transform cpm to the desired result (i.e., $\mu\text{Ci}/\text{gm}$ or Bq/L).

The MDA determined were 59, 3.3 and 3.3 Bq kg^{-1} , for ^{40}K , ^{232}Th and ^{226}Ra respectively. The measured data either for the efficiency or the activity determination was corrected for background, dead time, decay, decay during measurement, and where appropriate for coincidence summing. Using different disc-type reference standard sources supplied by M/s ECIL, the gamma ray spectrometer is calibrated up to 3 MeV. The counting time for each sample was 12,000 s and above to get a statistically small error.

4.6. COMPUTER HARDWARE AND RESRAD SOFTWARE

For this work, RESRAD calculations were conducted using RESRAD version 6.5 (RESRAD 6.5, Argonne National Laboratory, 9700 South Cass Avenue, EVS/900, Argonne, IL 60439) on a 1.0 GHz personal computer (HP). Data were collected and analyzed using standard, commercially available spreadsheet software (Microsoft Excel, Microsoft Corporation, version 11.3.7, 1 Microsoft Way, Redmond, WA 98073). Within its library, RESRAD version 6.5 contains dose conversion factors (DCF) from a variety of sources. All relevant calculations performed for this research used the ICRP (1995) age-dependent DCFs, excluding those for radon and its decay products. RESRAD calculations of dose due to inhalation of ^{222}Rn and ^{220}Rn use dose coefficients based on the Committee on the Biological Effects of Ionizing Radiation (BEIR) report IV and ICRP publication 32 and 47 (Yu et al 2001). The radon DCFs are not age – dependent in that their values remain constant for the various age-dependent DCF libraries in RESRAD. The use of RESRAD for such dose estimates depended on the models of radionuclide distribution into plants, livestock, and other sectors of the environment input. This was highly useful in considering the full range of dose pathways for chronic exposures. The dose calculations and estimations made with the procedural adaptation of RESRAD represent the use of theoretical values of certain hydrological, geological, and site specific constraints considered by RESRAD code. For the most accurate use of RESRAD to evaluate dose due to persistent exposures to NORM, as well as any other radioactive material, one should endeavor to base the calculation on as much accurate data about one's site as possible.

4.6.1 Test Cases for Procedural Adaptation

The RESRAD computer code was used for biosphere modeling and dose computations in this research. A dose due to Homa Mountain average concentrations of K, U and Th series radionuclides was then calculated. Our

study shows that house occupancy factor varies from 0.5 to 0.9 depending on sex and age. The as low as practicable achievable (ALAPA) frequently necessitates the evaluation of alternative actions and their costs and benefits. Collective dose is an important parameter in such comparisons. Estimates of collective dose from current and future use of the site can be derived with RESRAD by applying the appropriate site-specific parameters and integrating over the appropriate site occupancy.

ALARA Guidance Volumes 1 and 2 DOE (Yu et al. 2001) goals are to reduce potential radiation doses due to residual radioactive material to levels that are as near to background levels as is practicable. While it is not possible to reduce residual radioactive material levels to background levels in most cases, remedial actions (including necessary controls) should reduce levels such that potential doses under "actual" or "likely use" conditions would be a small fraction of the primary dose limits. While the pathway analyses conducted with RESRAD should consider and evaluate viable alternative remedial measures that reduce annual doses to a member of the general public from 1 mSv to a fraction of 1 mSv, the 1 mSv limit is for all pathways and sources combined (excluding background and medical exposures). Therefore, in order to comply with DOE Order 5400.5 and the proposed 10 CFR 834 requirements, potential doses from residual radioactive material must be well below the primary dose limit.

The derivation of guideline values for radionuclide concentrations in soil is based on a pathway analysis method known as the concentration factor method. With this method, the relationship between radionuclide concentrations in soil and the dose to a member of a critical population group is expressed as a sum of the products of "pathway factors." Pathway factors correspond to pathway segments connecting compartments in models of the environment between which radionuclides can be transported or radiation transmitted. Most pathway factors are assumed to be steady-state ratios of

concentrations in adjoining compartments. Some are factors for conversion from a radionuclide concentration to a radiation level or radiation dose; others are use and occupancy factors that affect exposure. Each term in the sum corresponds to a pathway of connected segments. In most cases, a pathway product or pathway factor may be added, deleted, or replaced without affecting the other pathways or pathway factors. This structuring facilitates the use of alternative models for different conditions or transport processes and the incorporation of additional pathways. Thus, in most cases, RESRAD can easily be modified or tailored to model any given situation by merely adding or replacing factors or terms in the pathway sum.

Chapter 5

RESULTS AND DISCUSSIONS

5.1 Summary

Using conventional experimental procedures measurements of the surface dose rate and activity concentrations of the naturally occurring radionuclides (^{40}K , ^{232}Th and ^{226}Ra) in geological samples were done and the results are presented in this chapter. The samples were mainly from and around Homa Mountain and they were measured using hyper pure Germanium (HpGe) detectors at the Institute of Nuclear Science and Technology (INST) of the University of Nairobi and National Radiation Protection Laboratory of the Radiation Protection Board (RPB). Calibration of hand held survey meters was done by comparing their responses to those of similar equipment in the Secondary Standards Dosimetry Laboratory (SSDL) at Kenya Bureau of Standards. RESRAD code was used with the inputs being primarily the activity concentrations in samples as deduced from equipment at INST and RPB.

5.2. Background Radiation Dose Measurements Using Hand Held Survey Meters

Using hand held survey meter the absorbed dose rates at the surface and at one meter above the ground were measured and the data subjected to statistical analysis using the computer software called Statistical Package for the Social Sciences (SPSS) computer program. Appendix B details the dose rates of various locations in and around Homa Mountain where survey meters readings were taken. The dose rates at other areas including Siaya, Vihiga, Busia and Nairobi were also measured so as to clearly show that the response of the survey meter in high background areas were significantly different. The latter are treated as control point measurements. SPSS analysis of the values obtained from the survey meters was done as contained in Table 5.1.

Table 5.1 Descriptive Statistical Analysis of Absorbed Dose Rates.

Dose Rate Descriptive	Statistic for Sample Size of 250 in nSv hr ⁻¹
Mean	474.1±17.7
95% Confidence Lower Bound	439.2
Interval for Mean Upper Bound	509.0
Median	418.7
Variance	78611.8
Standard Deviation	280.3
Minimum	108.4
Maximum	2681.0
Range	2572.6
Inter quartile Range	335.5
Skewness	2.6±0.1
Kurtosis	15.4±0.3

The median of 418.75 nSv hr⁻¹ is indicated by the vertical line that runs down the centre of the Fig 5.1. The range of 2572.6 nSv hr⁻¹ is represented by the horizontal distance between the smallest value and the largest value including any outliers. The inter quartile range is represented by the width of the box (Q3 minus Q1).

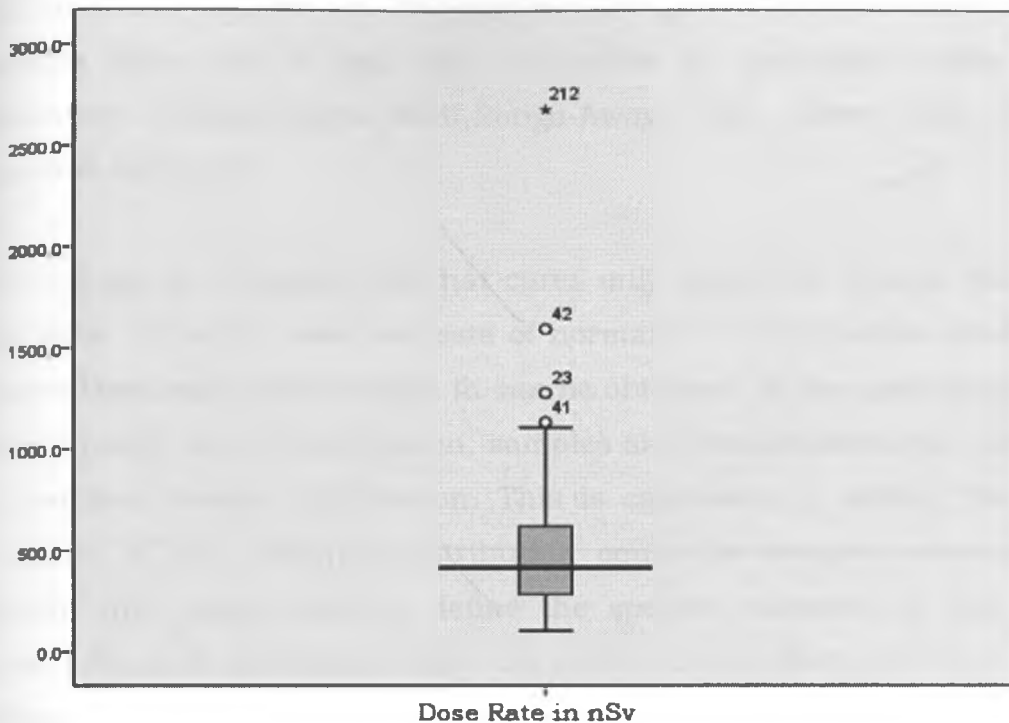


Fig. 5.1 Box plot of the Absorbed Dose Rates values

The Kolmogorov-Smirnov (KS) test tries to determine if two data sets differ significantly. The KS-test has the advantage of making no assumption about the distribution of data. One of the advantages of the KS-test is that it leads to a graphical presentation of the data, which enables the user to detect normal distributions. It can be modified to serve as a goodness of fit test see Table 5.2

Table 5.2. Tests of Normality for Data from Homa Mountain

Kolmogorov - Smirnov ^a				Shapiro - Wilk		
	Statistic	Df	Sig.	Statistic	Df	Sig.
Dose Rate	0.111	250	0	0.835	250	0

a. Lilliefors Significance Correction for sample size of 210 and control of 40

for the whole data set i.e. 250 points although it's possible to do the same for smaller data sets of less than 40 points for particular areas e.g. Homa Mountain, Chiewo-Ndiru Mbili-Rongo-Awaya Hills, Rawe beds, Bala gulley, Lambwe valley, etc.

The KS-test is a robust test that cares only about the relative distribution of the data and when used as tests of normality for data within and away from Homa Mountain a distribution fit can be obtained. In the special case of testing for normality of the distribution, samples are standardized and compared with a standard normal distribution. This is equivalent to setting the mean and variance of the reference distribution equal the sample estimate and it is known that using these to define the specific reference is true. One often rejects the null hypothesis when the p-value is less than 0.05 or 0.01. For the Homa Mountain data the distribution changes the null distribution of the null statistic. However, this test is less powerful for testing normality than the Shapiro-Wilk test. In practice the statistic requires relatively large number of data to properly reject the null hypothesis.

The behavior of Homa Mountain data are displayed on Fig. 5.2 on distribution fit superimposed on histogram. Each bar represents the dose rate range, and the height of the bar represents how many values fall into that range. It is evident that the data is skewed to the left, indicating that the tail of the right side is longer than the left side and bulk values lie to the left of the mean. Skewness of the data is indicated by the horizontal line that gravitates towards the end of the scale hence indicating that the data is skewed to the left. Skewness is a measure of the asymmetry of the probability distribution or a real valued random variable. A positive skew implies the data is skewed to the left implying that NORM levels are more towards less activity concentration of K, Th and U. Kurtosis is the measure of the peakedness of the probability distribution of the data points of Homa Mountain area which are real-valued

Chapter 5

RESULTS AND DISCUSSIONS

5.1 Summary

Using conventional experimental procedures measurements of the surface dose rate and activity concentrations of the naturally occurring radionuclides (^{40}K , ^{232}Th and ^{226}Ra) in geological samples were done and the results are presented in this chapter. The samples were mainly from and around Homa Mountain and they were measured using hyper pure Germanium (HpGe) detectors at the Institute of Nuclear Science and Technology (INST) of the University of Nairobi and National Radiation Protection Laboratory of the Radiation Protection Board (RPB). Calibration of hand held survey meters was done by comparing their responses to those of similar equipment in the Secondary Standards Dosimetry Laboratory (SSDL) at Kenya Bureau of Standards. RESRAD code was used with the inputs being primarily the activity concentrations in samples as deduced from equipment at INST and RPB.

5.2. Background Radiation Dose Measurements Using Hand Held Survey Meters

Using hand held survey meter the absorbed dose rates at the surface and at one meter above the ground were measured and the data subjected to statistical analysis using the computer software called Statistical Package for the Social Sciences (SPSS) computer program. Appendix B details the dose rates of various locations in and around Homa Mountain where survey meters readings were taken. The dose rates at other areas including Siaya, Vihiga, Busia and Nairobi were also measured so as to clearly show that the response of the survey meter in high background areas were significantly different. The latter are treated as control point measurements. SPSS analysis of the values obtained from the survey meters was done as contained in Table 5.1.

Table 5.1 Descriptive Statistical Analysis of Absorbed Dose Rates.

Dose Rate Descriptive	Statistic for Sample Size of 250 in nSv hr ⁻¹
Mean	474.1±17.7
95% Confidence Lower Bound	439.2
Interval for Mean Upper Bound	509.0
Median	418.7
Variance	78611.8
Standard Deviation	280.3
Minimum	108.4
Maximum	2681.0
Range	2572.6
Inter quartile Range	335.5
Skewness	2.6±0.1
Kurtosis	15.4±0.3

The median of 418.75 nSv hr⁻¹ is indicated by the vertical line that runs down the centre of the Fig 5.1. The range of 2572.6 nSv hr⁻¹ is represented by the horizontal distance between the smallest value and the largest value including any outliers. The inter quartile range is represented by the width of the box (Q3 minus Q1).

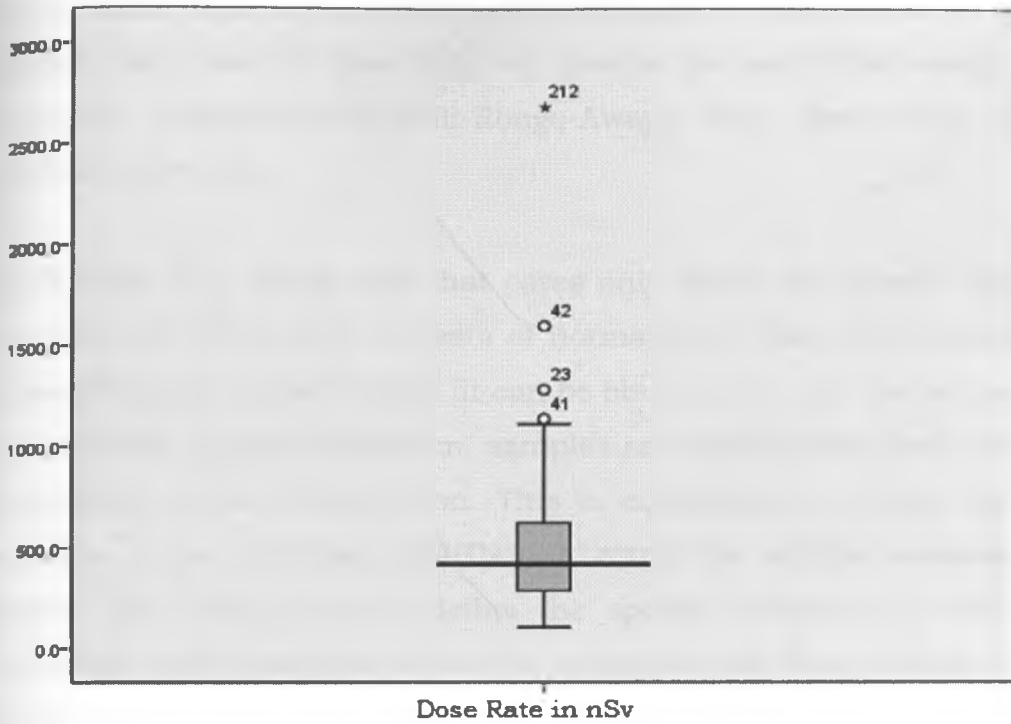


Fig. 5.1 Box plot of the Absorbed Dose Rates values

The Kolmogorov-Smirnov (KS) test tries to determine if two data sets differ significantly. The KS-test has the advantage of making no assumption about the distribution of data. One of the advantages of the KS-test is that it leads to a graphical presentation of the data, which enables the user to detect normal distributions. It can be modified to serve as a goodness of fit test see Table 5.2

Table 5.2. Tests of Normality for Data from Homa Mountain

Kolmogorov - Smirnov ^a				Shapiro - Wilk		
	Statistic	Df	Sig.	Statistic	Df	Sig.
Dose Rate	0.111	250	0	0.835	250	0

a. Lilliefors Significance Correction for sample size of 210 and control of 40

for the whole data set i.e. 250 points although it's possible to do the same for smaller data sets of less than 40 points for particular areas e.g. Homa Mountain, Chiewo-Ndiru Mbili-Rongo-Awaya Hills, Rawe beds, Bala gully, Lambwe valley, etc.

The KS-test is a robust test that cares only about the relative distribution of the data and when used as tests of normality for data within and away from Homa Mountain a distribution fit can be obtained. In the special case of testing for normality of the distribution, samples are standardized and compared with a standard normal distribution. This is equivalent to setting the mean and variance of the reference distribution equal the sample estimate and it is known that using these to define the specific reference is true. One often rejects the null hypothesis when the p-value is less than 0.05 or 0.01. For the Homa Mountain data the distribution changes the null distribution of the null statistic. However, this test is less powerful for testing normality than the Shapiro-Wilk test. In practice the statistic requires relatively large number of data to properly reject the null hypothesis.

The behavior of Homa Mountain data are displayed on Fig. 5.2 on distribution fit superimposed on histogram. Each bar represents the dose rate range, and the height of the bar represents how many values fall into that range. It is evident that the data is skewed to the left, indicating that the tail of the right side is longer than the left side and bulk values lie to the left of the mean. Skewness of the data is indicated by the horizontal line that gravitates towards the end of the scale hence indicating that the data is skewed to the left. Skewness is a measure of the asymmetry of the probability distribution or a real valued random variable. A positive skew implies the data is skewed to the left implying that NORM levels are more towards less activity concentration of K, Th and U. Kurtosis is the measure of the peakedness of the probability distribution of the data points of Homa Mountain area which are real-valued

random variables. A negative kurtosis indicates a distribution that is more peaked than normal.

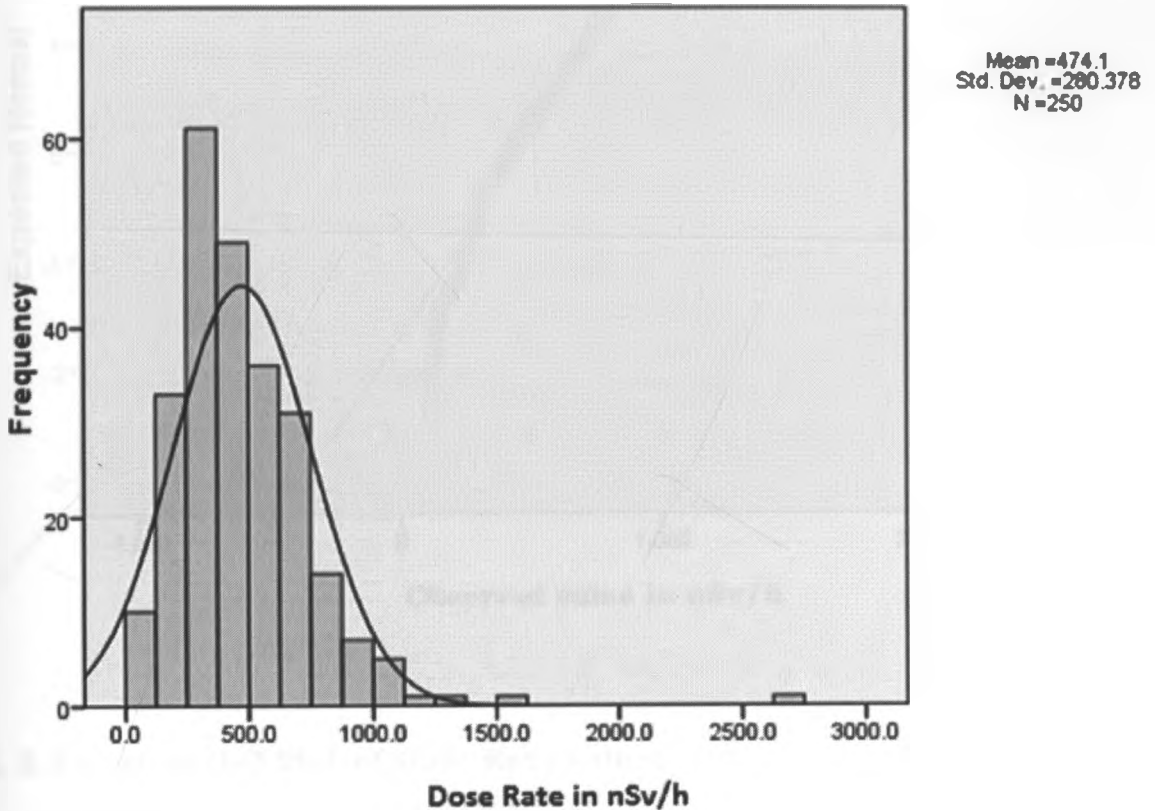


Fig. 5.2 Distribution Fit superimposed on Histogram for Absorbed Dose Rates values

An option for comparison with the normal distribution is given using the Q-Q plot which draws a quantile - quantile plot for the Homa mountain area data. Fig 5.3 shows the relationship between expected normal and observed value It can be seen that most of the data is normally distributed. Any values that touch the black line are normally distributed.

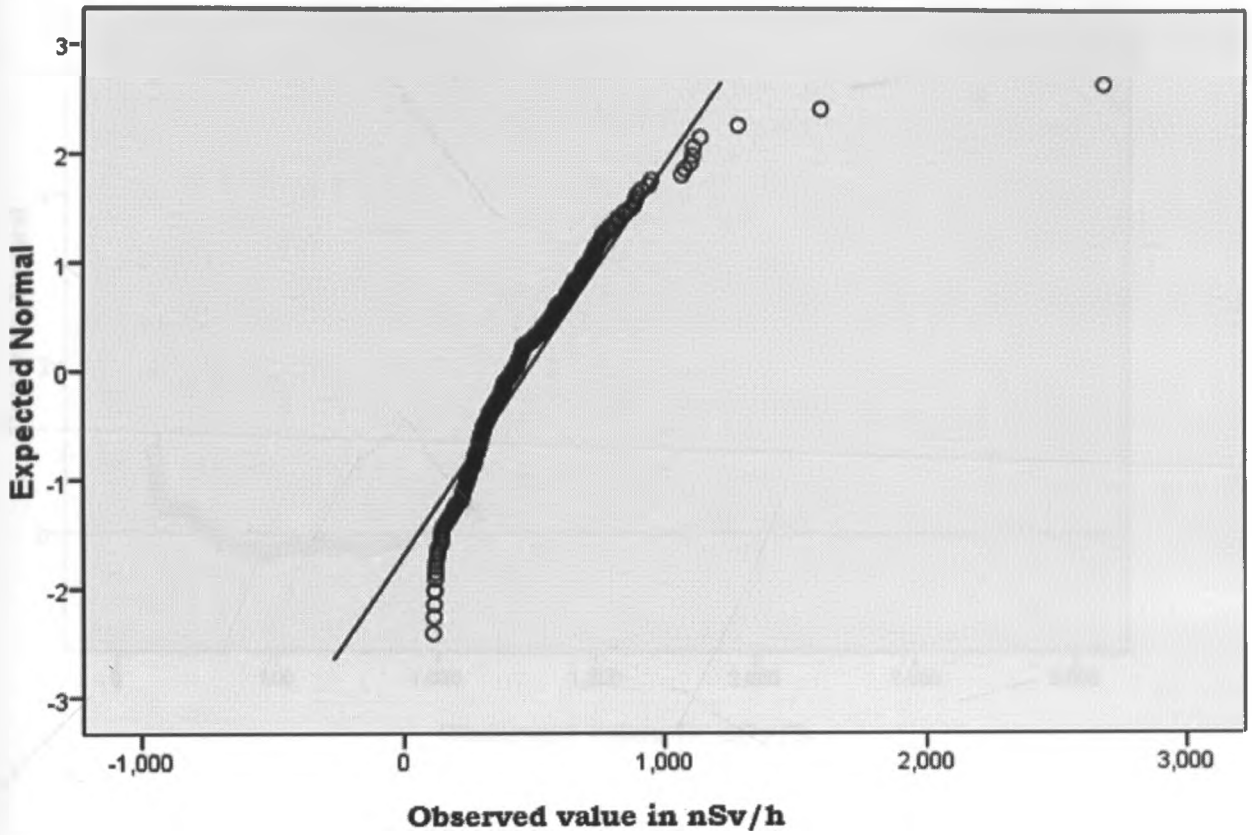


Fig. 5.3 Normal Q-Q Plot of Dose Rate values

Fig 5.4 shows the differenced data that is now stationary, on a Q-Q norm plot. The peakedness of the probability distribution of the data points of Homa Mountain area show a clear negative kurtosis. Homa Mountain data indicates a distribution that is more peaked than normal.

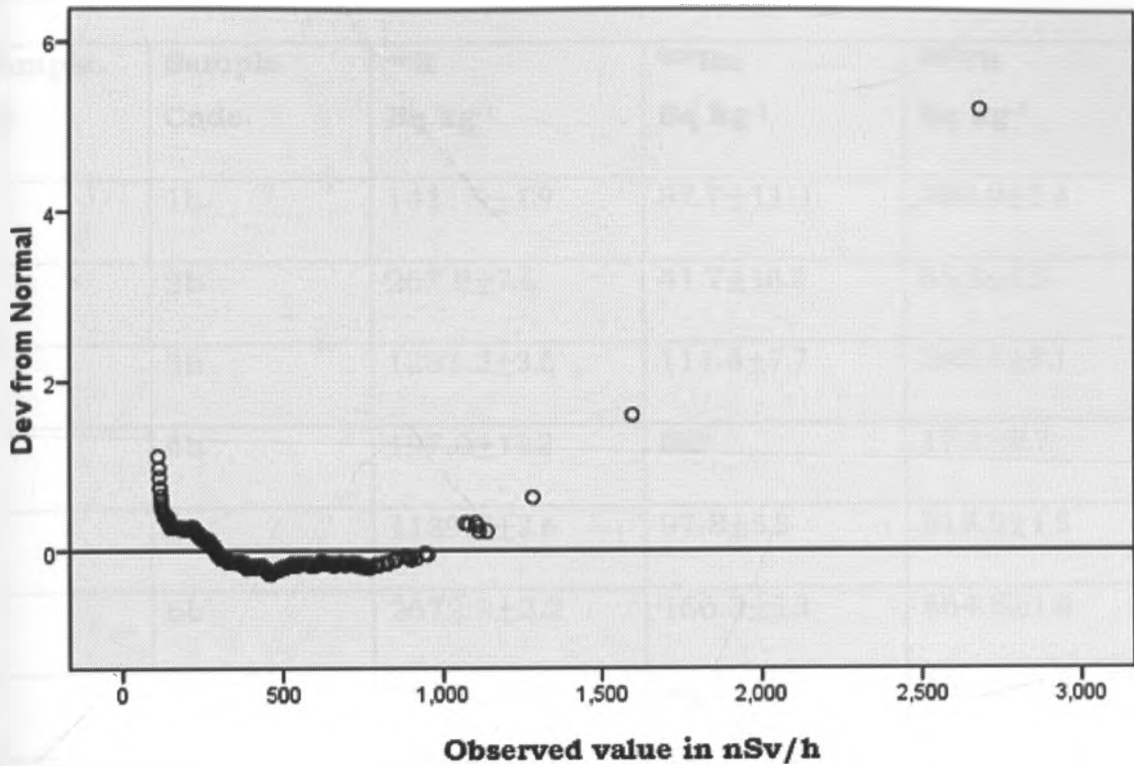


Fig. 5.4 Detrended Normal Q-Q Plot of Dose Rate values

5.3. Concentration of Uranium, Thorium and Potassium in samples

Activity concentration of ^{40}K , ^{232}Th and ^{226}Ra (^{238}U) results of rock and soil samples found in and around Homa Mountain areas are presented in Table 5.3. It shows the mean, range, standard deviation and standard error of mean activity concentrations (in Bq kg^{-1})

Table 5.3 Activity Concentrations of ^{232}Th , ^{226}Ra and ^{40}K in the Rock and Soil Samples.

Sample ID	Sample Code	^{40}K Bq kg⁻¹	^{226}Ra Bq kg⁻¹	^{232}Th Bq kg⁻¹
1	1b	1411.9±1.9	37.7±11.1	309.9±1.4
2	2b	267.2±7.4	41.7±10.2	65.3±5.5
3	3b	1231.2±3.6	111.4±7.7	242.1±3.1
4	4b	197.0±11.2	ND	17.1±8.7
5	5b	1139.5±2.6	97.8±5.3	318.9±1.5
6	6b	2672.9±2.2	166.3±5.3	564.5±1.6
7	7b	1674.2±2.1	95.5±6.4	456.0±1.3
8	8b	1092.3±2.6	49.1±9.9	156.0±3.4
9	9b	216.4±13.1	1567.5±0.4	1005.4±0.5
10	10b	323.2±6.3	49.3±6.8	45.5±6.9
11	11b	1468.5±2.8	ND	111.6±4.3
12	12b	1405.2±2.8	113.2±5.9	421.1±1.5
13	13b	661.6±3.8	47.5±10.2	568.8±1.1
14	14b	279.6±8.8	83.5±7.8	524.9±1.3
15	15b	514.7±4.1	52.4±8.2	231.0±1.8
16	16b	1279.5±2.5	ND	178.2±3.7
17	17b	186.8±11.2	54.3±11.2	675.1±1.1

Table 5.3 Activity Concentrations of ^{232}Th , ^{226}Ra and ^{40}K in the Rock and Soil Samples (cont).

Sample ID	Sample Code	^{40}K Bq kg⁻¹	^{226}Ra Bq kg⁻¹	^{232}Th Bq kg⁻¹
18	18b	260.1±8.7	44.5±13.8	476.3±1.6
19	19b	161.8±9.8	220.2±3.8	559.6±1.4
20	20b	1392.7±2.3	623.0±1.4	271.7±1.8
21	21b	573.3±2.9	487.9±0.9	564.4±0.8
22	22b	1253.6±2.2	ND	994.8±0.4
23	23b	1818.1±2.8	50.6±12.8	212.9±1.7
24	24b	496.0±3.8	80.8±5.3	439.6±1.0
25	25b	2064.5±2.2	454.4±1.9	444.3±1.8
26	26b	63.9±27.1	124.3±4.8	ND
27	27b	454.8±7.0	44.0±15.0	695.5±1.2
28	28b	872.2±3.0	27.5±10.6	67.4±4.1
29	29b	867.9±3.4	40.0±9.9	74.8±4.6
30	30b	2260.5±2.6	351.8±3.2	232.8±4.4
31	31b	1596.4±1.8	85.1±11.8	140.5±3.4
32	32b	108.3±9.8	174.7±5.9	75.1±7.8
33	33b	138.0±8.2	376.9±1.0	54.0±7.4
34	34b	183.5±12.3	421.3±5.0	582.4±1.2

Table 5.3 Activity Concentrations of ^{232}Th , ^{226}Ra and ^{40}K in the Rock and Soil Samples (cont).

Sample ID	Sample Code	^{40}K Bq kg⁻¹	^{226}Ra Bq kg⁻¹	^{232}Th Bq kg⁻¹
35	35b	1174.9±2.6	24.4±16.6	203.1±2.2
36	36b	1341.2±2.1	124.8±4.2	538.8±1.0
37	38b	3017.8±1.5	312.1±2.0	189.0±3.2
38	39b	ND	1398.8±1.1	1160.1±1.2
39	40b	333.5±4.4	36.8±7.2	74.0±3.3
40	41b	920.8±2.9	38.3±23.0	1153.8±0.7
41	42b	670.4±3.8	ND	1447.0±0.8
42	43b	559.3±4.7	76.4±6.9	648.1±0.9
43	44b	300.0±11.8	84.8±9.4	507.7±1.9
44	45b	1382.9±1.7	ND	117.7±2.3
Mean for 44 samples from Homa Mt area		915.6±5.5	195.3±8.3	409.5±4.1
Range		63.9– 3017.8	8.1 – 1567.5	6.3 – 1447.0
Standard Deviation		733.1	322.6	342.6
Standard error of mean		5.4	9.0	4.3

For each rock and soil type more than one measurement was done (at least one at the Institute of Nuclear Science and Technology of the University of Nairobi

and at the National Radiation Protection Laboratory of the Radiation Protection Board and what are shown in Table 5.3 are the mean activity concentrations. The cumulative mean activity concentration for the 44 Homa Mountain samples is 915.6, 195.3 and 409.5 Bq kg⁻¹, with corresponding standard deviation of 733.1, 322.6 and 342.6 Bq kg⁻¹, respectively. The standard deviations depict the spatial variation of the activity concentrations of the natural radionuclides in each rock and soil type. This ranged from non detectable (ND) to highest levels of 3017.8 ± 4.3, 1567.5 ± 9.0 and 1447.0 ± 5.4 Bq kg⁻¹, respectively. Uncertainties of ⁴⁰K, ²³²Th and ²²⁶Ra (²³⁸U) activity concentrations range from 0.05 % to 31.01%.

About 80% of the rock and soil collected at Homa Mountain show ²²⁶Ra (²³⁸U) activity concentration that is higher than the world average value of 35 Bq kg⁻¹ (UNSCEAR 2000), and the average ²²⁶Ra activity concentration value of 195.3 Bq kg⁻¹ is more than 5.58 times the world average value. In 95% of the samples from this study region, the ²³²Th activity concentrations exceed the world average value of 30 Bq kg⁻¹, and the mean ²³²Th activity concentration value of 409.5 Bq kg⁻¹ obtained in this work is 13.65 times higher than the world average value. The mean activity concentrations of ⁴⁰K of 915.6 Bq kg⁻¹ is more than 2 times the world average value of 400 Bq kg⁻¹ reported by UNSCEAR (2000). Only 15 out of 44 samples representing 34% of the samples analyzed in this work show ⁴⁰K activity concentrations lower than 400 Bq kg⁻¹ thw world average. The highest ²³⁸U (²²⁶Ra) activity concentration of 1567.5 ± 0.4 Bq kg⁻¹ (44 times the world average) was found in rhyolites or ijolites from the top of Got Chiewo where the hand held dose rate NaI meter gave a reading of 817 nSv h⁻¹. The highest ²³²Th activity concentration of 1447 ± 0.8 and highest ⁴⁰K activity concentration 3017.8 ± 1.5 came from rock samples taken on top of Homa Mountain. It is about 48 times the world average for ²³²Th and 7.5 times the world average for ⁴⁰K. Notable geological features of the Homa Mountain area that encompasses the hills are steep sided giant outcroppings of rocks that dominate the landscape. Comparatively high values of ²³⁸U (²²⁶Ra), ²³²Th

and ^{40}K in soil and rock samples from top of Chiewo and Homa Mountain may be attributed to the U, Th and K mineralization. Numerous studies such as those undertaken by Nyamai (1989), Mulaha (1989), Patel (1991), Mustapha (1999), Jibiri (2009), Oladele (2009), Shanthi (2009 and 2010) and Otansev et al. (2012)) have shown the presence of radioactive minerals such as zircon, allanite, apatite and monazite in the rocks together with high potassium feldspar correlate well with the high activity measured comparable to the values in Homa Mountain area.

A comparison of the mean activity concentration values obtained in this study with values from other regions of the world is presented in Table 5.4. Some are the national averages while others are of specific geological rock base or an area of interest. Table 5.4 shows that the mean activity concentration values obtained in this study are higher than those obtained in all the countries considered, while they are lower than those obtained in Yemen, Saudi Arabia and Turkey for ^{40}K only. Homa Mountain area thus qualifies to join the ranks of high background radiation areas in the world. Compared with the worldwide average concentration in soils and rocks, the present study results are higher for most of the analyzed samples indicating a possible accumulation of U, Th and K in Homa Mountain region, which may be due to geochemical processes.

Table 5.4: Comparison of mean activity concentration values (Bq kg-1) of rock and soil samples from different Countries

Sample ID	^{40}K	^{226}Ra	^{232}Th	Reference
Mean for 44 samples from Homa Mt area	915.6	195.3	409.5	This Study
Kenya (national average)	255.7	28.7	73.3	Mustapha (1999)
Kenya (Carbonatites)	185.6	179.0	950.2	Mustapha (1999)

Table 5.4: Comparison of mean activity concentration values (Bq kg⁻¹) of rock and soil samples from different Countries (cont).

Sample ID	⁴⁰ K	²²⁶ Ra	²³² Th	Reference
Southwestern Region(Nigeria)	286.5	54.5	91.1	Oladele (2009)
Turkey	1,207.0	115.0	192.0	Merdanoglu (2006)
HBRA, India	1585	44	215	Shanthi (2009)
Kenyakumari, India	940	20	114	Shanthi (2010)
Yemen (granite and gneiss)	1,742.8 and 2,341	53.6 and 22	27 and 121	Abd El-Mageed (2010)
Spain (national average)	650.0 (48 – 1570)	46.0 (13 – 165)	49.0 (7 – 204)	Baeza (1992)
Punjab Province (Pakistan)	615.0	35.0	41.0	Tahir (2005)
Bangalore (India)	635.1	26.2	53.1	Shiva Prasad (2008)
Bangladesh	833	42	81	Chowdhury (2005)
Saudi Arabia	1099	76.4	81	Alharbi (2011)
World's average	400	35	30	UNSCEAR, 2000

Using Eqs 3.5 to 3.11 the values for absorbed dose rate (D_R), annual outdoor effective dose equivalent (H_R), Radium equivalent activity (Ra_{eq}), representative level index (I_{γ}), gamma activity index (I), external hazard index (H_{ex}) and internal hazard index (H_{in}) were calculated for the 44 rock and soil samples from Homa Mountain area and are presented in Table 5.5.

Table 5.5 Calculated Radiological Indices for the Homa Mountain area.

	D _R	H _R	R _{a_{eq}}	I _{γ_t}	I	H _{ex}	H _{in}
1b	283.20	0.347	589.26	4.29	2.14	1.59	1.69
2b	72.78	0.089	155.58	1.10	0.55	0.42	0.53
3b	261.74	0.321	552.16	3.98	1.99	1.49	1.79
4b	23.31	0.028	47.70	0.35	0.17	0.12	0.15
5b	303.14	0.372	641.24	4.60	2.30	1.73	1.99
6b	561.90	0.689	1178.78	8.53	4.26	3.18	3.63
7b	416.46	0.511	876.03	6.31	3.15	2.36	2.62
8b	171.83	0.210	356.13	2.61	1.30	0.96	1.09
9b	1348.22	1.654	3020.87	20.64	10.32	8.16	12.39
10b	65.25	0.080	139.20	0.99	0.49	0.37	0.50
11b	137.47	0.168	272.55	2.09	1.04	0.73	0.73
12b	389.21	0.477	823.15	5.90	2.95	2.22	2.52
13b	427.55	0.524	911.25	6.44	3.22	2.46	2.59
14b	397.26	0.487	855.11	5.99	2.99	2.31	2.53
15b	198.35	0.243	422.13	3.00	1.50	1.14	1.28
16b	180.31	0.221	368.66	2.73	1.36	0.99	1.03
17b	480.83	0.590	1033.40	7.23	3.61	2.79	2.93
18b	347.40	0.426	745.16	5.23	2.61	2.01	2.13
19b	473.67	0.581	1032.3	7.17	3.58	2.78	3.38
20b	506.85	0.622	1118.4	7.79	3.89	3.02	4.70
21b	608.87	0.747	1338.5	9.27	4.63	3.61	4.93
22b	724.04	0.888	1535.8	10.90	5.45	4.14	4.19
23b	348.60	0.427	747.1	5.26	2.63	2.01	2.23
24b	241.57	0.296	494.8	3.68	1.83	1.33	1.47
25b	578.70	0.710	1248.2	8.84	4.42	3.37	4.60
26b	60.01	0.073	138.2	0.93	0.46	0.37	0.70
27b	501.54	0.615	1072.8	7.55	3.77	2.89	3.01

Table 5.5 Calculated Radiological Indices for the Homa Mountain area (cont).

	D _R	H _R	Ra _{eq}	I _{yr}	I	H _{ex}	H _{in}
28b	94.13	0.115	190.9	1.43	0.71	0.51	0.59
29b	104.21	0.127	213.7	1.59	0.79	0.57	0.68
30b	402.46	0.493	858.5	6.18	3.09	2.31	3.27
31b	198.55	0.243	408.7	3.03	1.51	1.10	1.33
32b	129.27	0.158	290.3	1.98	0.99	0.78	1.25
33b	202.83	0.248	464.6	3.14	1.57	1.25	2.27
34b	283.20	0.347	1267.6	8.75	4.37	3.42	4.56
35b	196.20	0.240	405.0	2.97	1.48	1.09	1.16
36b	469.80	0.576	998.0	7.13	3.55	2.69	3.03
38b	388.90	0.477	814.5	5.98	2.99	2.20	3.04
39b	1369.91	1.681	3056.6	20.92	10.46	8.25	12.04
40b	79.33	0.097	168.2	1.20	0.60	0.45	0.55
41b	824.37	1.011	1757.9	12.40	6.20	4.74	4.85
42b	992.52	1.218	2119.3	14.91	7.45	5.72	5.72
43b	488.30	0.599	1045.6	7.36	3.68	2.82	3.03
44b	387.23	0.475	833.4	5.84	2.92	2.25	2.48
45b	145.24	0.178	291.9	2.21	1.10	0.78	0.83
Sum	16625.15	20.403	36405.9	256.94	128.47	98.36	120.74
Mean	383.33	0.470	838.6	5.93	2.96	2.26	2.77
max	1369.91	1.681	3056.6	20.92	10.46	8.25	12.39
Min	23.32	0.028	47.70	0.35	0.17	0.12	0.15
StDev	302.06	0.370	671.10	4.61	2.30	1.81	2.52

Absorbed dose rates in air, D_R , values

The mean absorbed dose rate of $383.36 \text{ nGy hr}^{-1}$ shown on Table 5.5 is higher than the estimate of average global terrestrial radiation which ranges $24 - 160 \text{ nGy hr}^{-1}$ (UNSCEAR 2000). The maximum level of $1.37 \text{ } \mu\text{Sv h}^{-1}$ which translate to 12 mSv y^{-1} for a resident living there that was measured is way beyond the dose limit of 1 mSv y^{-1} for the general public and compares more with the 20 mSv y^{-1} for radiation workers (Kenya Government 1982, IAEA 1996), while the inhabitant of Homa Mountain area possibly will receive 60 mSv in 5 years a value tolerated for radiation workers whose limit as cumulative dose is 100 mSv in any 5 years. As noted by Al-Saleh and Al-Berzan (2007) due to the health risks associated with the exposure to indoor radiation, many governmental and international bodies such as the International Commission on Radiological Protection (1983, 1984, 1990, 1995 and 2007), the World Health Organization (2001), IAEA (1996, 1999 and 2004) etc. have adopted strong measures aimed at minimizing such exposures. In this context, limits have been set on the concentrations of radionuclides in various building materials and the use of materials with abnormally high levels of radioactivity has been banned. Local authorities lead by the Radiation Protection Board (RPB), National Environmental Management Authority (NEMA) etc. can limit the use of building materials that cause a significant increase in radiation exposure due to high levels of indoor Radon and external gamma exposure.

Annual outdoor effective dose equivalent, H_R , values

The results for the calculation of annual outdoor effective dose equivalent values are displayed in Table 5.5. The values vary between 0.028 to 1.68 mSv y^{-1} with a mean value of 0.470 mSv y^{-1} and a standard deviation of 0.370 mSv y^{-1} . This is above the world average of $0.070 \text{ mSv year}^{-1}$ for outdoor terrestrial radiation for regions of normal radiation background (UNSCEAR 2000) by a factor of 6.71 but compare, to those reported by Mustapha (1999) i.e. effective dose of 0.509 mSv y^{-1} from natural stone ranging between 0.155 to 1.559 mSv

y^{-1} . The logical conclusion is that Homa Mountain area is a high background radiation area. Alharbi et al. (2011) while noting dose to members of the Public for granite in the southeastern Arabian Shield areas concluded that results above the world average of $0.07 \text{ mSv } y^{-1}$ would show that the radiation burdens do pose as a source of radiation contamination or hazard to the environment. According to international recommendations (UNSCEAR 1988, 1993 and 2000), which the Radiation Protection Act (Kenya Government 1982) adopts in case of non local law, quoted in the Basic Safety Series No 115 from the International Atomic Energy Agency (IAEA 1996), the use of building materials containing enhanced concentrations of NORM should be controlled and restricted under the application of radiation safety standards.

Radium equivalent activity, Ra_{eq} , values

The Radium equivalent activity, Ra_{eq} , provides a basis for comparing the activity concentrations of ^{226}Ra , ^{232}Th and ^{40}K in rocks and soils so as to obtain the total radioactivity. The results displayed in Table 5.5 vary from 47.7 to 3,056.6 Bq kg^{-1} with a mean of 838.6 Bq kg^{-1} and a standard deviation of 671.1 Bq kg^{-1} . The mean value is higher than the permissible maximum value of 370 Bq kg^{-1} (UNSCEAR 1988; OECD 1979). Since the annual effective dose for an Ra_{eq} value of 370 Bq kg^{-1} corresponds to an effective dose of 1.0 mSv for the general population (Tahir et al. 2005), the observed mean Ra_{eq} value of 838.60 Bq kg^{-1} corresponds to an annual effective dose of about 2.26 $\text{mSv } y^{-1}$. Note that the use of building materials with Ra_{eq} values higher than 370 Bq kg^{-1} is restricted to avoid health hazards of radiation (Beretka and Mathew 1985). Therefore the use of 33 out of the 44 sampled (75%) rocks and soils for buildings (especially mud block or soil brick houses) should be discouraged by appropriate authorities led by the Radiation Protection Board (RPB) and National Environment Management Authority (NEMA).

Representative level index, $I_{\gamma r}$, values

The ICRP-60 (1990) recommended that any exposure above the natural background radiation should be kept as low as reasonably achievable (ALARA) but below the individual dose limits, which for radiation workers averaged over 5 years is 100 mSv and for members of the general public is 1 mSv y^{-1} . These dose limits have been established on the prudent approach by assuming that there is no threshold dose below which there would be no effect. This means that any additional dose will cause a proportional increase in the chance of a health effect. This relationship has not yet been established in the low dose range where the dose limits have been set. It is therefore important to measure the quantities (concentrations of radionuclides and their radiation hazard indices) in the environment in order to enable assessment of their health impacts. The calculated values of the representative level index ($I_{\gamma r}$) are also presented in Table 5.5. This index varies from 0.35 to 20.92 with a mean value of 5.93 and a standard deviation of 4.61. The mean value exceeds the limit of 1.00 for $I_{\gamma r}$, and also the mean (1.13) for Bangalore (India) soils reported by Prasad et al (2008) and for cement in China reported by Xinwei (2005). It is exceeded in over 92% of the investigated rock and soil samples. Grazing of cattle, growing food on such soils and residing in Homa Mountain area guarantees one of high background radiation exposure.

Gamma activity, I , index

Table 5.5 shows the gamma activity index I to vary from 0.17 to 10.46 with a mean value of 2.96 and a standard deviation of 2.30. The mean value is higher than the upper limit of 1.0 for undisturbed soil in more than 81% of the rock and soil samples. Given (Malozewski et al. 2004; Tahir et al. 2005; Ryan et al. 2004; Mohsen et al. 2007; Mossman 2009) that a value less than 1.0 (or 0.5) corresponds to an absorbed gamma dose rate in air of less than 1.00 mSv y^{-1} (or 0.30 mSv y^{-1}), greater than 81% (97%) of the sampled areas show an absorbed gamma dose rate of more than 1.00 mSv y^{-1} (0.30 mSv y^{-1}). On

average an inhabitant of Homa Mountain area receives an absorbed dose rate in air that results in excess of 1.00 mSv y^{-1} .

External hazard index, H_{ex} , values

From Table 5.5 H_{ex} values vary from 0.12 to 8.25 with a mean of 2.26 and a standard deviation of 1.81. For the radiation hazard of a building raw material to be considered acceptable, the value of this hazard index must be less than 1.00 corresponding to less than $1.50 \text{ mSv year}^{-1}$. It turns out that the mean value of H_{ex} (2.28) for the Homa Mountain area is higher than 1.00 for 71% of the rock and soil samples criterion (Alharbi et al. 2011) which considers only the external exposure risks due to gamma rays and corresponds to the maximum R_{eq} of 370 Bq kg^{-1} for the material. The model although accepted by former Soviet Union and Norway (OECD 2011) was considered conservative and later corrected after considering a finite thickness of walls and the existence of windows and doors through the application of a weighing factor of 0.7 in each case resulting in the maximum permissible concentrations being increased by a factor of 2. For the maximum value of H_{ex} to be less than unity, the maximum value of R_{eq} must be less than 370 Bq kg^{-1} and hence applying the criterion for gamma activity the results indicate that most samples from Homa Mountain should not be used in building construction as they would surpass the proposed radiation criterion level. This implies that their use for buildings (especially mud block or soil brick houses) should be discouraged by appropriate authorities led by the RPB and NEMA.

Internal hazard index, H_{in} , values

In addition to the external irradiation radon and its short-lived products are also hazardous to the respiratory organs. The internal exposure to radon and its daughter products is quantified by the internal hazard index, H_{in} . If the maximum concentration of radium is half that of the normal acceptable limit then H_{in} will be less than 1.0. For safe use of material in the construction of dwellings, H_{in} , should be less than unity. From Table 5.5 H_{in} values vary from

0.15 to 12.39 with a mean value of 2.77 and a standard deviation of 2.52. H_{in} describes the risk from radon (^{222}Rn), a progeny of ^{226}Ra , and its short-lived decay products to the internal respiratory organs whose account is suggested by Eq. 3.11. The limit 1.00 for H_{in} was exceeded for 76% of the rock and soil samples implying that most samples under investigation should not be used as building construction as they would exceed the proposed radioactivity criterion (Viruthagiri and Ponnarasi 2011). Rock and soil from Homa Mountain area and their use for buildings (especially mud block or soil brick houses) should be discouraged by appropriate authorities led by the RPB and NEMA.

5.4 Exposure Pathways and Dose Estimation using RESRAD

A procedural adaptation of RESRAD was developed in order to use the code to estimate dose due to continual exposure to and intake of NORM, and is presented in this study. The dose limit or dose constraint used as a basis for the guidelines depends on the requirements of the regulation, as does the selection of the land use scenario for demonstrating compliance. When the mean activity concentration for the 44 Homa Mountain samples shown on Table 5.3 i.e. 915.6, 195.3 and 409.5 Bq kg⁻¹ of ^{40}K , ^{232}Th and ^{226}Ra , respectively is used in the RESRAD code the TED for the resident farmer exposure scenario for an infant, 1, 5, 10, 15 year old and adult for water independent pathways for ground, inhalation, Rn, plant, meat, milk and rock/soil is as shown in Table 5.6.

Table 5.6 Total Effective Dose Contributions for individual radionuclides and pathways for water independent pathways (inhalation excludes Rn)

(a)

Infant resident farmer exposure scenario						
Element/water pathway	Ground mSv y ⁻¹	Inhalation mSv y ⁻¹	Plant mSv y ⁻¹	Meat mSv y ⁻¹	Milk mSv y ⁻¹	Rock/soil mSv y ⁻¹
⁴⁰ K	0.15	1.44E-6	1.52	0.77	0.32	0.0016
²²⁶ Ra	0.22	3.01 E-4	2.36	0.071	0.081	0.023
²³² Th	0.084	0.0062	6.85	0.18	0.23	0.11
Total	0.46	0.0065	10.73	1.02	0.62	0.13
Total Effective Dose from all pathways is 12.94 mSv y⁻¹						

(b)

1 year resident farmer exposure scenario						
Element/water pathway	Ground mSv y ⁻¹	Inhalation mSv y ⁻¹	Plant mSv y ⁻¹	Meat mSv y ⁻¹	Milk mSv y ⁻¹	Rock/soil mSv y ⁻¹
⁴⁰ K	0.14	9.62 E-7	0.97	0.49	0.20	0.001
²²⁶ Ra	0.22	2.72 E-4	0.59	0.018	0.018	0.008
²³² Th	0.22	0.0066	2.70	0.75	0.093	0.028
Total	0.58	0.0069	4.26	0.58	0.31	0.037
Total Effective Dose from all pathways is 5.76 mSv y⁻¹						

(c)

5 year resident farmer exposure scenario						
Element/water pathway	Ground mSv y ⁻¹	Inhalation mSv y ⁻¹	Plant mSv y ⁻¹	Meat mSv y ⁻¹	Milk mSv y ⁻¹	Rock/soil mSv y ⁻¹
⁴⁰ K	0.15	4.50E-7	0.51	0.26	0.11	5.39 E-5
²²⁶ Ra	0.25	1.67 E-4	0.32	0.0098	0.011	0.0033
²³² Th	0.084	0.0043	0.77	0.020	0.026	0.010
Total	0.46	0.0045	1.61	0.29	0.14	0.014
Total Effective Dose from all pathways is 2.51 mSv y⁻¹						

(d)

10 year resident farmer exposure scenario						
Element/water pathway	Ground mSv y ⁻¹	Inhalation mSv y ⁻¹	Plant mSv y ⁻¹	Meat mSv y ⁻¹	Milk mSv y ⁻¹	Rock/soil mSv y ⁻¹
⁴⁰ K	0.15	2.70 E-7	0.32	0.16	0.067	3.34 E-4
²²⁶ Ra	0.22	1.07 E-4	0.39	0.012	0.013	0.0036
²³² Th	0.084	0.0034	0.88	0.023	0.029	0.010
Total	0.46	0.0035	1.59	0.19	0.11	0.014
Total Effective Dose from all pathways is 2.49 mSv y⁻¹						

(e)

15 year resident farmer exposure scenario						
Element/water pathway	Ground mSv y ⁻¹	Inhalation mSv y ⁻¹	Plant mSv y ⁻¹	Meat mSv y ⁻¹	Milk mSv y ⁻¹	Rock/soil mSv y ⁻¹
⁴⁰ K	0.15	1.50 E-7	0.19	0.094	0.039	1.94 E-4
²²⁶ Ra	0.25	8.91 E-5	0.71	0.021	0.025	0.0012
²³² Th	0.084	0.0032	1.18	0.031	0.040	0.012
Total	0.46	0.0032	2.08	0.15	0.10	0.018
Total Effective Dose from all pathways is 2.85 mSv y⁻¹						

(f)

Adult resident farmer exposure scenario						
Element/water pathway	Ground mSv y ⁻¹	Inhalation mSv y ⁻¹	Plant mSv y ⁻¹	Meat mSv y ⁻¹	Milk mSv y ⁻¹	Rock/soil mSv y ⁻¹
⁴⁰ K	0.15	1.26E-7	0.15	0.077	0.032	1.59 E-4
²²⁶ Ra	0.22	8.44 E-5	0.14	0.0042	0.0048	0.0013
²³² Th	0.084	0.003	0.16	0.0042	0.0052	0.0038
Total	0.46	0.003	0.45	0.085	0.042	0.0053
Total Effective Dose from all pathways is 1.03 mSv y⁻¹						

The contribution of dose from ground, inhalation and Rn is similar for all age sets, about 0.46, 0.003 and 0 mSv y⁻¹, respectively, but there are differences for contribution from plant with the infant and 1 year old child scenario registering higher dose (10.73 and 4.26 mSv y⁻¹ respectively) while adult registers least dose (0.45 mSv y⁻¹). The same is seen for milk which again infants (0.62 mSv y⁻¹) show highest exposure with adults displaying the lowest (0.042 mSv y⁻¹). Both the U.S. Department of Energy (DOE) and the U.S. Nuclear Regulatory Commission (NRC) use 0.25 mSv y⁻¹ as the general limit or constraint for soil cleanup or site decontamination (Yu et al. 2001). For all age sets (born and raised, spending all their childhood and adult life in Homa Mountain) the amount of dose from NORM from all sources (K, U and Th) and sum of all pathways (ground, inhalation, Rn, plant, meat, milk and rock/soil) that exceeds the compliance limit of 0.25 mSv y⁻¹ is 52 times (for an infant whose TED is 12.94 mSv y⁻¹) while for an adult it is 4 times.

For Homa Mountain Fig 5.5 gives the RESRAD deduced dose for summation of ⁴⁰K, ²²⁶Ra and ²³²Th when all pathways are summed. It can be seen that for an infant and child the exposure due to ⁴⁰K is significant contributing up to 1 mSv y⁻¹ for the first four years, while beyond 5 years ²³²Th becomes dominant. It is joined by ²²⁶Ra after 11 years of the individual residing in Homa Mountain. Hence a resident farmer or fisher-man/woman living around Homa Mountain all his/her life receives an additional dose beyond 3 mSv y⁻¹ after age 10 to the normal background.

DOSE: All Nucleides Summed, Pathways Summed

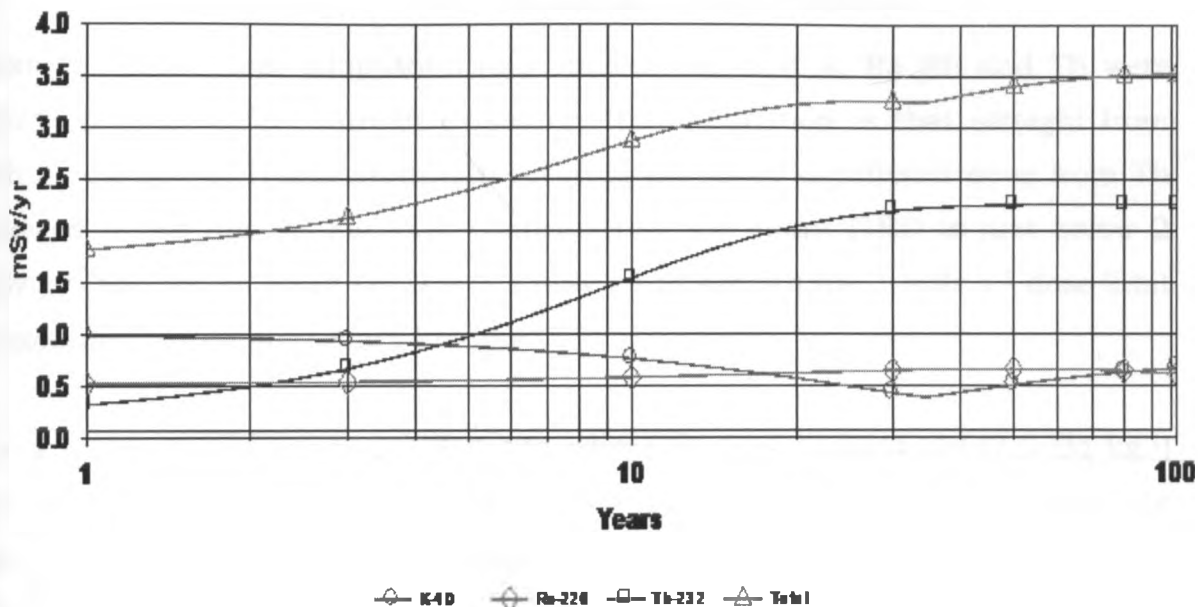


Fig. 5.5 Annual dose when Mean Activity Concentrations of ^{40}K , ^{226}Ra and ^{232}Th all pathways is summed

First, the annual radiation dose received by a member of the general public from residual radioactive material — predicted by a realistic but reasonably conservative analysis of the actual or likely future use of the site and calculated as the TED — should not exceed the dose constraint of 0.25 mSv y^{-1} . Second, doses should be ALARA when health and environmental impacts, economics, cultural and natural resources, and other appropriate factors are taken into account. DOE guidance indicates that the final authorized limits should be based on a realistic assessment of future use of the subject property yet be sufficiently protective to ensure that the other less likely, but plausible, use scenarios would not cause potential doses to exceed 1 mSv y^{-1} . The worst-case use scenario is typically the resident farmer/fisher/herder scenario. In cases in which this scenario is not realistic but is plausible, it can generally be assumed to be the most restrictive use and, therefore, may be used to

demonstrate that the potential uses for all plausible scenarios will not exceed the 1 mSv y⁻¹ dose limit.

From the procedural adaptation and considering that K, Ra (U) and Th were always present before human existence, the implication is that straight from birth a resident of Homa Mountain receives the most significant dose from Th followed by Ra and K. Fig. 5.5. confirms that an infant (TED is just below 2 mSv y⁻¹) and for an adult (TED is 3.5 mSv y⁻¹ at age 70) the 1 mSv y⁻¹ dose limit is exceeded throughout one's lifetime.

For a resident farmer at sampled site where Th was highest (1447.0 Bq kg⁻¹) the summation of dose due to ⁴⁰K, ²²⁶Ra and ²³²Th when all pathways are added is shown in Fig 5.6. Beyond age 2 the contribution due to Th is most significant and remains that way leveling at age 12 around 6 mSv y⁻¹ for the remainder of the inhabitants lifetime. From procedural adaptation the implication is that from birth to adulthood an inhabitant here receives TED of almost 6 mSv y⁻¹ a value 6 times the dose limit for public exposure limit.

For a resident farmer at sampled site where U was highest (1567.5 Bq kg⁻¹) the summation of dose due to ⁴⁰K, ²²⁶Ra and ²³²Th when all pathways are added is shown in Fig 5.7. The ²²⁶Ra is significant from age 1 and remains dominant for the rest of the lifetime of the individual. From procedural adaptation the implication is that from birth to adulthood the resident farmer receives TED of almost 9 mSv y⁻¹, a values 9 times the dose limit for members of the public.

For a resident farmer at sampled site where K was highest (3,017.8 Bq kg⁻¹) the summation of dose due to ⁴⁰K, ²²⁶Ra and ²³²Th when all pathways are added is shown in Fig 5.8. The contribution of K is only significant for the first 10 years and its overtaken thereafter by Ra first and later Th. The TED from all radionuclides for all pathways is less than 3 mSv y⁻¹ though showing that Ra and Th give considerable doses due to their progenies. Using procedural

adaptation the TED for a resident farmer from birth to adulthood is above 1.5 times the dose limit.

DOSE: All nuclides Summed, Pathways Summed

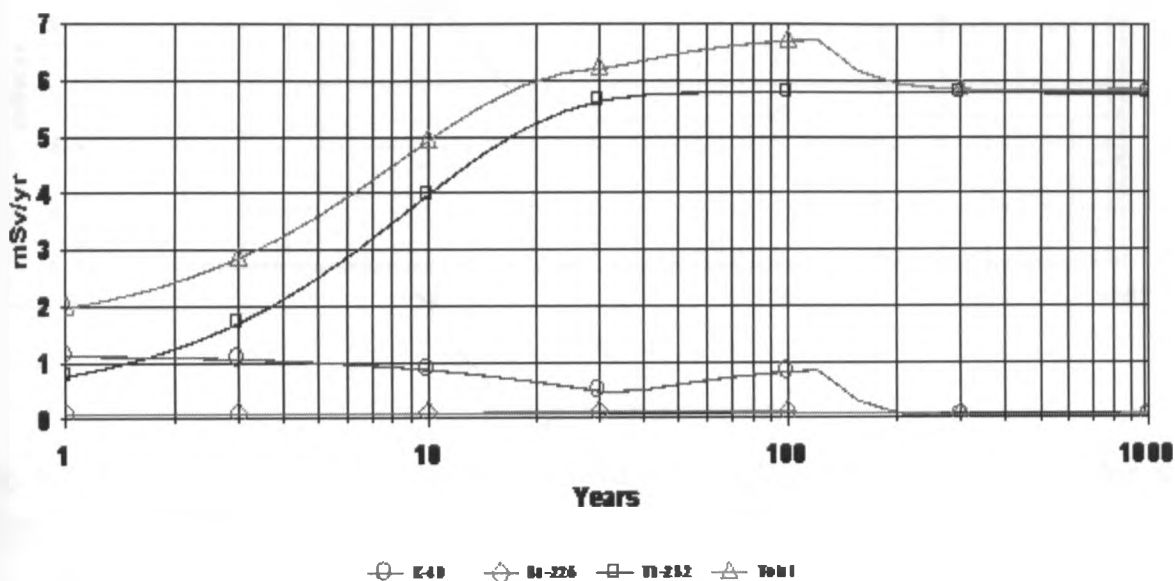


Fig. 5.6 Annual dose when ^{40}K , ^{226}Ra and ^{232}Th all pathways summed for a 1,000 year extrapolation for sample with highest Th.

In all the three cases in which the resident farmer scenario is the likely future use, the 0.25 mSv y^{-1} constraint as used in USA for developing the guideline values would render Homa Mountain area not habitable. When all significant exposure pathways for the critical population group are considered in deriving soil guidelines an extrapolation of 1000 years still renders the Homa Mountain area not usable for release to a resident farmer as shown in Figs 5.6, 5.7 and 5.8.

DOSE: All nuclides Summed, Pathways Summed

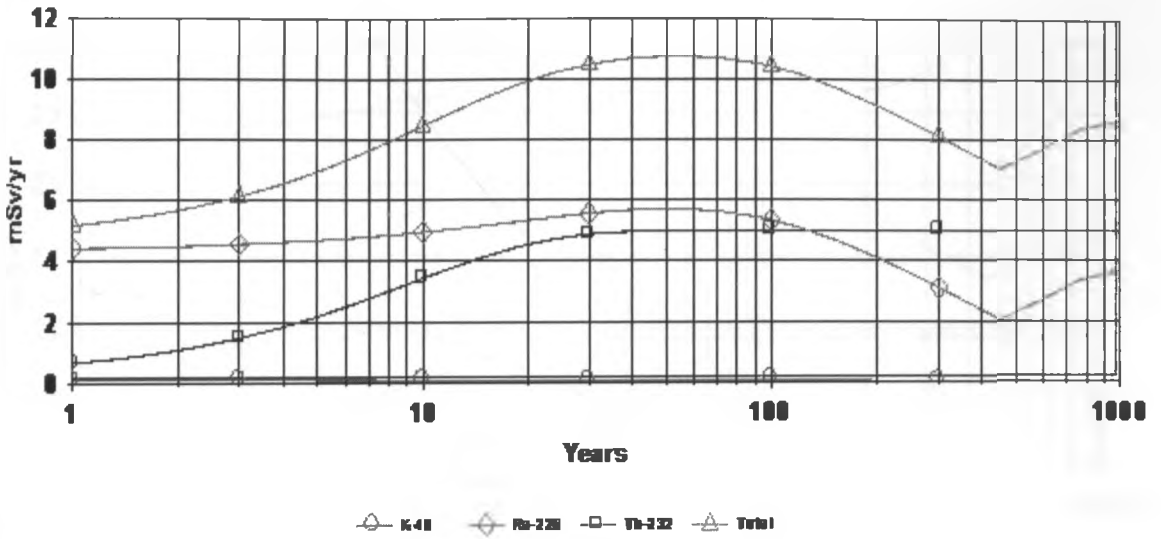


Fig. 5.7 Annual dose when ^{40}K , ^{226}Ra and ^{232}Th all pathways summed for a 1,000 year extrapolation for sample with highest U

In the procedural adaptation of RESRAD described earlier, the TED calculated by RESRAD is adjusted to account for deviations from the user specified radionuclide concentrations in those calculated by RESRAD. The magnitude of the deviation from the user specified values is dependent on the 'Time Since Material Placement' (TI). Since RESRAD is primarily used to model the movement of radioactive materials following a spill, leak, or artificial placement, the use of TI stands to reason. However, with respect to NORM and the general assumption of time constant concentration, a TI cannot be determined and has

DOSE: All Nuclides Summed, Pathways Summed

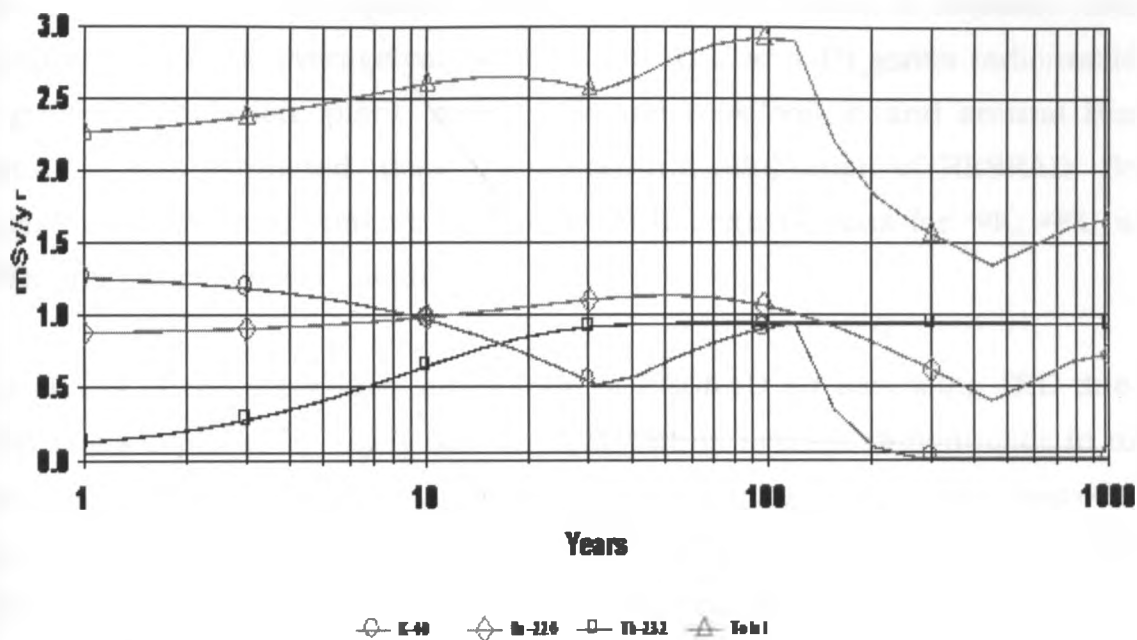


Fig. 5.8 Annual dose when ^{40}K , ^{226}Ra and ^{232}Th all pathways summed for a 1,000 year extrapolation for sample with highest K

no true meaning. Additionally, ^{40}K , ^{238}U and ^{232}Th are primordial in origin and the time since their placement into the environment is not relevant and outside the scope of possibility for modeling. RESRAD is designed with the assumption that the radionuclide concentration in ground water is due to leaching of radioactive materials through the rock and soil. This assumption can be overridden with the input of a TI and a water concentration, although TI must agree with the input water concentration or else the code is designed to override the user specified concentration and compute one based on the leaching from the soil (Yu et al. 2001).

As a general trend, RESRAD calculated for rock/soil concentration varied more for larger values of TI, which is expected because a larger time allows for greater movement of radioactivity in the environment. RESRAD calculated

radionuclide concentration in soil did not vary from the user specified value for any calculation encountered. The pattern of variances was fairly erratic. The TED to infants, 1, 5, 10 and 15 year olds plus adults in a resident farmer scenario due to the average concentration of K, U and Th series radionuclides in ground, inhalation, plant, meat, milk and rock/soil in and around Homa Mountain was estimated using the procedural adaptation of RESRAD. Both water dependent and water independent TED contributions for ^{40}K , ^{238}U and ^{232}Th and pathways were deduced.

The effects of the procedural adaptation of RESRAD for assessing TED due to NORM was explored by using the Homa Mountain average radionuclide in rock and soil samples and comparing the value estimated using the procedural adaptation of RESRAD yields interesting observations. The estimated annual TED to the adult from all pathways was calculated to be 1.05 mSv y^{-1} , which is 4.2 times higher than the US EPA dose limit of 0.25 mSv y^{-1} (Yu 2001) for actual or likely use of the site. For adults at Homa Mountain exposed in a resident farmer scenario, TED estimated using the default procedures was 4 times greater than the 0.25 mSv y^{-1} dose constraint, but 16 times higher when compared to that derived from hand held dose rate meters and 13 times higher when compared to the value from activity concentration values obtained from HpGe measurements. The estimated annual TED to infants from sum of all water independent and dependent pathways is 12.97 mSv y^{-1} . The highest contributor to the infant estimated TED is the water independent plant ingestion pathway, accounting for 10.73 mSv y^{-1} . It is possible so due to the fact that most foodstuffs taken by local inhabitants and children in particular consist of high intake of plant food (maize, beans, vegetables, fruits etc.) account for more intake than animal and fish products.

As the basis for the concept of EDFs, linearity of TED with environmental radionuclide concentration was necessary. Consequently, TED estimated using the procedural adaptation of RESRAD is a strong linear function of both

rock/soil and groundwater concentration. The factors used to estimate TED due to K, U and Th using elemental activity concentrations, EDFs, were calculated for various age groups and exposure scenarios. Generally the EDFs for U and K decrease as age increases with slightly increased dose for teenagers. This trend is graphically shown in Figs 5.7 and 5.8. For Th in rock and soil, including dose due to Rn inhalation, Th EDFs ranged for adults recreationists to $116 \mu\text{Sv kg (Bq yr)}^{-1}$ for infants exposed in a resident farmer scenario. The differences in Th EDFs caused by the dose due to inhalation of Rn were negligible.

The contribution to the total EDF for U corresponding to the resident farmer exposure scenario were separated by pathway and compared for various age groups. For the rock and soil EDFs corresponding to infants, the primary dose contributing pathway was the combined 'Foodstuff' pathway, with plant contributing 82% of the TED per Bq kg^{-1} K, U and Th. For adults, the primary dose contributing pathway was also foodstuff pathway with plant accounting for 43% of the TED per Bq kg^{-1} U. The contribution of each pathway is shown in Table 5.6.

The variations in the age dependent DCFs are further illustrated in Figs 5.5 and 5.8. Since RESRAD did not consider the age dependence of dose due to Rn inhalation, the contribution due to Rn inhalation is constant for each age group for a given exposure scenario; however, the present contribution to the whole dose, and in particular the EDF, due to Rn is not constant since the magnitude of the dose from the other pathways is age dependent. The use of constant Rn DCF corresponding to an age constant Rn dose is reasonable. According to BEIR VI, the ratio between the dose to adults and infants, as extrapolated from the 'k-factors' presented in that report, is nearly unity (OECD 2011). Accuracy of the Rn DCF used by RESRAD is open to additional debate since the various approaches to calculation yield highly different results. By using a DCF that utilized dosimetric methods in its derivation, the calculated

dose due to Rn could be more than three times greater than that calculated with DCF derived from epidemiological data.

A comparison of EDFs on the basis of age is shown in Figs 5.5 and 5.8, with a slight deviation from the general trend occurring between the ages 13 and 17 yr in each of the four exposure scenarios. In each scenario, though most noticeable for the resident farmer, the age dependent EDFs increase slightly for the ages between 13 and 17 yr. This is a direct reflection of an increase in the ICRP age dependent DCF for this age group. As described in ICRP 69, K, Ra and Th both seek bone as they have similar chemical properties to alkaline earth metals and calcium in particular (ICRP 1995). Moreover, U and Ra attach themselves to new growth bone and thus give a higher dose to those who are growing. This is illustrated by an increased dose coefficient to bone surfaces from the 5 yr old age group to the 15 yr old group for ^{226}Ra and each of the natural U isotopes. Additionally, there is an increased dose coefficient in red marrow and effective dose between 10 yr old and 15 yr old age groups in ^{226}Ra and each of the natural U isotopes (ICRP 1995).

CONCLUSIONS AND RECOMMENDATIONS

6.1. Dose Rates using hand held Survey Meters

After measuring the surface distribution of gamma radiation dose rate in Homa Mountain area was done the mean dose rate of 474.1 nSv h^{-1} translates to 4.15 mSv annual dose due to external radioactivity. The maximum level of $2.6 \mu\text{Sv.h}^{-1}$ which translate to 22.7 mSv y^{-1} for a resident living there is way beyond the dose limit of 1 mSv y^{-1} for the general public and is also more than the 20 mSv y^{-1} for radiation workers who are not supposed to receive cumulative dose of 100 mSv in any 5 years, while the inhabitant of Homa Mountain area will possibly receive 113.5 mSv in 5 years.

Interpretation of the data signifies as above normal background radiation exposure qualifying Homa Mountain and surroundings as a high background radiation area. The NORM exposure to the public at Homa Mountain calls for recommendation to regulatory authorities to provide acceptable exposure values and guidelines on mitigation actions to reduce external exposure due to K, Th and U in rocks and soils.

6.2. Radiation Hazard/Indices Conclusions

Subsequent to finding the activity concentrations of ^{238}U , ^{226}Ra , ^{232}Th and ^{40}K radionuclides in rock and soil samples, the pattern of high and/or low values of the radiological indices follows that of the corresponding activity concentrations. After determining the external exposure of inhabitants of Homa Mountain area to terrestrial gamma rays from the primordial radionuclides in the ground, the average value of 0.47 mSv y^{-1} qualified the region as a high background radiation area. This was collaborated by the radiological indices

with Total Effective Dose (TED) of 5.05 mSv y^{-1} being the calculated using dose conversation factors. The determination of the external exposure of the population of the study area to terrestrial gamma radiation is useful to relevant authorities namely the Radiation Protection Board (RPB) and National Environmental Management Authority (NEMA).

These indices are important parameters for the radiological protection of the population since soils are used for making earthen huts, bricks and pottery materials. The data obtained in this study will serve as baseline data for proper assessment of radiation exposure of the dwellers. On applying the radioactivity criterion and from the results of the Homa Mountain samples it can be seen that the indices varied significantly due to the elevated values of K, U and Th.

Most are above the internationally accepted values so they should not be used in building construction as they exceed the radioactivity criterion. The data obtained here are reference value to be used as baseline data for drawing a radiological map of the region. The health burden due to NORM from rocks and soils on the inhabitants of this area is high and hence may carry significant health hazards. Homa Mountain study has established data on radiation dose to the population qualifies the area as a high background radiation area and appropriate authorities led by RPB and NEMA need to take obligatory corrective action.

6.3. RESidual RADIation (RESRAD) Adaptation Conclusions

An assumption of secular equilibrium of decay products within a series was made for the calculations presented in this work. This enabled modeling the dose rate from activity concentrations within assumed lifestyle declarations for various exposure scenarios. The exposure scenarios are used as a base generalization to allow for the hypothetical scenarios presented, and to thus better represent different sections of the population. For future site

assessments, using the procedural adaptation presented here, it is appropriate to abandon this assumption when more information is known about the activity concentrations of the different radionuclides present. Additionally, several assumptions regarding dietary lifestyles of inhabitants of a site under consideration are factored into the input parameters listed for each of the specified exposure scenarios. Once again, if supplementary information is known, about the daily life habits of inhabitants of a site under consideration, the exposure scenarios should be disregarded in exchange for the more exact data.

A resident farmer exposure scenario was used in the calculation of the estimated TED due to Homa Mountain average concentration of non technologically enhanced NORM. Although the resident farmer scenario and its associated assumptions of a diet consisting of high fractions of contaminated food may not be indicative of a typical resident of Kenya, the typical resident does obtain a substantial portion of his/her food from domestic sources. Since the NORM concentrations used in the calculation are Homa Mountain averages, it follows that there is an equal chance that these are the concentrations for the hypothetical residence as for the site on which the food was produced.

6.4. Recommendations

1. The combined results of dose rates (obtained by hand held dose rate meters) the concentrations of K, U and Th (used in calculations of various radiological indices) and the dose calculations and estimations (obtained using RERAD code) can be considered as base values for distribution of natural radionuclides in Homa Mountain region. They will be used as reference information to assess any changes in the radioactive background level due to geological process and progressive development of the nuclear

and other industries. The later will enable detection of humanly manufactured contamination so as to protect the population and the environment but more important enable comparison of existing exposures compared to newly developed ones. Hence examination and identification of any new natural radiation exposure pathways as well as any critical populations or groups will be possible in subsequent studies if technically enhanced NORM activities occur.

2. The estimate of TED due to average K, U and Th concentrations in Homa Mountain is greater than the estimate in Kenya. It is also above world wide average background radiation due to terrestrial radionuclides. The estimate presented in this study for adults of 4.93 (from RESRAD); 5.05 (by calculation using Dose Conversion Factors) and 4.15 (by use of hand held radiation detectors) mSv yr⁻¹ compare favourably when sources of uncertainty are considered. For K, U and Th series rock and soil concentrations of 915.6, 195.3 and 409.5 Bq kg⁻¹, respectively they are above worldwide K, U and Th series concentrations of 400, 35.0 and 37.0 Bq kg⁻¹, respectively. It is recommended that the use of these samples under investigation in the construction of dwellings should not be considered safe for inhabitants.
3. Environmental monitoring ought to be carried out where people might be exposed to radioactivity and epideomological studies done to follow resident population to compare trends in diseases. It is important accurate information concerning the marble and granite be done, because simple mistakes on that can produce serious economic and social consequences. Since data that provides pertinent information on the potential high values of TED are indicative of enhanced radiological risk when such areas are used for land utilization it is recommended that human settlements should not be encouraged in Homa Mountain area.

4. Deviation of the estimate presented from that in the literature could be caused by misuse of exposure scenario, as discussed previously, by deviations from the assumption of secular equilibrium, by use of hypothetical values for hydrological and geological parameters, or by an inaccurate or inappropriate calculation of Rn dose within RESRAD. The estimate of TED due to exposure to Homa Mountain average terrestrial NORM concentrations, using the default procedures of RESRAD was much greater than that using the procedural adaptation. The enormous difference is primarily explained by the difference in dose integration between the two procedures. As explained in Chapter 4, the TED estimated using the procedural adaptation reflects only the input radionuclide concentrations at time 0 whereas the default procedure integrates the dose over the duration of the first year. Due to environmental movement during the first year, as modeled by RESRAD, there is a considerable higher concentration of each radionuclide present in Homa Mountain average scenario in groundwater and surface water at the end of the first year. The TED calculated using the default procedures incorrectly reflects this, while the procedural adaptation purposely does not. It is recommended that procedural adaptation be utilized when using the RESRAD code to interpret primordial radionuclides impacts.

5. Environmental Dose Factors (EDF) were defined and generated for estimation of TED due to certain NORM using elemental concentrations of K, U and Th. The EDFs were calculated for several age groups and exposure scenarios. The Tables of EDFs allow for estimates of dose to be made without the direct use of RESRAD. Hence from direct measurements with hand held dose rate meters we have a value of 4.15 mSv yr^{-1} , while from HpGe we deduced 5.05 mSv yr^{-1} and from RESRAD 4.93 mSv yr^{-1} . These diverse methods that arrive at similar conclusions are proving to be valuable tools in determining the necessity of further assessment of radiation dose and risk in areas of high background. One recurring conclusion from these

results is that Homa Mountain is a high background radiation area. It is recommended that the regulatory authorities led by RPB and NEMA needs to issue guidelines on future land use in cognizance of new knowledge availed on radiation exposure and environmental impact.

6. Additional studies to validate the RESRAD code would enable further information about a site or a general area to be known, such as hydrological parameters considered by RESRAD, or deviations from the assumptions stipulated in the computation of EDFs to more accurately provide TED estimates for specific sites. The progressive development of the nuclear industry and other contaminating technologies is very important. When widespread and ever increasing use of radiation and radioactive isotopes happen, it make it extremely necessary to evaluate the background of natural radiation in order to distinguish humanly manufactured contamination to protect the population and the environment. As a baseline studies it is recommended follow ups be done to note any additional burden due to additional human activities in mining, settlements and industrial development.

REFERENCES:

Achola S.O., Patel J.P., Mustapha A.O., and Angeyo H.K. (2012) Natural Radioactivity in the High Background Radiation Area of Lambwe East, Southwestern Kenya, Radiation Protection Dosimetry, pp 1-6, Oxford University Press

Ademoli A.K., Olaide S.H., and Ajumobi C.(2008) Radioactivity and Dose Assessment of Marble Samples from Igneti Mines, Nigeria. Radiation Protection Dosimetry, Vol 132, No. 1 pp 94 -97

Alencar, A.S. and Freitasn, A.C. (2005) Reference levels of natural radioactivity for the beach sands in a Brazilian southeastern coastal region, Radiation Measurements, 40, 76 – 83

Alharbi W.R., AlZahrani J.H. and Abbady A.G.E. (2011) Assessment of Radiation Hazard Indices from Granite Rocks of the Southeastern Arabian Shield, Kingdom of Saudi Arabia. Australian Journal of Basic and Applied Sciences, 5(6): 672-682

Aliyeva S. (2004) Radionuclide contamination of Natural Environment of Absheron Peninsula (Azerbaijan), NORM IV Proceedings of an International Conference, Szczyrk, Poland. IAEA-TECDOC-1472, 138 - 146

Al-Saleh F.S. and Al-Berzan B. (2007) Measurements of Natural Radioactivity in Some Kinds of Marble and Granite Used in Riyath Region. Journal of Nuclear and Radiation Physics, Vol. 2, No. 1, pp 25-36

Al-Sulaiti H.A., Regan P.H., Bradley D.A., Mathews M., Santawamaitre T. and Malain D. (2008) Preliminary Determination of natural Radioactivity

Levels of the State of Qatar using High-Resolution Gamma-ray Spectrometry. IX Radiation Physics & Protection Conference, Nasr City, Cairo, Egypt

Aly-Abdo A.A., Hassan M.H. and Huwait M.R.A. (1999) Radioactivity assessment of fabricated phosphogypsum mixtures, Fourth Radiation Physics Conference, 15–19 November, Alexandria, Egypt, 632–640.

Akerblom, G. (1995) The Use of Airborne Radiometric and Exploration Survey Data and Techniques in Radon Risk Mapping in Sweden. Application of Uranium Exploration Data and Techniques in Environmental Studies, IAEA-TECDOC 827, 159-180.

Ansoborlo E., Chazel V., Henge-Napoli M.H., Pihet P., Rannou, A., Bailey M.R. and Stradling N. (2002) Determination of the Physical and Chemical Properties, Biokinetics, and Dose Coefficients of Uranium Compounds handled during Nuclear Fuel Fabrication in France, Health Physics, 82(3), 279-289.

Baeza, A., del Rio, M., Mir C. and Paniagua, J.M. (1992) Natural Radioactivity in Soils of the Province of Caceres, Spain, Radiation Protection Dosimetry (45) 261-263

Beauvais Z.S., Thompson K.H. and Kearfott K.J. (2009) Evaluation of Total Effective Dose due to certain environmentally placed naturally occurring radioactive materials using a procedural adaptation of RESRAD Code, Health Physics, 97(1), 50-67

Bell K., (1989) Carbonatites, Genesis and Evolution. Unwin Hyman Ltd 46, 48, 72,& 73,

Beretka J. and Mathew P.J. (1985) Natural Radioactivity of Australian Building Materials, Industrial Wastes and By-products, Health Physics, 48, 87

Bolivar J.P., García-Tenorio R. and García-León M., (1996) Radioactive impact of some phosphogypsum piles in soils and salt marshes evaluated by gamma-ray spectrometry. Appl. Radiat. Isot. 47 (9/10), 1069–1075.

Briquet C., Silva K.M. and Cipriani M. (2004), Improving Criteria for Remediation of Monazite by Products contaminated sites in Brazil, NORM IV Proceedings of an International Conference, Szczyrk, Poland, IAEA-TECDOC-1472, 488 – 492

Canoba A., Lopez F.O., Arnaud M.I., Oliveria A.A., Neman R.S., Hadler J.C., Iunes P.J., Paulo S.R., Osorio A.M., Aparecido R., Rodriguez C., Moreno V., Vasquez R., Espinosa G., Golzarri J.I., Martinez T., Navarrete M., Cabrera I., Sagovia N., Pena P., Tamez E., Pereyra P., Lopez-Herrera M.E. and Sajo-Bohus L. (2001) Indoor radon measurements and methodologies in Latin American Countries, Radiation Measurements, 34, 483–486.

Chalupnik S. (2004) Theoretical study of Radium Behaviour in Aquifers, NORM IV Proceedings of an International Conference, Szczyrk, Poland, IAEA-TECDOC-1472, 67 – 78

Chowdhury M.I., Kamal M., Alam M.N., Yeasmin S. and Mostafa M.N. (2005) Distribution of Naturally Occurring Radionuclides in Soils of the Southern Districts of Bangladesh. Radiation Protection Dosimetry, 1-5

Clouvas A., Xanthos S., Takoudis G., Antonopoulos-Domis M. and Guilhot J. (2010) Nuclear Instruments and methods in Physics Research A, 614, 57

<http://www-ub.iaea.org/mtcd/meetings/PDFplus/2010/38924/TM-38924/Presentations/Clouvas.pdf>

Cocksedge W., Rankin W., Tostowaryk K., Charbonneau B.W. and Grasty R.L. (1993) National Native Home Radon Survey - Maximizing Resources through Radon Potential Assessment. Proceedings of the 26th Midyear Topical Meeting of the Health Physics Society, Environmental Health Physics, January 24th-28th, Lake Coeur d'Alene, Idaho, 391-402.

Crespo, M.T. (2000) On the determination of ²²⁶Ra in environmental and geological samples by alpha-spectrometry using ²²⁵Ra as yield tracer. Applied Radiation Isotope 53, 109-114.

Degrange J.P. and Lepicard S. (2004) Evaluation of Occupational Radiological Exposures Associated with Fly Ash from French Coal Power Plant, NORM IV Proceedings of an International Conference, Szczyrk, Poland, IAEA-TECDOC-1472, 230 – 239

Doring J., Gerler J., Beyermann M., Schkade U.K. and Freese J. (2004) Identification of Enhanced concentrations of ²¹⁰Pb and ²¹⁰Po in Iron Ore Industry, NORM IV Proceedings of an International Conference, Szczyrk, Poland, IAEA-TECDOC-1472, 213 – 216.

Doyle, P.J., Grasty, R.L. and Charbonneau B.W. (1990). Predicting geographic variations in indoor radon using airborne gamma-ray spectrometry. Current Research, Part A, Geological Survey of Canada, Paper 90-1A, pp. 27-32.

Eckerman K.F. and Ryman J.C. (1993) External Exposure to Radionuclides in Air, Water, and Soil, Exposure to Dose Coefficients for General Application, Based on the 1987 Federal Radiation Protection Guidance, EPA 402-R-93-076, Federal Guidance Report No. 12, prepared by Oak Ridge National Laboratory, Oak Ridge, Tenn., for U.S. Environmental Protection Agency, Office of Radiation and Indoor Air, Washington, D.C.

Elegba S.B. and Funtua I.I. (2004) Naturally occurring Radioactive Material (NORM) Assessment of oil and Gas production instillation in Nigerla, NORM IV Proceedings of an International Conference, Szczyrk, Poland, IAEA-TECDOC-1472, 256 – 258

Ekdal E., Karali T. and Sac M. M. (2006) ^{210}Po and ^{210}Pb in soils and vegetables in Kucuk Menderes basin of Turkey Radiation Measurements 41 pp 72-77

El-Mageed A.A.I., El-Kamel A.H., Abbady A., Harb S., Youssef A.M.M. and Saleh I.I. (2010) Assessment of Natural and Anthropogenic Radioactivity levels in rocks and soils in the environs of Juban town in Yemen, Tenth Radiation Physics & Protection Conference, 27-30 November 2010, Nasr City, Egypt

Espinosa G. and Gammage R.B. (2003) A representative survey of indoor radon in the sixteen region in Maxico city. Radiat. Prot. Dosim. 103, 73–76.

European Commission (EC) (1994) Radiation Protection 73, Technical Recommendations for monitoring individuals occupationally exposed to external radiation, Published by the European Commission Directorate –

General XI Environment, Nuclear Safety and Civil Protection, Luxembourg.

European Commission (EC) (1999) Radiological Principles Concerning the Natural Radioactivity of Building Materials. European Commission Radiation Protection Report 112, Luxembourg.

EURACHEM/CITAC (2000) Guide CG 4 Quantifying Uncertainty in Analytical Measurement 2nd Edition

<http://www.eurachem.ul.pt/guides/QUAM2000-1.pdf>

Faanhof A. and Kempster P. (2004), Examining the Natural Radioactivity of water sources to Evaluate the import on surrounding communities, NORM IV Proceedings of an International Conference, Szczyrk, Poland, IAEA-TECDOC-1472, 280 – 290

Friedmann H., (2002) Radon in Austria. In: Bukart,W., Shorabi, M., Bayer, A. (Eds.), Proceeding of 5th International Conference on High Levels of Natural Radiation and Radon Areas: Radiation Dose and Health Effects. Munich, Germany, 4–7 September, 2000, p. 162.

Gbadago J. K., Faanhof A., Darko E.O. and Schandof C. (2011) Investigation of the Environmental Impacts of Naturally Occurring Radionuclides in the processing of Sulfide ores for Gold Using Gamma Spectrometry, Journal of Radiological Protection 31 pp 337-352

Geraldo L.P., Serafim A.M., Correa B.A.M., Yamazaki I.M. and Primi M.C. (2010) Uranium Content and Dose Assessment for Sediment and Soil Samples from the Estuarine System of Santos and Sao Vicente, SP, Brazil. Radiation Protection Dosimetry, Vol 140, No. 1 pp 96 -100

Gonzalez A.J. (2009) The 12th Congress of the International Radiation Protection Association: Strengthening Radiation Protection Worldwide. Health Physics Vol. 97, no 1 pp 6-43

Gonzalez J.C., Fernandez I.M., Ferrera E.C. and Castro G.R. (2008) Determination of radionuclides in environmental test items at CPHR: Traceability and uncertainty calculation. Applied Radiation Dosimetry 66(11) pp 1632-8

Harb S., El-Kamel A.H., El-Mageed A.I.A., Abbady A. and Rashed W. (2008) Concentration of ²³⁸U, ²³⁵U, ²²⁶Ra, ²³²Th and ⁴⁰K for some Granite samples in Eastern Desert of Egypt. Proceedings of the 3rd Environmental Physics Conference, Aswan, Egypt pp 109-117

Hashim N.O., Rathore I.V.S., Kinyua A.M. and Mustapha A.O. (2004) Natural and artificial radioactivity levels in sediments along the Kenyan coast. Radiation Physics and Chemistry (71) pp 805 - 806

Hayumbu P., Mulenga S., Nomai M., Mulenga P., Katebe R., Shaba P., Chunga T., Inambao D., Mangala F., Tembo P. and Malama Y. (2004) Status of Radon Dosimetry in Zambian underground, NORM IV Proceedings of an International Conference, Szczyrk, Poland, IAEA-TECDOC-1472, 24-28

Henrich E., Jonssens A., Ryan T.P., Daroussin J.L., Smith K.R. and Gerchitor M.Y. (2004) The rapid identification of NORM Discharges Requiring Regulatory Control – A possible screening methodology, NORM IV Proceedings of an International Conference, Szczyrk, Poland, IAEA-TECDOC-1472, 377 – 388

Iakovleva V.S. and Karataev V.D. (2001) Radon levels in Tomsk dwellings and correlation. *Radiation Measurements* (34) 501 - 504

Ibrahim N. (1999) Natural activities of ^{238}U , ^{232}Th and ^{40}K in building materials, *Journal of Environmental Radioactivity*, **43**, pp 255–258.

Ibrahiem N.M., Abdel-Ghani A.H., Shawky S.M., Ashraf E.M. and Farouk M.A., (1993) Measurement of radioactivity levels in soil in the Nile Delta and Middle Egypt. *Health Phys.* 64, pp 620–627.

International Atomic Energy Agency (1987) Preparation and Certification of IAEA Gamma Spectrometry Reference Materials. IAEA/RL/148, IAEA, Vienna

IAEA Safety Series No. 115. (1996) International Basic Safety Standards for Protection against Ionizing Radiation and for the Safety of Radiation Sources. International Atomic Energy Agency, Vienna.

IAEA Technical Reports Series No. 393 (1999) Nuclear Geophysics and its Applications. International Atomic Energy Agency, Vienna.

IAEA (2004) Quantifying uncertainty in nuclear analytical measurements, IAEA Tecdoc 1401, Vienna.

ICRP (1983) Radionuclide Transformations: Energy and Intensity of Emissions, ICRP Publication 38, *Annals of the International Commission on Radiological Protection*, Vols. 11–13, Pergamon Press, New York, N.Y.

ICRP (1984). Principles for Limiting Exposure of the Public to Natural Sources of Radiation. International Commission on Radiological Protection Publication 39, *Annals of the ICRP* 14(1)

ICRP (1991) Annual limits on Intake of Radionuclides by Workers based on 1990 Recommendations of ICRP. International Commission on Radiological Protection Publication 61, Annals of the ICRP 21(4)

ICRP (1995) Age-dependent Doses to Members of the Public from Intake of Radionuclides: Part 3 - Ingestion Dose Coefficients. International Commission on Radiological Protection Publication 69, Annals of the ICRP 25 (1)

ICRP-60 (1990) Radiation Protection: 1990 recommendations of the International Commission on Radiological Protection. Oxford: Pergamon Press.

ICRP (2005) low Dose Extrapolation on Radiation related Cancer Risk. International Commission on Radiological Protection Publication 69, Annals of the ICRP 34 (4)

ICRP (2007). The 2007 Recommendations of the International Commission on Radiological Protection. ICRP Publication 103, Annals of the ICRP.

ISO (1993) Guide to the Expression of Uncertainty in Measurement. Geneva: ISO, corrected reprint (1995).

ISO (2000) Determination of the detection limit and decision threshold for ionizing radiation measurements – Part 1: Fundamentals and application to counting measurements without the influence of sample treatment. (Geneva, ISO)

Ivanov V.K., Tsyb A.F., Panfilov A.P., Agapov A.M., Kaidalov O.V., Korelo A.M., Maksioutov A., Chekin, S.Y. and Kashcheyeva P.V. (2009) Estimation of Individualized Radiation Risk from Chronic Occupational Exposure in Russia, *Health Physics*, 97(2), 107-114

Jackson S.A. (1992) Estimating Radon Potential from an Aerial Radiometric Survey, *Health Physics*, 62(5), 450-452

Jibiri N.N., Alausa S.K. and Farai I.P. (2009) Assessment of external and internal doses due to farming in high background radiation area in old tin mining localities in Jos-plateau, Nigeria, *Radioprotection* Vol 44 139-151

Joshua E.O., Ademola J.A., Akpanowo M.A., Oyebanjo O.A. and Olorode D.O. (2009) Natural radionuclides and hazards of rock samples collected from Southeastern Nigeria *Radiation Measurements*, *Radiation Measurements*, 44, 401-404

Kebwaro J. M., Hashim N.O. and Mustapha A.O. (2011) Construction of a generic reference material for gamma ray spectrometric analysis, *Indonesian Journal of Physics* Vol 22 No. 4, 105 - 106

Kenya Government (1982) *The Radiation Protection Act Cap 243 Laws of Kenya*. Government Printers. Nairobi

Komosa A., Chibowski S. and Reszka M. (2004) Natural Radiosotope Level Differentiation in Arable and Non Cultivated soils of Leczne – Wlodowa Lake District, pp. 117 – 126 *TECDOC 1472*

Lavi N., Steiner V. and Alfassi Z.B. (2009), Measurement of radon emanation in construction materials, *Radiation Measurements*, 44, 396 – 400

Lazar I., Toth E., Marx G., Cziegler I. and Kotdes G.J. (2003) Effects of residential radon on cancer incidence, *J. Radioanal. Chem.* 258 (3), 519–524

Le Bas M.J. (1977) *Carbonatite – Nephelinite Volcanism. An African Case History*, John Wiley & Sons Ltd, United Kingdom

Letourneau E.G., McGregor R.G and Walker W.B. (1984) Design and Interpretation of Large Surveys for Indoor Exposure to Radon Daughters. *Radiation Protection Dosimetry*, Vol. 7, No. 1-4, pp. 303-308.

Malance A., Gaidolfi L., Pessina V. and Dallara G. (1996) Distribution of ^{226}Ra , ^{232}Th , and ^{40}K in soils of Rio Grande do Norte, Brazil. *J. Environ. Radioactiv.* 30, 55–67.

Malozewski D., Teper L., Lizurek G. and Dorda J. (2004) In Situ Gamma Ray Spectrometry in Common Rock Raw Materials mined in Krakow Vicinity, Poland, NORM IV Proceedings of an International Conference, Szczyrk, Poland, IAEA-TECDOC-1472, 368 – 376

Mangala J.M. (1987) A multi-channel x-ray fluorescence analyses of fluorspar ore and rock from Mrima hills, Kenya. M.Sc. thesis, UoN, Unpublished.

Martínez-Aguirre A., García-León M., Gascó C. and Travesí A. (1996) Anthropogenic emissions of ^{210}Po , ^{210}Pb and ^{226}Ra in an estuarine environment. *Radioanal. Nucl. Chem. Art.* 207 (2), 357–367.

McCall G.J.H. (1958) Geology of the Gwasi area, Ministry of Commerce and Industry, Geological Survey of Kenya, Dept. No. 45

Mohsen N., Bahari I., Abdullah P. and Jaafa A. (2007) Gamma Hazards and risk Associated with NORM on Sediment from Amang processing Recycling Ponds. The Malaysian Journal of Analytical Sciences, Vol II, No 1; pp 314-323

Mossman K.L. (2009) Policy Decisions - Making under Scientific Uncertainty; Radiological Risk Assessment and the Role of Expert Advisory Groups. Health Physics 97 (2) 101 - 106

Mujahid A., Hussain S., Dogar H. and Karim S. (2005) Determination of porosity of different materials by radon diffusion, Physics Radiation Division, PINSTECH, P.O. Nilore, Islamabad, Pakistan. Radiation Measurements, 40, 106 - 109

Mulaha T.O. (1989) The Ndiru Hill Carbonatite, South Nyanza District, Western Kenya. MSc thesis in Geology and Mineralogy, Department of Geology, University of Helsinki, Unpublished

Mustapha A.O., Narayana D.G. S., Patel J.P. and Otwoma D. (1997) Natural Radioactivity in Some Building Materials in Kenya and the Contributions to the Indoor External Doses, Radiation Protection Dosimetry, 71, 65-69 Oxford University Press

Mustapha A.O., Patel J.P. and Rathore I.V.S., (1999) Assessment of human exposure to natural sources of radiation in Kenya, Radiat. Prot. Dosim, 82, 285-292, Oxford University Press

Mustapha A.O (1999) Assessment of Human Exposures to Natural Sources of Radiation in Kenya, PhD thesis, University of Nairobi, Unpublished

Mustapha A.O., Patel J.P. and Rathore I.V.S. (2002) Preliminary Report on Radon Concentration in Drinking Water and Indoor Air in Kenya, *Environmental Geochemistry and Health*, 24(4), 387-396

Mustapha A.O., Patel J.P., Rathore I.V.S., Hashim N.O. and Otwoma D. (2004) An investigation of the repeatability of calibration factors in gamma-ray spectrometry of geological materials. *Applied Radiation and Isotopes* 60 pp 79 - 82

Myrick T.E., Berven B.A. and Haywood F.F. (1983) Determination of the concentration of selected radionuclides in surface soil in USA, *Health Physics*, 45, 361.

Nair R.R.K., Rajan B., Akiba S., Jayalekshmi P., Nair M.K., Gangadharan P., Koga T., Morishima H. and Nakamura S. (2009) Background Radiation and Cancer Incidence in Kerali, India – Karunagappally Cohort Study. *Health Physics* 96(1) 55 - 66

NRPB (2002) W26 Radon Atlas of England and Wales-Northamptonshire, National Radiological Protection Board, Chilton, United Kingdom

NCRP (1987) National Council on Radiation Protection and Measurement Report No. 93, Ionizing Radiation Exposure of the Population of the United States NCRP, Bethesda, Maryland.

NCRP (1993) Limitation of Exposure to Ionizing Radiation. NCRP Report

116. National Council on Radiation Protection and Measurements, Bethesda, Maryland. March 31, 1993.

Nyamai C.M. (1989) The Mineralogy of Uncompahgrites and Turjaites from South Rangwa Complex, Western Kenya. MSc in Geology and Mineralogy, Department of Geology, University of Helsinki, Unpublished

Oatway W.B., Jones J.A., Shaw P.V. and Mobbs S.F. (2004) Radiological Impact on the UK population of Industries which use or produce materials containing enhanced levels of Naturally Occurring Radionuclides: Zircon sands industries, NORM IV Proceedings of an International Conference, Szczyrk, Poland, IAEA-TECDOC-1472, 246 – 255

OECD (1979) Organisation for Economic Cooperation and Development. Exposure to radiation from natural radioactivity in building materials. Report by a Group of Experts of the OECD Nuclear Energy Agency, OECD, Paris.

OECD (2011) Evolution of ICRP Recommendations 1977, 1990 and 2007, Changes in Underlying Science and protection policy and their Impact on European and UK Domestic Regulation, OECQ Publishing, Paris

Ohde S. (2004) Instrumental neutron activation analysis of carbonatites from Homa Mountain, Kenya, Journal of Radioanalytical and Nuclear Chemistry, 260(1), 213-218

Oladele S.A. (2009) Measurement of activity concentration of ^{40}K , ^{226}Ra and ^{232}Th for assessment of radiation hazards from soils of the southwestern region of Nigeria, Radiat Environ Biophys (48) 323-332

Osman A.A.A., Salih I., Shaddad I.A., Din S.E., Siddeeg M.B., Eltayeb H., Idriss H., Hamza W. and Yousif E.H., (2008) Investigation of natural radioactivity levels in water around Kadugli, Sudan, Applied Radiation and Isotopes, 1650-1653

Otansev P., Karaha G., Kan E., Barut I. and Taskin H. (2012) Assessment of Natural Radioactivity Concentration and Gamma Dose Rate Levels in Koyseri, Turkey. Radiation Protection Dosimetry Vol. 148 No. 2 227 - 236

Otton J. K., Gundersen L.C.S., Schumann R.R., Reimer G.M. and Duval J.S. (1995) Uranium Resource Assessment and Exploration Data for Geologic Radon Assessments in the United States. Application of Uranium Exploration Data and Techniques in Environmental Studies, IAEA- TECDOC-827, 135-137.

Otwoma D. and Mustapha A.O. (1998) Measurement of ^{222}Rn concentration in Kenyan groundwater, Health Physics, 74, 91-95

Patel J.P., Van der Voo R. and Meert J.G., (1987) Paleomagnetic investigations of the Precambrian in Kenya: Report of Investigations I, Kenya Division of Mines and Geology Open File Report, 29 pages

Patel J.P. (1991) Environmental radiation survey of the area of high natural radioactivity of Mrima hill of Kenya, Discovery and Innovation, Vol. 3, No. 3, P 31-36

Personal Communication (2007) Unpublished personal communication with Don Riario, Chief Geologist; Wanjie, Geo-Chemist and; Chebet Geologist; Geology Department, Ministry of Energy, Kenya

Pietrzak-Flis Z.I. Kaminsta and Chrzanowski E. (2004) Uranium Isotopes in Public Drinking water in Poland, NORM IV Proceedings of an International Conference, Szczyrk, Poland, IAEA-TECDOC-1472, 291 – 298

Prasad S.N.G., Nagaiah N. and Karunakara N. (2008) Concentrations of ^{226}Ra , ^{232}Th and ^{40}K in the Soils of Bangalore Region, India. Health Physics (94) pp 264 - 271

Reilly D., Ensslin N., Smith H. and Kreiner S. (1991) Passive Nondestructive Assay of Nuclear Materials, United States Nuclear Regulatory Commission, Washington DC

Ryan T.P., Jonssens A., Herich E., Daroussin J.L., Hillis Z.K. and Meijne E.I.M. (2004) Industries giving rise to NORM Discharges in the European Union – A Review, NORM IV Proceedings of an International Conference, Szczyrk, Poland, IAEA-TECDOC-1472, 169 – 187

Salman K.A. and Amany Y.S. (2008) Assessment of Natural Radioactivity in TENORM Samples Using Different Techniques, IX Radiation Physics & Protection Conference, 15-19 November 2008, Nasr City - Cairo, Egypt also <http://rphysp.com/proceeding/4142.pdf>

Shanthi G., Maniyan C.G., Raj A.G. and Thampi T.K. (2009) Radioactivity in Food Crops from High Background Radiation Area in South West India, Curr. Sci. 97(9), 1331 - 1335

Shanthi G., Thampi J., Kumaran T., Raj G.A.G. and Maniyan C.G. (2010) Measurement of Activity Concentration of Natural Radionuclides for the Assessment of Radiological Indices. Radiation Protection Dosimetry Vol. 141 No. 1 90 - 96

Shives R.B.K, Charbonneau B.W. and Ford K.L. (1997) The detection of potassic alteration by gamma ray spectrometry - recognition of alteration related to mineralization. In: Geophysics and Geochemistry at the Millennium, Proc. Fourth Decennial Int. Conference on Mineral Exploration (Exploration 7) Toronto, Ontario, Canada . Also in http://gsc.nrcan.gc.ca/gamma/exp97/index_e.php

Singh S., Singh B. and Kumar A. (2003) Natural radioactivity measurements in soil samples from Hamirpur district. Radiat. Meas. 36, 547-549

Singha S., Rania A. and Mahajanb R.K. (2005). ^{226}Ra , ^{232}Th and ^{40}K analysis in soil samples from some areas of Punjab and Himachal Pradesh, India using gamma ray spectrometry, Radiation Measurements (39) 431 – 439

Singha S., Kumara M. and Mahajanb R.K. (2005) The study of indoor radon in dwellings of Bathinda district, Punjab, India and its correlation with uranium and radon exhalation rate in soil, Radiation Measurements (39) 535 – 542

Sugahara T. (2009) Background Radiation and cancer incidences in Kerala, India – Karunagappaly Cohort Study. Health Physics January 2009, Volume 96 pp 55-66

Tahir S.N.A., Jamil K., Zaidi J.H., Arif M., Ahmed N. and Ahmad S.A. (2005) Measurements of Activity Concentrations of Naturally Occurring Radionuclides in Soil Samples from Punjab Province of Pakistan and Assessment of Radiological Hazards, Radiat. Prot. Dosimetry 113 (4), 421-427

Tomazini da Conceicao F., Bonotto D. M., Jimenez-Rueda J. R. and Roveda J. A. F (2009) Distribution of ^{226}Ra , ^{232}Th and ^{40}K in soils and sugar cane crops at Corumbatai river basin, Sao Paulo, Brazil, Applied Radiation and Isotopes (67) 1114-1120

UNSCEAR (1988) United Nations Scientific Committee on Effects of Atomic Radiation, Sources, Effects and Risks of Ionising Radiation, Report to the General Assembly, United Nations, New York

UNSCEAR (1993) United Nations Scientific Committee on Effects of Atomic Radiation, Sources and Effects of Ionising Radiation, UNSCEAR Report, New York

UNSCEAR (2000) United Nations Scientific Committee on the Effects of Atomic Radiation, Exposures from natural radiation sources, United Nations, New York.

Van Velzen L.P.M. and Timmermons C.W.M. (2004) Importance of sampling in relation to the Gamma Spectroscopic Analysis of NORM Material, NORM IV Proceedings of an International Conference, Szczyrk, Poland, IAEA-TECDOC-1472, 347-356

Veiga R., Sanches N., Anjos R.M., Macario K., Bastos J., Iguatemy M., Aguiar J.G., Santos A.M.A., Mosquera B., Carvalho C., Baptista F.M. and Umisedo N.K. (2006) Measurement of natural radioactivity in Brazilian beach sands, Radiation Measurements (41) 189-196

www.elsevier.com/locate/radmeas

Viruthagiri G. and Ponnarasi K. (2011) Measurement of Natural Radioactivity in Brick Samples. *Advances in Applied Science Research*, 2(2), 103-108

Whicker J.J. and McNaughton M.W. (2009) Work to Save Dose: Contrasting Effective Dose Rates from Radon Exposure in Workplaces and Residences against the backdrop of Public and Occupational Regulatory Limits, *Health Physics*, 97(3) 248-261

WHO (2001) World Health Organisation 2001, Guidelines for Drinking Water Quality – General Considerations, last modified 17 Oct 2002, http://www.who.int/water_sanitation_health/GDWQ/General_Considerations.htm, accessed 20 Apr 2001.

Xinwei L. (2005) Radioactive Analysis of Cement and its Products Collected from Shaanxi, China. *Health Physics*. 88(1):84-86, January 2005.

Yii M.W., Zaharudin A. and Abdul K. (2009) Distribution of naturally occurring radionuclides activity concentration in East Malaysian marine sediments *Applied Radiation and isotopes* 67 pp 630-635

Yu C., A. Zielen A.J., Cheng J.J., LePoire D.J., Gnanapragasam E., Kamboj S., Arnish J., Wallo A., Williams W.A. and Paterson H. (2001) User's Manual for RESRAD Version 6, Environmental Assessment Division Argonne National Laboratory, United States Department of Energy.

A.1 Nyasanja Peak

Nyasanja is a small carbonatite intrusion peak separated with Homa summit by Nyasanja valley. It reaches 1,600 m in height and contains a secondary peak around 200 m to the North East called Ratieng which could suggest double cone formations (Fig A. 1).



Fig: A.1 Nyasanja peak – the forest cover have been cleared by charcoal burners.

The carbonatitic intrusions are cut by dykes and veins of a later volcanic activity. East of Nyasanja's main peak is also another Nyasanja affiliate, separated from the main peak by a depression probably caused by faulting. The depression formation looks more of a sedimentary

agglomerates, but could also be of volcanic origin (Personal Communication with Wanjie, 2007). These could be volcanic pyroclastics containing various rock assortments cemented together during the magmatic episode. Feldpars rich veins are seen cutting in all directions.

The carbonatites boulders not only occur on Nyasanja but also on Homa Mountain as seen on Fig. A. 2 below.



Fig A. 2: A lineament cutting across the northern side of Homa Mt in a NE-SW direction.

A.2 Nyamatoto Peak

South-East of Nyasanja about 1 km apart occurs the Nyamatoto phonolite plug. It is a steep sided peak covered by vegetation. The phonolites range from small sizes to large boulders, and could suggest a

later volcanic activity in the area. They are found as intruded and extruded of which erosion followed. A single outcrop shows poorly bedded phonolitic agglomerate, and the field relationship supports the view that the plug was intruded into a cover including this agglomerate.

A.3 Kanam and Rawe Beds

North-West of Nyasanja arise the Kanam beds. It consists mainly of soils and alluvial which range from light brown clays and greenish tuffs varying from the fine grained ash to fine grained agglomerates.



Fig A.3 Rawe beds composed of brown clay, ash and gravel beds overlain by alluvials.

To the east of Kanam and lying at the foot of Nyasanja are the Rawe beds. The latter are composed of layers upon layers of brown clay, ash and gravel overlain by alluvials see Fig A. 3. Gravel beds are seen to occur throughout the sequence and often contain well rounded pebbles, suggesting transportation over a distance by water.

The streams flow towards Lake Victoria and when the sources are sought they emanate from the hot springs. Two streams of Nyagot Pala and Abundu Pala were located and veins were a common feature in the discharge zones (Figs. A.4, A.5 and A.6).



Fig A. 4 Veins, a common feature in the hot water discharge zones.

The hot springs are about 2 km apart, separated by a formation of country shattered Nyanzian rock and alluvial deposits. Two main fault line accompanied by numerous fractures seem to be the main factors controlling the hot spring. The main Rock formations found in the area range from the shattered Nyanzian, cemented pyroclastics, tuffs, sandstone, red iron-stones and alluvial deposits

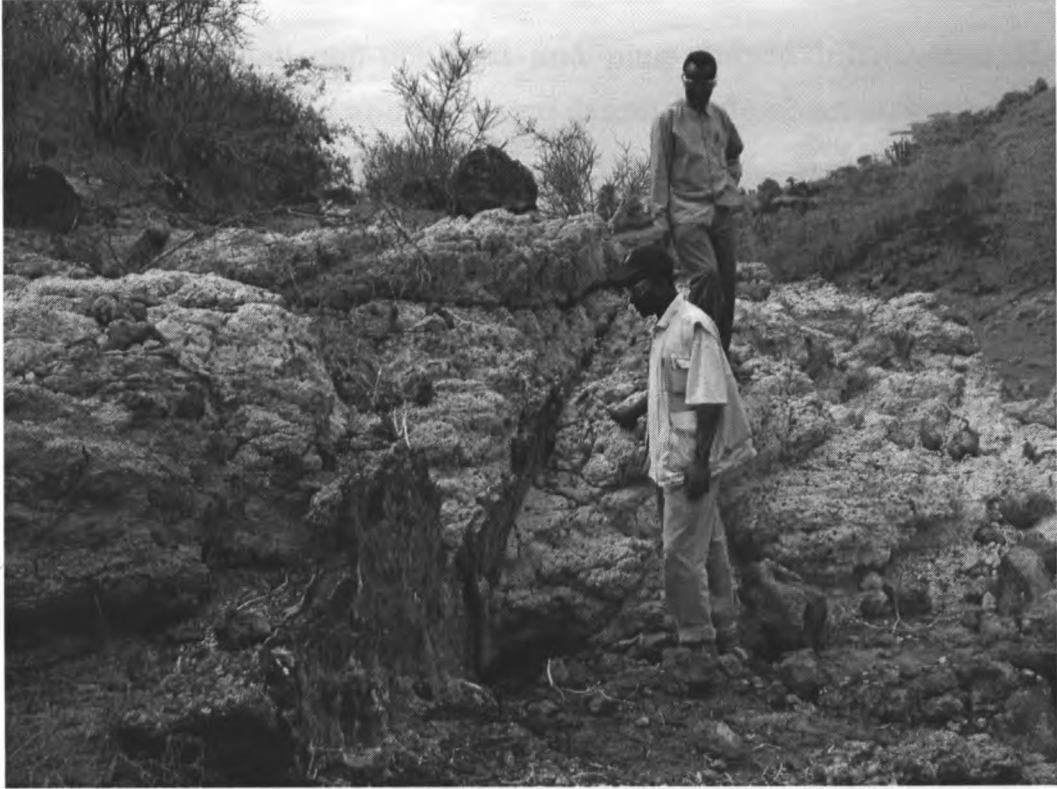


Fig A.5 Veins, a common feature in the hot water discharge zones.

Travertine deposits occur some (100 m) distance north-west of Abundu hot spring. Hot water discharge from the hot springs take a linear orientation showing either a contact of two different rock types or a veining intrusion see Figures A. 4, 5 and 7. A trend of about 20 – 40 m long line was noted of which the water temperatures ranged between 25 – 83°C. Hydrothermal veins and infillings of quartz and calcite are

common occurrence within the country rock on the geothermal area. Similar formations to Kanam beds were found exposed in a gully on the banks of Nyagoto stream. An intrusion of welded pyroclasts was encountered close to the same place indicating volcanic eruptions contemporaneous to Rawe beds see Fig A.6.

A.4 Odiawo

Odiawo is a small cliff-bounded and plug-shaped hill around 150 m high, east of Nyasanja and shows no definite cone-sheet structure.



Fig A.6 An inclusion of welded pyroclastics in Rawe beds exposed on the banks of Nyagot Pala stream.

The rock formations are similar to that of the Nyasanja peak (carbonatites). Again, veins are seen cutting in all directions. The outline of the hill is defined by concentric faults. Got Akom, is a small hill around 50 m high to the north of Odiawo and appears as a reworked carbonatites (brecciated) relating to its doming.

A.5 Awaya

Awaya is a small hill east of Homa Mountain rising over 400 m above the surrounding plains. Its subdued relief is in contrast to other carbonatite peaks around Homa Mountain. Exposed carbonatites is scanty and most of the exposed rocks are Nyanzian volcanics.



Fig A.7 Clear water discharging from a formation contact zone.

The drainage pattern is radial about the summit with geological structures mainly being concentric fractures along intrusive carbonatites. East of Awaya peak is a low relief area covered by vegetation with the geology being mainly alluvial deposits.

A.6 Chiewo – Ndiru Mbili –Yusoo

Nyanzian, ijolites, bedded pyroclasts, carbonatites intrusions, K-feldspars, gypsum, lime and breccias occur abundantly from Ndiru, Yusoo, Ndiru Mbili and Chiewo volcanic peak.

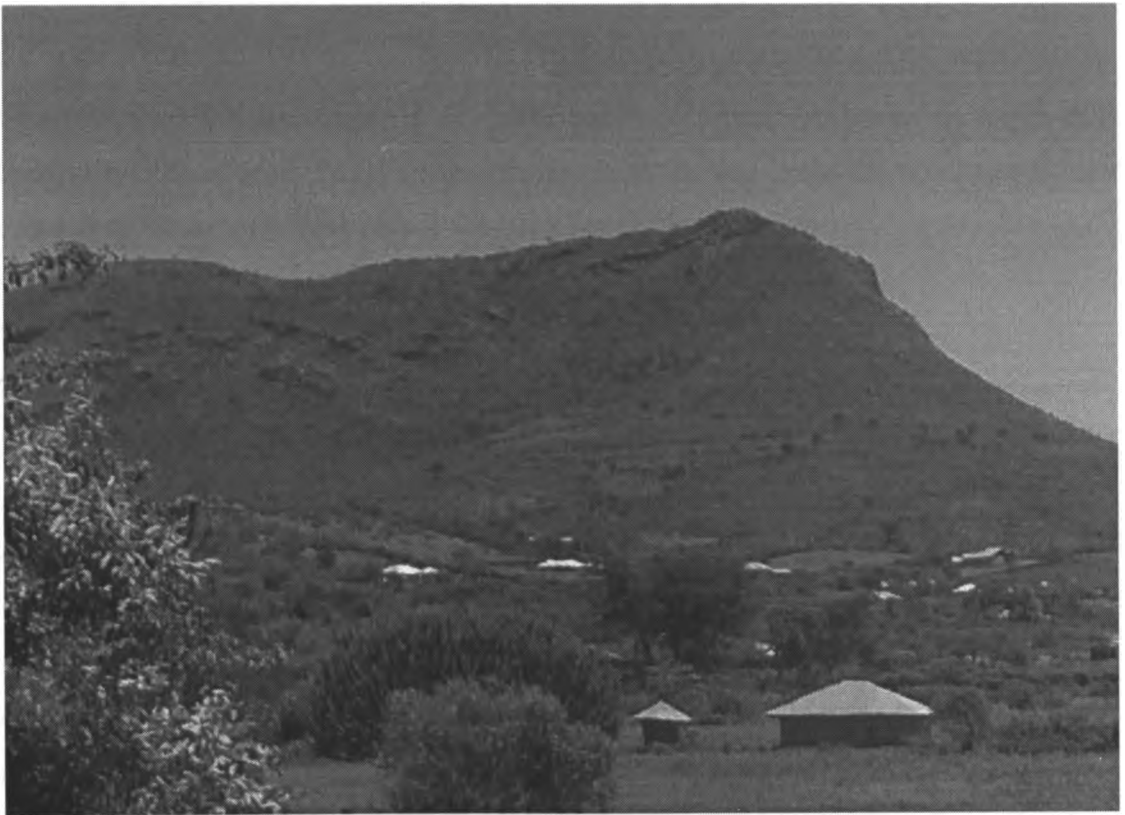


Fig A. 8 Habitations encroaching Got Chiewo viewed from Ndiru Mbili

At Homa Mountain, the satellite vent of Got Chiewo consists of a well preserved carbonatite cone composed of bedded, grey lapilli turfs.

Porphyritic textures with platy, rectangular pseudomorphs made up of polycrystallized as alkali carbonatite.

Observations at Got Chiewo showed that the grey carbonatite tuffs are composed of juvenile and accretionary lapilli set in an ash matrix of similar texture and composition to the lapilli themselves. Got Chiewo clearly demonstrates the highly fluid nature of erupting carbonatite lava. Welding and agglutination in the proximal crater rim facies show that the juvenile pyroclasts were in a fluid or plastic state at the moment of deposition. Pyroclastic fall deposits of shard rich tuffs from Got Chiewo are produced by the violent disruption of a carbonatite melt by rapidly expanding gases. Agglomerates are common and are typically made up of agglutinated accumulations of carbonatite bombs. Increase in explosive intensity results in lava fountaining that forms extensive, topography mantling, spatter veneers.

The Ndiru Hill carbonatite lies 1.5 km South of the Homa Mountain carbonatite centre. It belongs to the tertiary alkaline province of Western Kenya (Mulaha 1989). The main outcrop constitutes about one half alvikite, one fourth sovite and one fourth ferrocarnatite. The two outliers consist of almost equal amounts of dyke alvikite and ijolite with sovite occurring mainly as inclusions. Dykes of ferrocarnatite cut all the carbonatite types in the outcropping areas. The Ndiru Hill carbonatite shows the basis of cross cutting relationships, a sequential intrusion from sovite through alvikite to ferrocarnatite classified as C1, C2 and C3 type carbonatite respectively. With late stage mineralization as cross cutting vein lets.

A.8 Types of Houses

Most of the houses in the surveyed area are semi permanent houses and partially ventilated and only a few are mud-type with poor ventilation. The concrete houses are built using cement, sand, bricks, marble and concrete as the construction materials. Most of the houses are single storey while a few have a second storey. Each house has two to three rooms with common walls and in some cases interconnected doors. Usually windows are not in operation and remain open with no additional exhausting fans, which result in the good ventilation conditions. The mud-type earthen-floored houses are built with local mud, unfired bricks and woods. The houses are very well ventilated almost always, especially during the day when inhabited having the windows and doors open.

Appendix B**List of Surveyed Areas**

Table B.1 List of sites at and around Homa Mountain that the hand held survey meters were used showing the dose rates.

S/No **Dose rate (nSv. hr⁻¹)** **Location description and coordinates**

<u>S/No</u>	<u>Dose rate (nSv. hr⁻¹)</u>	<u>Location description and coordinates</u>
1	588.4	Off Bala Road on 16th October 2007
2	386.0	At Gulley - carbonatite intrusions in ijolites
3	425.5	Pholonite Boulder
4	1068.0	Carbonatite Boulders
5	165.0	Dykes washed by water H ₂ O
6	238.0	Limestone after growth
7	286.9	Limestone lower cr
8	305.5	Limestone Upper
9	292.0	Hot Springs at Bala gulley
10	281.9	Hot Springs at Bala gulley
11	385.0	Hot Springs at Bala gulley
12	532.0	Kendu Bay room

S/No	Dose rate (nSv. hr⁻¹)	Location description and coordinates
13	622.0	Kendu Bay room
14	329.0	Kendu Bay hotel outside
15	130.0	Kendu Bay hotel outside
16	353.2	Junction Gogo & Kenyament Sec School
17	417.9	06/68/333/99/53/163/1227/
18	541.1	066 8349 / 995 3218 / 1236 (Picked sample from Huntney Nongi's farm)
19	591.6	066 8349 / 995 3218 / 1236 (Picked sample from Huntney Nongi's farm)
20	594.6	066 8349 / 995 3218 / 1236 (Picked sample from Huntney Nongi's farm)
21	587.6	066 8349 / 995 3218 / 1236 (Picked sample from Huntney Nongi's farm)
22	581.3	0668467 / 9953280 / 1238 shattered Nyanzian
23	1282.0	0668492 / 9953329 / 1243 carbonite dyke or intrusion
24	182.5	0668275 / 9953474 / 1247 (Breccia)
25	533.9	0668409 / 9954372 / 1276 (Aluvial / black cotton soil)
26	735.0	0668770 / 9955327 / 1332 (Shattered Nyanzian intrusion)

S/No	Dose rate (nSv. hr⁻¹)	Location description and coordinates
27	620.0	0668717 / 9955452 / 1344 (Nyanzian rock sample taken at Ndiru Mbili)
28	574.0	0668717 / 9955450 / 1339 or 40
29	578.0	0668717 / 9955450 / 1339 or 40
30	440.8	0668721 / 9955454 / 1344 (K- feldspar at Ndiru Mbili)
31	434.7	0668721 / 9955454 / 1344 (K- feldspar at Ndiru Mbili)
32	899.8	0668709 / 9955458 / 1341 (After taking soil / rock pebbles)
33	1109.0	0668709 / 9955458 / 1341 (After taking soil / rock pebbles)
34	254.0	0668387 / 9955689 / 1360 (Pyroclasts (cemented limestone) to sample)
35	584.4	0667932 / 9956059 / 1413 (rutile fine soil)
36	524.4	0667932 / 9956059 / 1413 (Limestone cemented pyroclasts)
37	724.6	0667932 / 9956059 / 1413 (Pebbles)
38	370.5	0667890 / 9956276 / 1443 (K - feldspar looks like gurtz gypsum)
39	500.0	0667897 / 9956286 / 1436 (bedded Pyroclasts)
40	646.5	0667896 / 9956292 / 1443 (Triffa collected sample)
41	1138.0	0667820 / 9956301 / 1478 (altered carbonite took sample)

S/No	Dose rate (nSv. hr⁻¹)	Location description and coordinates
42	1596.7	0667810 / 9956304 / 1472
43	825.0	0667676/ 9956329 / 1480 (The survey meters reverted to nSv h ⁻¹)
44	675.2	0667648 / 9956254 / 1499 (alluvial soil cover)
45	718.4	0667592 / 9956232 / 1506 (Chiewo volcano top)
46	724.5	0667469 / 9956129 / 1512 (Top of Chiewo)
47	745.3	0667444 / 9956119 / 1506
48	787.8	0667551 / 9956147 / 1501 (bedded pyroclast)
49	823.6	0667594 / 9956143 / 1498 (Ryolites or Ijolites - took samples)
50	1080.0	0667636 / 9956132 / 1476 (Bedded Pyroclasts - took sample)
51	752.3	0667679 / 9956059 / 1450 (Iron rock intrusion cutting across country)
52	432.2	0667946 / 9955971 / 1445 (Carbonite Intrusions Nyanzian Pyroclasts)
53	463.8	0667671 / 9955950 / 1434 (Pyroclasts tuffs at Yusoo)
54	789.9	0667674 / 9955857 / 1419 (Pyroclastics)
55	297.7	0667690 / 9955755 / 1410 (Alluvial cover)
56	463.7	0667946 / 9955183 / 1340 (Carbonite sheets)

S/No	Dose rate (nSv. hr⁻¹)	Location description and coordinates
57	331.5	06678047 / 9954708 / 1307 (Okiki Amayo)
58	314.0	0668044 / 9954720 / 1308 (Building at Kendu Bay Hotel)
59	228.5	0668044 / 9954720 / 1308 (Building at Kendu Bay Hotel)
60	126.0	06 / 6982 / 3 / 99 / 58 / 01 / 1 / 1323
61	143.7	06 / 69 / 62 / 4 / 99 / 58 / 23 / 1 / 1326
62	113.7	06 / 69 / 58 / 3 / 99 / 58 / 118 / 1359 (Breccia (brecciated carbonatite dykes))
63	108.4	06 / 69 / 43 / 5 / 99 / 57 / 92 / 6 / 1392 (with r- probe brecciated carbonites)
64	361	06 / 69 / 43 / 5 / 99 / 57 / 92 / 6 / 1392 (with r- probe brecciated carbonites)
65	114.7	Cross – path (with r – probe)
66	110.7	0669494 / 99/ 57 / 948 / 1406 (Pyroclasts)
67	116.4	0669540 / 9957967 / 1410 (with r – probe)
68	116.4	Awaya peak has Pyroclasts
69	249.0	Awaya peak has Pyroclasts
70	146.7	0669485 / 9957858 / 1389

S/No	Dose rate (nSv. hr⁻¹)	Location description and coordinates
71	238.0	066/94/79/995/76/67/1422 (K - feldspar intrusion at peak of dome)
72	568.5	066/94/79/995/76/67/1422 (K - feldspar intrusion at peak of dome)
73	570.9	066/94/79/995/76/67/1422 (K - feldspar intrusion at peak of dome)
74	140.3	066/93/71/9957639/1404 (foot of Homa mountain on Eastern part)
75	317.0	066/92/77/995/75/39/1408 (Pyroclasts)
76	157.8	066/92/77/995/75/39/1408 (Pyroclasts)
77	149.5	066/92/77/995/75/39/1408 (Pyroclasts)
78	178.0	0669204/9957512/1440 (Pyroclasts)
79	121.5	0669204/9957512/1440 (Pyroclasts)
80	120.8	0669204/9957512/1440 (Pyroclasts)
81	287.7	0669204/9957512/1440 (Pyroclasts)
82	436.0	0668956 / 9957261 / 1409 (shattered Nyanzian)
83	331.4	0668956 / 9957261 / 1409 (shattered Nyanzian)
84	323.8	0668956 / 9957261 / 1409 (shattered Nyanzian)

S/No	Dose rate (nSv. hr⁻¹)	Location description and coordinates
85	307.5	0668867 / 9957225 / 1403 (Y - section of path covered with shattered)
86	433.0	0668855 / 9957027 / 1381 (Ngou / Omukhuyu, Fig tree aluvials)
87	455.5	0668855 / 9957027 / 1381 (Ngou / Omukhuyul, Fig tree aluvials)
88	327.5	0668833 / 9956935 / 1391 (Alluvial in garden)
89	286.5	0668833 / 9956935 / 1391 (Alluvial in garden)
90	410.6	0668833 / 9956935 / 1391 (Alluvial in garden)
91	454.4	0660951 / 9956911 / 1387 (Alluvial in garden)
92	455.6	0660951 / 9956911 / 1387 (Alluvial in garden)
93	509.4	0669010 / 9956884 / 1390 (Fe-rich carbonanites mixed with breccia, nyanzian, lime, soviets, pyroclastic)
94	541.0	0669202 / 9956855 / 1385 (moved 20 m away)
95	281.8	0669202 / 9956855 / 1385 (moved 20 m away)
96	683.1	0669163 / 9956861 / 1380 (intruding dyke)
97	412.9	0669200 / 9956785 / 1402 (Shattered Nyanzian phonolites at Rongo)

S/No	Dose rate (nSv. hr⁻¹)	Location description and coordinates
98	942.2	0669101 / 9956756 / 1383 (carbonatite dykes)
99	292.7	0668794 / 9956681 / 1406 (carbonititic dykes)
100	274.6	0668755 / 9956758 / 1426 (One of Rongo peaks carbonititic dykes)
101	419.6	0668755 / 9956758 / 1426 (One of Rongo peaks carbonititic dykes)
102	273.0	0668581 / 9956727 / 1424 (shattered pebbles of pre-existing rocks)
103	533.5	0668342 / 9956786 / 1420 (Alluvial (soil) cover)
104	688.8	0668228 / 9956743 / 1424
105	698.5	0668075 / 9957037 / 1438 (Soil cover from weathering of rocks from Homa mountain)
106	688.3	0667897 / 9957004 / 1449 (Pyroclasts in river gulley)
107	679.4	0667897 / 9957004 / 1449 (Pyroclasts in river gulley)
108	703.5	0667897 / 9957004 / 1449 (Pyroclasts in river gulley)
109	516.3	0667601 / 9957082 / 1486 (Tuffecias formation)
110	872.9	0667566 / 9957082 / 1490 (Pyroclast)
111	452.0	0667301 / 9956947 / 1516 (Pyroclast)

S/No	Dose rate (nSv. hr⁻¹)	Location description and coordinates
112	762.5	0667424 / 9956858 / 1511 (Shattered Nyanzian)
113	657.2	0667561 / 9956755 / 1506 (Shattered Nyanzian)
114	623.1	0667610 / 9956729 / 1498 (Pyroclastics composed among others rhyolites)
115	733.9	0667618 / 9956717 / 1490 (Pyroclastics)
116	770.0	0667642 / 9956695 / 1484 (Pyroclastics)
117	684.9	0668040 / 9956608 / 1425 (Aluvials)
118	712.9	0668073 / 9956485 / 1414 (Aluvials)
119	846.7	0668143 / 9956089 / 1394
120	298.4	0667978 / 9954922 / 1324
121	328.0	06678047 / 9955183 / 1340 (Okiki Amayo had soda here mud hut)
122	337.1	06678047 / 9955183 / 1340 (Okiki Amayo had soda here mud hut)
123	122.2	Kendu Bay Hotel
124	266.0	Kendu Bay Hotel
125	311.8	0666751 / 9961912 / 1151 (Limestone deposits took sample)
126	343.6	0666828 / 9961749 / 1153 (Lime cemented scree (pyroclasts)

S/No	Dose rate (nSv. hr⁻¹)	Location description and coordinates
127	348.7	0666873 / 9961723 / 1157 (Chalk sample in Nyangot Pala gulley)
128	525.8	0666908 / 9961641 / 1154 (Rawe beds sediments had detector inside hole took sample)
129	625.6	Pyroclast in the middle of Rawe (Nyogot pole) gulley
130	239.7	indripping rock formation to ask Prof. Opiyo
131	217.5	0666882 / 9961403 / 1165 (alluvial sediments aeron pics)
132	320.9	0666882 / 9961403 / 1165 (alluvial sediments aeron pics)
133	402.5	0666805 / 9961267 / 1168 (alluvial cover of erosion surface below the limestone in Rawe river bed)
134	562.8	0667010 / 9961141 / 1179 (alluvial cover previous area had > 400)
135	566.0	0667010 / 9961141 / 1179 (alluvial cover previous area had > 400)
136	584.0	0667010 / 9961141 / 1179 (alluvial cover previous area had > 400)
137	630.9	0667109 / 9961109 / 1198 (alluvial cover look sample)
138	643.0	0667109 / 9961109 / 1198 (alluvial cover look sample)

S/No	Dose rate (nSv. hr⁻¹)	Location description and coordinates
139	643.6	0667109 / 9961109 / 1198 (alluvial cover look sample)
140	415.7	0667359 / 9960964 / 1175 (Alluvial on Rawe bed)
141	397.5	0667580 / 9960627 / 1178 (Limestones have reddish coloration fe-riche stone siderites feco3)
142	547.0	0667580 / 9960627 / 1178 (Limestones have reddish coloration fe-riche stone siderites feco3)
143	560.0	0667580 / 9960627 / 1178 (Limestones have reddish coloration fe-riche stone siderites feco3)
144	369.0	0667628 / 9960548 / 1180 (Sampled water (vial 1))
145	387.0	0667628 / 9960548 / 1180 (Sampled water (vial 1))
146	364.1	0667609 / 9960538 / 1193 (sampled water (vial 2) NY1)
147	360.1	0667538 / 9960471 / 1202 (Pyroclasts near hot springs 83 degrees C)
148	406.7	0667538 / 9960471 / 1202 (Pyroclasts near hot springs 83 degrees C)
149	376.6	0667538 / 9960471 / 1202 (Pyroclasts near hot springs 83 degrees C)

S/No	Dose rate (nSv. hr⁻¹)	Location description and coordinates
150	482.7	0667538 / 9960471 / 1202 (Pyroclasts near hot springs 83 degrees C)
151	850.7	0667645 / 9960540 / 1198 (Dyke of Fe stone took sample)
152	764.6	0667645 / 9960540 / 1198 (Dyke of Fe stone took sample)
153	638.3	0667618 / 9960591 / 1197 (Alluvial - Lake Victoria to Nysengu)
154	555.5	0667727 / 9960789 / 1209 (Alluvial)
155	600.3	0667693 / 9960993 / 1213 (Nyanzian system)
156	654.8	0667910 / 9961059 / 1211 (Nyanzian andesite took sample near hot spring, Abundo Primary School)
157	353.2	0668000 / 9961027 / 1183 (water sample from hot spring)
158	437.8	0668000 / 9961027 / 1183 (water sample from hot spring)
159	454.8	0671159 / 9962587 / 1152 (alluvial)
160	637.1	
161	379.8	Picked water sample Omari, Sam, Okello credit & legal
162	380.7	0671167 / 9962597 / 1154 (Picked water sample #5)
163	129.6	00683272 / 9959246 / 1166 (Back to hotel in Kendu Bay)
164	392.0	00683272 / 9959246 / 1166 (Back to hotel in Kendu Bay)

S/No	Dose rate (nSv. hr⁻¹)	Location description and coordinates
165	238.1	0669633 / 9952289 / 1165
166	376.3	0669633 / 9952289 / 1165
167	374.5	0669774 / 9952267 / 1165 (Garden with aluvial cover)
168	191.6	0669824 / 9952250 / 1186, 1184 (Rhyolite)
169	269.1	0669834 / 9952264 (Ijolites)
170	381.0	0669833 / 9952186 / 1181 (Carbonititic dykes cutting across ijolites, thinner dyke)
171	449.4	0669833 / 9952186 / 1181 (Carbonititic dykes cutting across ijolites, thinner dyke)
172	455.8	0669833 / 9952186 / 1181 (Carbonititic dykes cutting across ijolites, thinner dyke)
173	445.9	0669822 / 9952172 / 1186 (Rhyolite)
174	915.6	0669828 / 9952170 / 1188 (Carbonatite)
175	119.6	0669815 / 9952142 / 1182 (Banded carbonititic intrusion)
176	385.5	0669633 / 9951649 / 1158 (shattered Nyanzian)
177	531.4	0669595 / 9951563 / 1163 (Bala Springs, carbonatite intrusions in Nyanzian)
178	436.7	0669636 / 9951527 / 1154 (Hot spring at Bala)

S/No	Dose rate (nSv. hr⁻¹)	Location description and coordinates
179	490.8	
180	251.0	without probe
181	247.4	without probe
182	225.7	NRPL
183	293.6	NRPL
184	394.0	MTRL
185	302.0	MTRL
186	303.6	LSC - 16 oils counted all ABA ABI removed
187	189.8	Outreach with Hez
188	143.9	Lake view Hotel at Kendu Bay
189	361.0	Kodula Market
190	721.9	0.5 - 1 km Kodula market
191	298.1	0.5 - 1 km Kodula market
192	439.9	0.5 - 1 km Kodula market
193	169.4	chief's camp - Homa Mountain
194	385.2	Mzee Aman Ogira
195	412.0	Path to Homa Mt.

S/No	Dose rate (nSv. hr⁻¹)	Location description and coordinates
196	797.9	Pyroclasts on way to Adiags (vying for Councilor)
197	663.7	Pyroclasts on way to Adiags (vying for Councilor)
198	488.5	Pyroclasts on way to Adiags (vying for Councilor)
199	653.9	Path at Vuma to Homa Mt
200	692.4	Path at Vuma to Homa Mt
201	445.0	Foot of Homa peak
202	623.1	Facing Homa peak on path with intrusions
203	461.1	Facing Homa peak on path with intrusions
204	615.5	
205	552.3	Peak of Homa Mt.
206	1112.0	Peak of Homa Mt.
207	894.5	Took sample at 11.15 a.m.
208	742.1	Took sample at 11.15
209	888.7	Took sample at 11.15
210	951.0	Homa Mt through brown boulder
211	451.6	Took sample at 11.35
212	2681.0	Took sample at 11.35

S/No	Dose rate (nSv. hr⁻¹)	Location description and coordinates
213	756.0	Soil alluvial Homa Mt.
214	884.5	Soil alluvial Homa Mt.
215	1101.0	Boulder cave
216	311.4	Top of Homa peak inside boulder 12.15 p.m.
217	475.9	alluvial on top of Homa peak
218	811.2	alluvial on top of Homa peak
219	442.6	Opposite Homa peak on Homa Mt
220	144.2	Lake View Hotel at Kendu Bay
221	345.1	Bathroom Ebusiralo, Vihiga County
222	655.0	
223	380.0	with γ - probe inserted
224	325.4	in bed rock
225	294.4	with γ -probe in bedroom
226	339.4	
227	219.6	Outside house
228	345.4	Window tofali's being built
229	735.3	2.67 n Sv.h ⁻¹

S/No	Dose rate (nSv. hr⁻¹)	Location description and coordinates
230	225	00 38.926/34019.756 Kamato Gate
		00 64876/34 32929 Ruma National Park
231	200	00 38 55476/34 19558/1244 m
232	293	00 63796/34 30979/ 1173 m
233	271	00 63438/34 0040/ 1180 m Lambwe River
234	248	00 62676/34 29519/ 1186 m
235	278	00 60713/34 3060/ 1173 m
236	229	00 60855/34 30949/ 1165 m
237	270	00 60438/34 28534/ 1183 m TRAP 7
238	306	00 58737/34 29975/ 1165 m TRAP 15
239	235	00 58707/34 30301/ 1163 m TRAP 16
240	271	00 35051/34 17568/ 1151 m TRAP 11
241	268	00 57943/34 29492/ 1167 TRAP 10
242	305	00 57741/34 30838/ 1141 TRAP 14
243	285	00 57671/34 28192/ 1179 TRAP 9
244	261	00 57499/ 34 26386/1217 TRAP 8 NYATOTO
245	223	00 58926/34 30311/ 1332 M Ruma National Park KWS office

S/No	Dose rate (nSv. hr⁻¹)	Location description and coordinates
246	284	00 67202/34 25147/ 1187 m TRAP 5
247	252	00 67206/34 25147/ 1172 m TRAP 6
248	504	Radiation Protection Board Office at Nyanza General Hospital
249	501	EBUSIRALO, Vihiga County
250	204	SIO PORT, Busia County

Key to Global Positioning readings

GPS satellites broadcast signals from space, and each GPS receiver uses these signals to calculate its three-dimensional location (latitude, longitude, and altitude) and the current time . For example 00 67202/34 25147/ 1187 is interpreted as latitude (0⁰ (degrees) South of the equator, 67 minutes, 20 seconds with an error/uncertainty of 2 seconds)); longitude (34⁰ West of the meridian, 25 minutes, 14 seconds with an error/uncertainty of 7 seconds) and altitude of 1,187 meters above sea level.

IAEA-RGU-1 , Uranium Ore

Inorganic , Ores

- Unit Size: 500g
- Price per Unit: 50 EUR
- Report: IAEA/RL/148
- Date of Release: 1987-01-01

Both, IAEA-RGU-1 and IAEA-RGTh-1 reference materials were prepared on behalf of the International Atomic Energy Agency by the Canada Centre for Mineral and Energy Technology by dilution of a uranium ore BL-5 (7.09% U) and a thorium ore OKA-2 (2.89% Th, 219 µg U/g) with floated silica powder of similar grain size distribution, respectively (IAEA 1987).

Table C.1 IAEA –RGU-1

Analyte	Value	Unit	95% C.I.	N	R/I/C
²³² Th	< 4	Bq/kg	-	None	I
²³⁵ U	228	Bq/kg	226 - 230	None	R
²³⁸ U	4940	Bq/kg	4910 - 4970	None	R
⁴⁰ K	< 0.63	Bq/kg	-	None	I
K	< 20	mg/kg	-	None	I
Th	< 1	mg/kg	-	None	I
U	400	mg/kg	398 - 402	None	R

No evidence for between-bottles inhomogeneity was detected after mixing and bottling. BL-5 has been certified for uranium, ²²⁶Ra and ²¹⁰Pb confirming that it

is in radioactive equilibrium. The agreement between radiometric and chemical measurements of thorium and uranium in OKA-2 shows both series to be in radioactive equilibrium.

(Value) Concentration calculated as a mean of the accepted laboratory means
(N) Number of accepted laboratory means which are used to calculate the recommended or information values and their respective confidence intervals
(R/I/C) Classification assigned to the property value for analyte.

Recommended/Information/Certified) (IAEA 1987) Natural radionuclide activity concentrations derived from the elemental concentrations on basis of isotopic abundance and half-life data. The values listed above were established on the basis of a gravimetric dilution of materials with known uranium, thorium and potassium composition. The details concerning the criteria for qualification as a recommended or information value can be found in the respective report (attached).

IAEA-RGTh-1 , Thorium Ore

Inorganic , Ores

- Unit Size: 500g
- Price per Unit: 50 EUR
- Report: IAEA/RL/148
- Date of Release: 1987-01-01

Both, IAEA-RGU-1 and IAEA-RGTh-1 reference materials were prepared on behalf of the International Atomic Energy Agency by the Canada Centre for Mineral and Energy Technology by dilution of a uranium ore BL-5 (7.09% U) and a thorium ore OKA-2 (2.89% Th, 219 µg U/g) with floated silica powder of similar grain size distribution, respectively. No evidence for between-bottles

inhomogeneity was detected after mixing and bottling. BL-5 has been certified for uranium, ^{226}Ra and ^{210}Pb confirming that it is in radioactive equilibrium. The agreement between radiometric and chemical measurements of thorium and uranium in OKA-2 shows both series to be in radioactive equilibrium.

Table C.2 IAEA -RGTh-1

Analyte	Value	Unit	95% C.I.	N	R/I/C
^{232}Th	3250 [?]	Bq/kg	3160 - 3340	155	R
^{235}U	3.6 [?]	Bq/kg	3.3 - 3.9	145	R
^{238}U	78 [?]	Bq/kg	72 - 84	145	R
^{40}K	6.3 [?]	Bq/kg	3.1 - 9.5	45	I
K	200	mg/kg	100 - 300	45	I
Th	800	mg/kg	784 - 816	155	R
U	6.3	mg/kg	5.9 - 6.7	145	R

(Value) Concentration calculated as a mean of the accepted laboratory means
 (N) Number of accepted laboratory means which are used to calculate the recommended or information values and their respective confidence intervals
 (R/I/C) Classification assigned to the property value for analyte

Recommended/Information/Certified) (?) Natural radionuclide activity concentrations derived from the elemental concentrations on basis of isotopic abundance and half-life data

The values listed above were established on the basis of a gravimetric dilution of materials with known uranium, thorium and potassium composition. The details concerning the criteria for qualification as a recommended or information value can be found in the respective report (attached).

IAEA-RGK-1 , Potassium Sulfate

Inorganic , Ores

- Unit Size: 500g
- Price per Unit: 50 EUR
- Report: IAEA/AL/148
- Date of Release: 1987-01-01

The IAEA-RGK-1 material is produced from high purity (99.8%) potassium sulphate supplied by the Merck Company. The potassium property value and its uncertainty were obtained from repeated measurements performed at the IAEA Laboratories Seibersdorf and the results confirmed the value certified by Merck. The upper limits for the uranium and thorium property values were estimated by the IAEA Laboratories Seibersdorf using fluorimetry and activation analysis, respectively.

Table C.3 IAEA -RGK-1

Analyte	Value	Unit	95% C.I.	N	R/I/C
⁴⁰ K	14000 [?]	Bq/kg	13600 - 14400	20	R
K	448000	mg/kg	445000 - 451000	20	R
Th	< 0.01	mg/kg	-	20	I
U	< 0.001	mg/kg	-	20	I

(Value) Concentration calculated as a mean of the accepted laboratory means

(N) Number of accepted laboratory means which are used to calculate the recommended or information values and their respective confidence intervals

(R/I/C) Classification assigned to the property value for analyte

(Recommended/Information/Certified) (?) Natural radionuclide activity concentrations derived from the elemental concentrations on basis of isotopic abundance and half-life data

The values listed above were established on the basis of a gravimetric dilution of materials with known uranium, thorium and potassium composition. The details concerning the criteria for qualification as a recommended or information value can be found in the respective report (IAEA 1987).

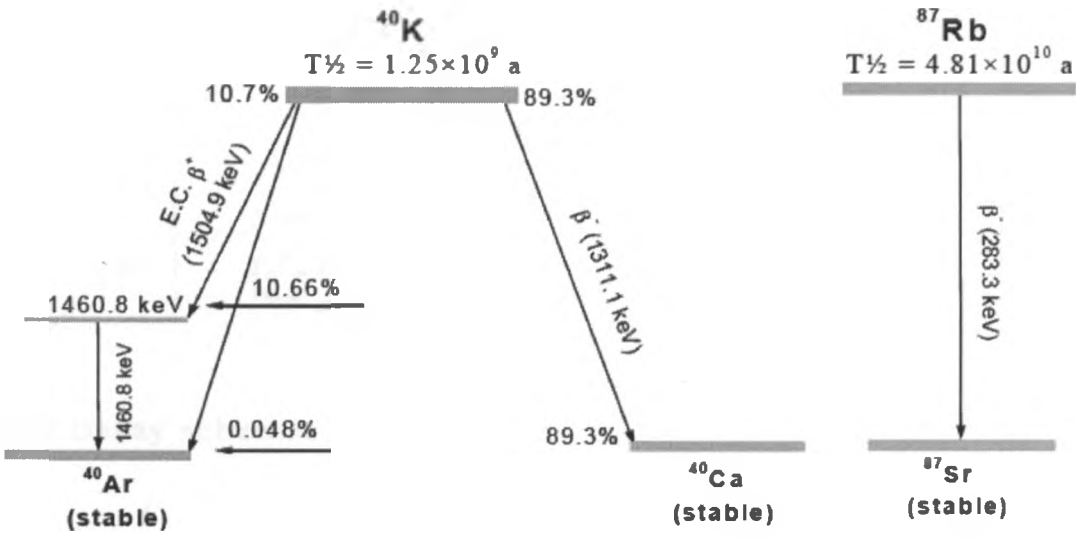


Fig. C. 1 Decay schemes of ^{40}K and ^{87}Rb .

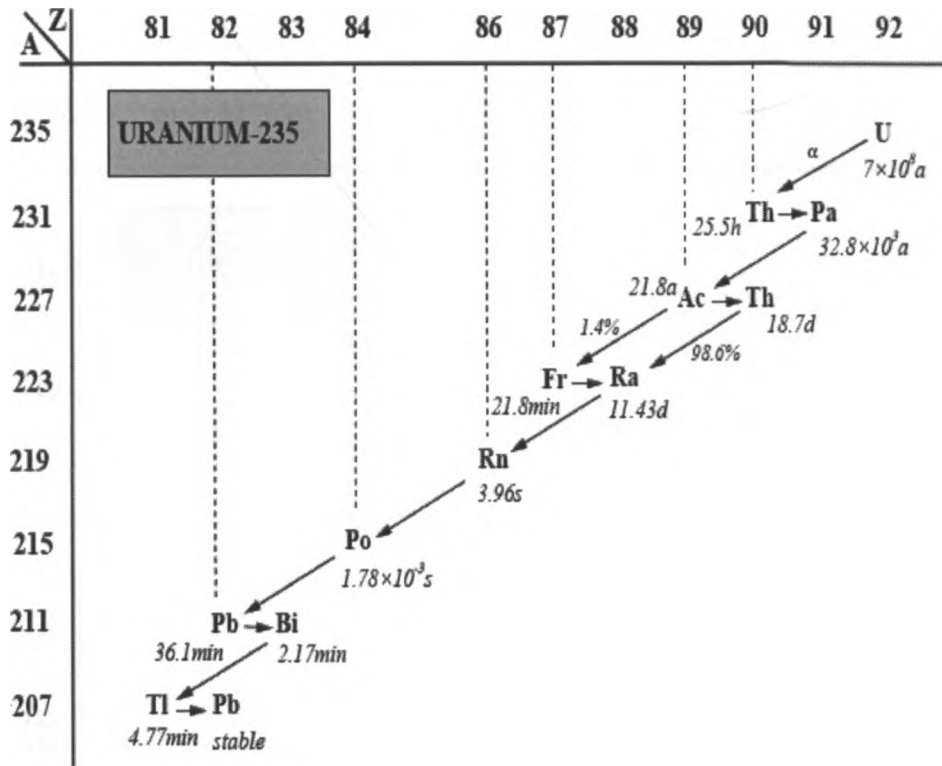


Fig. C. 2 Decay schemes of ^{235}U

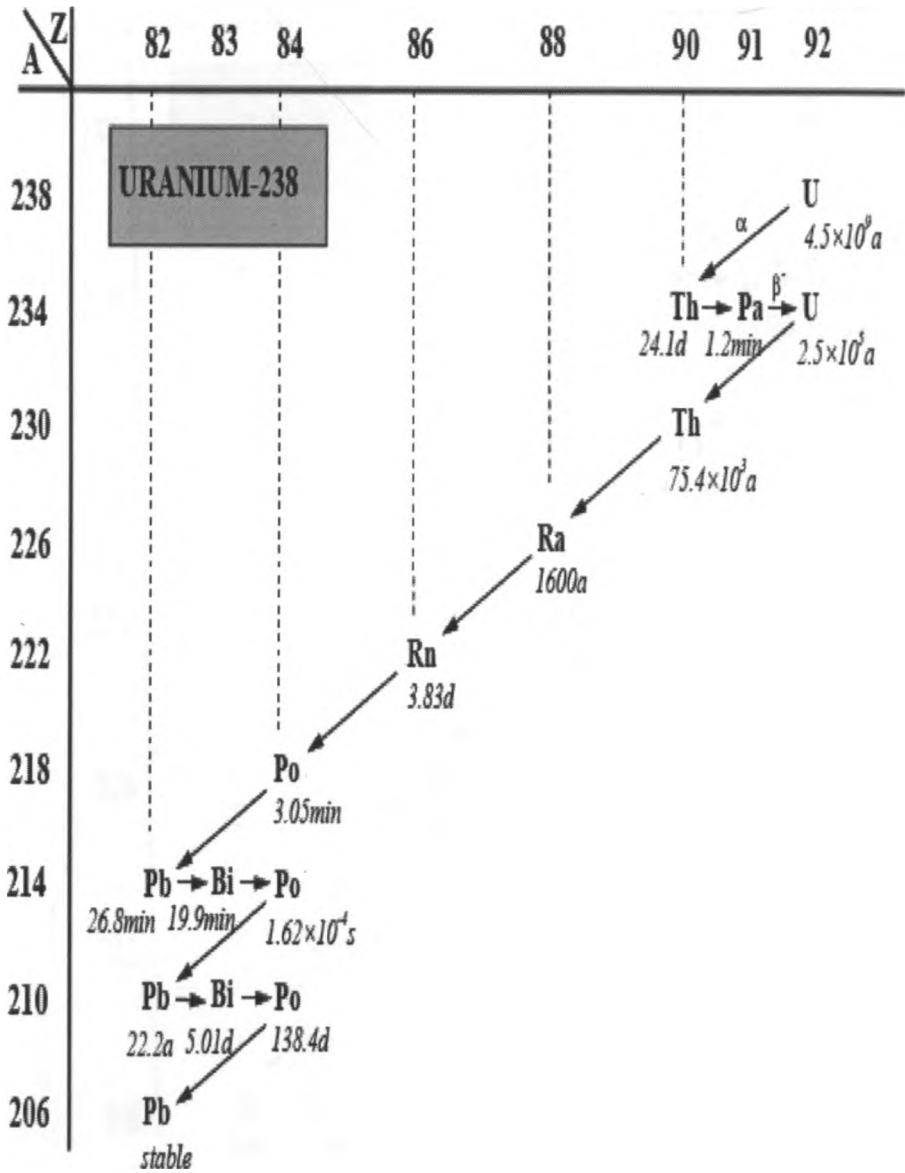


Fig. C. 3 Decay schemes of ^{238}U

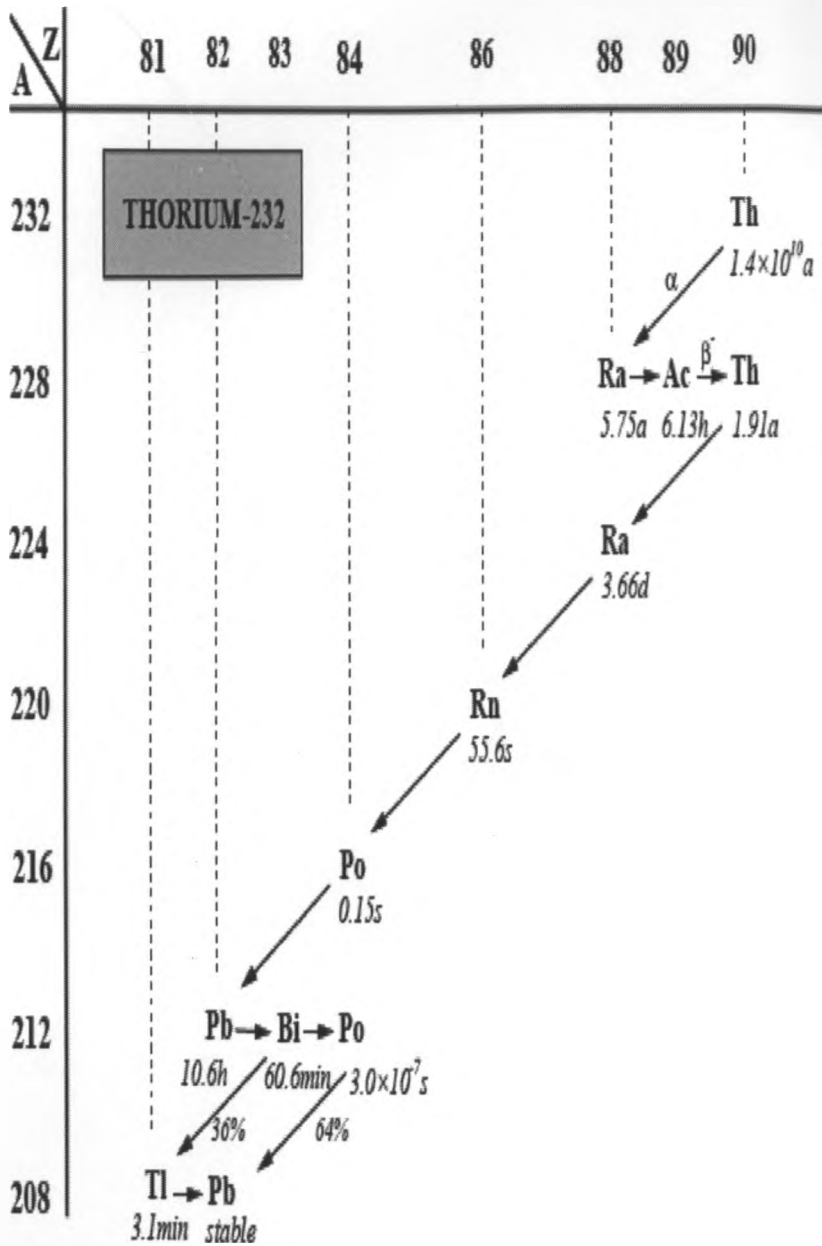


Fig. C. 4 Decay schemes of ^{232}Th